USGS
science for a changing world

# Systematic Comparisons Between PRISM Version 1.0.0, BAP, and CSMIP Ground-Motion Processing

By Erol Kalkan and Christopher Stephens

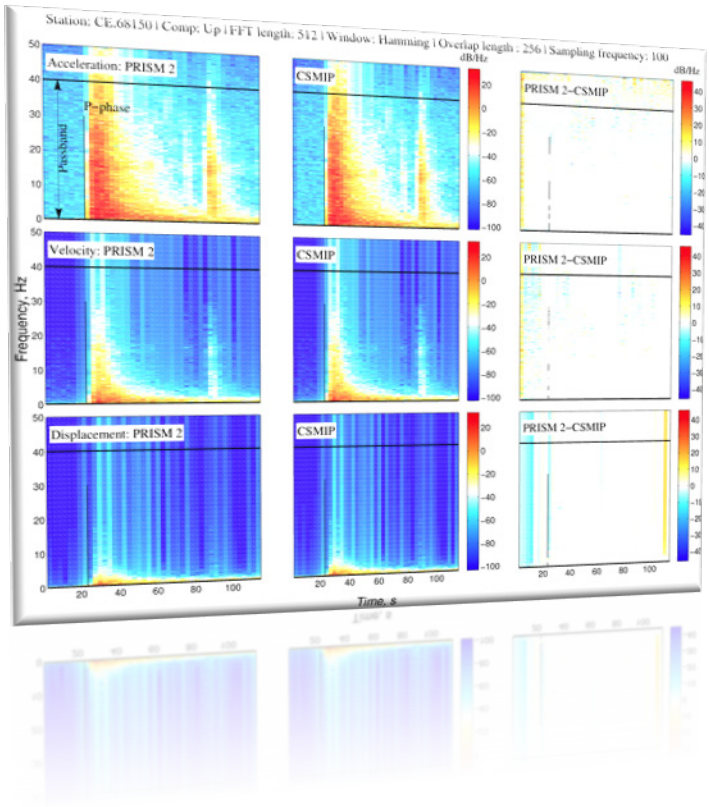


Open-File Report 2017–1020

U.S. Department of the Interior
U.S. Geological Survey

Cover: Spectrograms showing acceleration, velocity, and displacement time series obtained by using Processing and Review Interface for Strong Motion data (PRISM) and California Strong Motion Instrumentation Program (CSMIP) processing.

U.S. Geological Survey
William H. Werkheiser, Acting Director

U.S. Geological Survey, Reston, Virginia: 2017



Suggested citation:
Kalkan, E., and Stephens, C., 2017, Systematic comparisons between PRISM version 1.0.0, BAP, and CSMIP ground-motion processing: U.S. Geological Survey Open-File Report 2017–1020, 108 p., https://doi.org/10.3133/ofr20171020.

ISSN 2331-1258 (online)

# Acknowledgments

The authors would like to thank Bob Darragh, Jamie Steidl, Tadahiro Kishida, and Brad Aagaard for their thorough reviews. Special thanks are extended to Joe Fletcher for fruitful discussions on cross-correlation and phase spectrum, and Sarah Nagorsen and Elisabeth Brouwers for editing.

# Contents



## Figures

## Tables

# Abbreviations

| | |
|---|---|
| ANSS | Advanced National Seismic System |
| BAP | Basic Strong-Motion Accelerogram Processing software |
| COSMOS | Consortium of Organizations for Strong-Motion Observation Systems |
| CSMIP | California Strong Motion Instrumentation Program |
| FAS | Fourier amplitude spectrum |
| FFT | fast Fourier transform |
| FIR | finite-impulse-response |
| *M* | moment magnitude |
| ML | local magnitude |
| NCCM | Normalized cross-correlation measure |
| NSMP | National Strong-Motion Project |
| PGA | peak ground acceleration |
| PGD | peak ground displacement |
| PGV | peak ground velocity |
| PRISM | Processing and Review Interface for Strong Motion data |
| PSD | power spectral density |
| RMS | root mean square (square root of the mean of the squared values) |
| s | second |
| sps | samples-per-second |
| V1 | COSMOS volume 1 |
| V2 | COSMOS volume 2 |

# Notation

| | |
|---|---|
| $A(t)$ | waveform amplitude at time *t* |
| $C_{xy}(f)$ | magnitude-squared coherence of signal *x* and *y* |
| *d* | sample delay |
| *f* | frequency |
| *i* | imaginary number equal to square root of −1 |
| $m_b$ | body-wave magnitude |
| *mx* | mean of signal *x* |
| *my* | mean of signal *y* |
| *n* | Butterworth filter order |
| *N* | number of data points in the input time series |
| $P_{xx}(f)$ | power spectral density of signal *x* |
| $P_{yy}(f)$ | power spectral density of signal *y* |
| $P_{xy}(f)$ | cross power spectral density of signals *x* and *y* |
| $R_{xx}$ | normalized cross-correlation sequence |
| *s*(*t*) | time series |
| $\theta_{xy}(f)$ | relative phase between signals *x* and *y* |
| $\tau_0$ | time delay |
| $\omega$ | cyclic frequency, in radians |
| $\varphi(t)$ | waveform phase |

# Systematic Comparisons Between PRISM Version 1.0.0, BAP, and CSMIP Ground-Motion Processing

By Erol Kalkan and Christopher Stephens

## Abstract

A series of benchmark tests was run by comparing results of the Processing and Review Interface for Strong Motion data (PRISM) software version 1.0.0 to Basic Strong-Motion Accelerogram Processing Software (BAP; Converse and Brady, 1992), and to California Strong Motion Instrumentation Program (CSMIP) processing (Shakal and others, 2003, 2004). These tests were performed by using the MatLAB implementation of PRISM, which is equivalent to its public release version in Java language. Systematic comparisons were made in time and frequency domains of records processed in PRISM and BAP, and in CSMIP, by using a set of representative input motions with varying resolutions, frequency content, and amplitudes. Although the details of strong-motion records vary among the processing procedures, there are only minor differences among the waveforms for each component and within the frequency passband common to these procedures. A comprehensive statistical evaluation considering more than 1,800 ground-motion components demonstrates that differences in peak amplitudes of acceleration, velocity, and displacement time series obtained from PRISM and CSMIP processing are equal to or less than 4 percent for 99 percent of the data, and equal to or less than 2 percent for 96 percent of the data. Other statistical measures, including the Euclidian distance ($L^2$ norm) and the windowed root mean square level of processed time series, also indicate that both processing schemes produce statistically similar products.

## Introduction

PRISM (Processing and Review Interface for Strong Motion data) originally was conceived as a modern graphical user interface (GUI) to replace the outdated, command-line driven software program BAP (Basic Strong-Motion Accelerogram Processing Software; Converse and Brady, 1992) developed and used by the U.S. Geological Survey (USGS) National Strong-Motion Project (NSMP) to process earthquake strong-motion acceleration records. PRISM incorporates basic processing procedures from BAP, and interacts with a database or workflow management system; a complete description of this software is provided in Jones and others (2017).

This report presents results for a series of benchmark tests that compared processing results of PRISM version 1.0.0 (henceforth referred to as PRISM), with those from BAP, and with those processed by the California Strong Motion Instrumentation Program (CSMIP; Shakal and others, 2003, 2004). The benchmark tests were performed by using the MatLAB implementation of PRISM, which is equivalent to its public release version in Java language. In development stage, the baseline correction and acausal bandpass filtering were performed in the velocity domain after integrating acceleration to velocity; the acceleration and displacement time series were derived by differentiating and integrating the corrected velocity, respectively. When compared with corresponding products derived by using

BAP, it was observed that amplitudes of the time series were systematically lower. Investigations showed that discrepancies in part resulted from numerical differentiation, particularly for lower time resolution (100 samples-per-second [sps] or less) records characterized by relatively high-frequency content, and to the method of trapezoidal integration acting as a low-pass filter, so that when bandpass filters were applied in velocity rather than in acceleration, the amplitudes of high-frequency content were disproportionately reduced. In PRISM the baseline correction is still computed in the velocity domain, but its derivative is applied as a baseline correction to the acceleration waveform, which is subsequently bandpass-filtered and integrated and double integrated to obtain velocity and displacement, respectively. Other improvements in PRISM include the use of a 5-point central difference operator, which was found to be superior to the 3-point central difference used earlier in development version; and interpolation of low time resolution digital records to at least 200 sps before processing.

Systematic comparisons are made in the time and frequency domains of records processed in PRISM and BAP, and in CSMIP, by using a set of representative input motions with different sampling rates, frequency content, and amplitude. The details of strong-motion records output by each of these processing procedures are identical, and, for each component and within the frequency passband common to these procedures, differences are minor. These findings are substantiated through a comprehensive statistical evaluation considering more than 1,800 ground-motion components recorded from various magnitude earthquakes and at a wide range of distances.

## Integration and Filtering

In the BAP software, acausal bandpass filtering of ground-motion data was performed on acceleration. In development stage of PRISM, bandpass filters were applied in velocity. Because integration acts as a low-pass filter (fig. 1), resultant amplitudes of higher frequencies were systematically lower when bandpass filters were applied in velocity as compared with acceleration. To avoid this distortion in frequency content of the signals, PRISM now applies bandpass filters in acceleration.

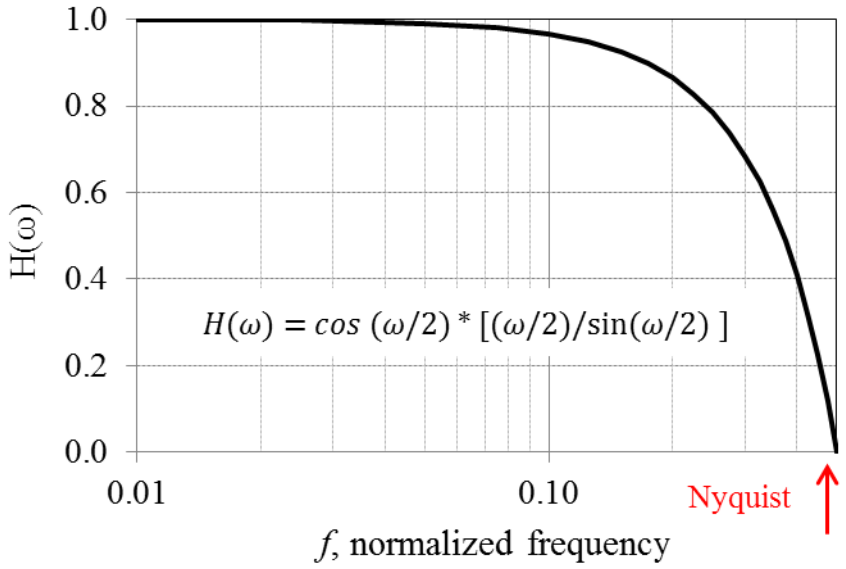


Figure 1. Graph showing frequency response of trapezoid integration (modified from Hamming, 1989).

## Central-Difference Formula

Numerical differentiation of nonstationary random signals is sensitive to rounding errors, and the error increases as the sampling rate decreases. The 3-point central difference operator was found to be sufficient for records sampled at 200 sps. This sample rate is recommended for Advanced National Seismic System (ANSS) strong-motion reference sites (COSMOS, 2001; Whittaker and others, 2005) and is the standard adopted for NSMP stations. Other strong-motion networks, however, often use a lower sampling rate, typically 100 sps, which requires a higher order differentiation operator.

One improvement to PRISM includes use of a 5-point central difference operator as default. Its superior performance in reducing error is demonstrated in figure 2, where an acceleration time series originally sampled at 100 sps is integrated to velocity and differentiated back to acceleration. The graphs in figure 2 compare initial acceleration with derived acceleration. This simple test involved neither a baseline correction (other than a simple correction by subtracting the mean of the time series) nor filtering. The numerical error (difference in time series) is significant—11.5 percent for peak ground acceleration (PGA) solely resulting from the low sampling rate. The 5-point central difference operator reduces this error to 5.3 percent.

Interpolating the time series to a higher sampling rate before differentiating further reduces numerical errors. The interpolation process applies an anti-aliasing (low-pass) finite-impulse-response (FIR) filter to time series with a Kaiser window (Oppenheim and others, 1999). The linear-phase FIR filter minimizes the weighted, integrated squared error between an ideal piecewise linear function and the magnitude response of the filter over a set of desired frequency bands (Parks and Burrus, 1987). In figure 3, the previous acceleration time series in figure 2 is resampled to 200 sps, integrated to velocity, and then differentiated back to acceleration. The derived acceleration time series is downsampled to the original 100 sps for comparison. In this case, the error in PGA is reduced from 11.5 percent to 1.4 percent. Resampling at 400 sps reduces the error in PGA to 0.4 percent (fig. 4).

If the V1 acceleration has low time resolution (less than about 200 sps), PRISM resamples the time series to 200 sps as default prior to the V2 processing.

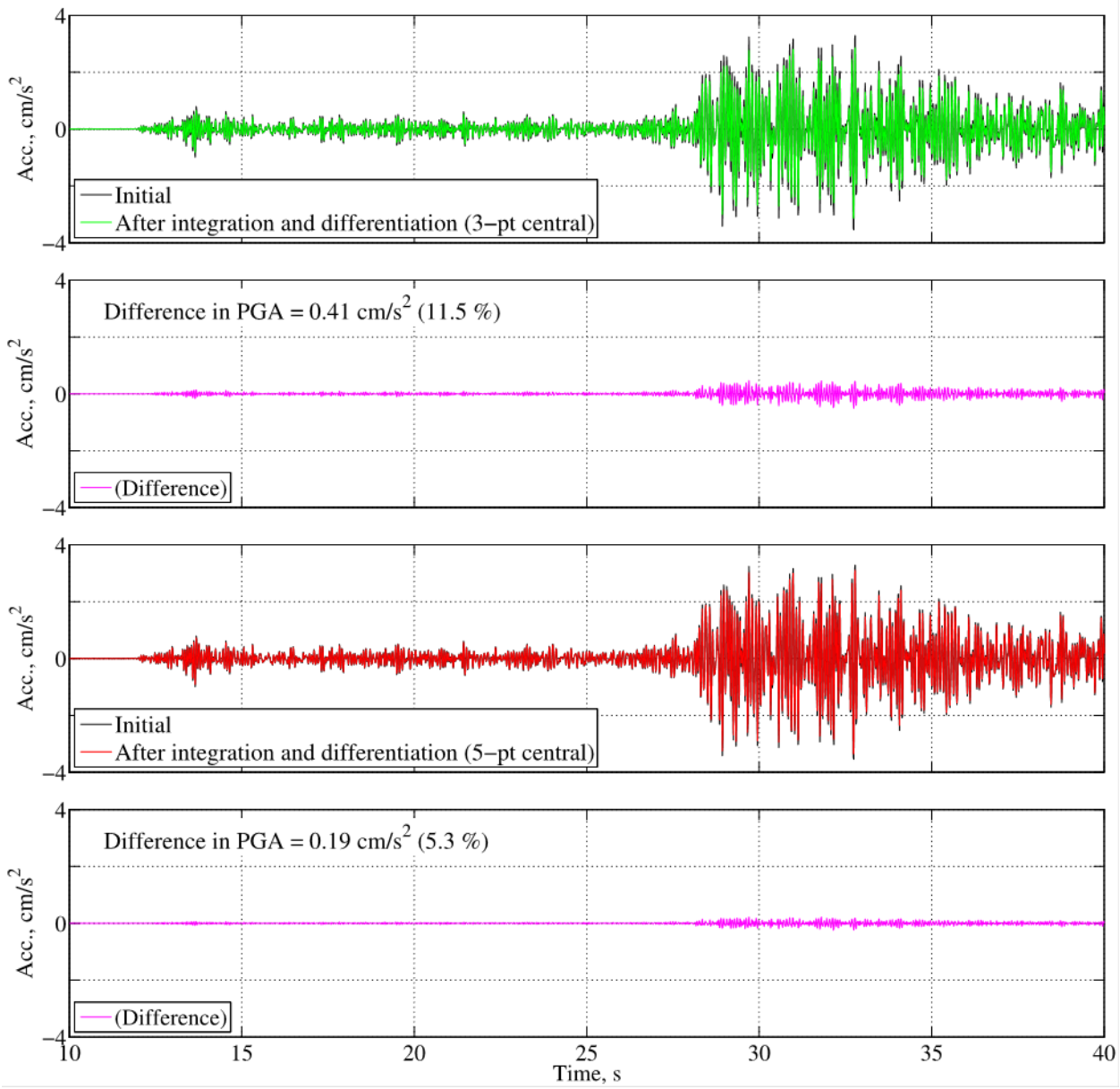


Figure 2. Graphs showing numerical error (difference in time series) resulting from differentiation by using 3- and 5-point central difference operator (input motion sampling rate is 100 samples-per-second [sps]). Using a 5-point central difference operator reduces error in peak ground acceleration (PGA) by 6.2 percent. acc., acceleration; cm/s$^2$, centimeters per second squared; pt, point; s, seconds.

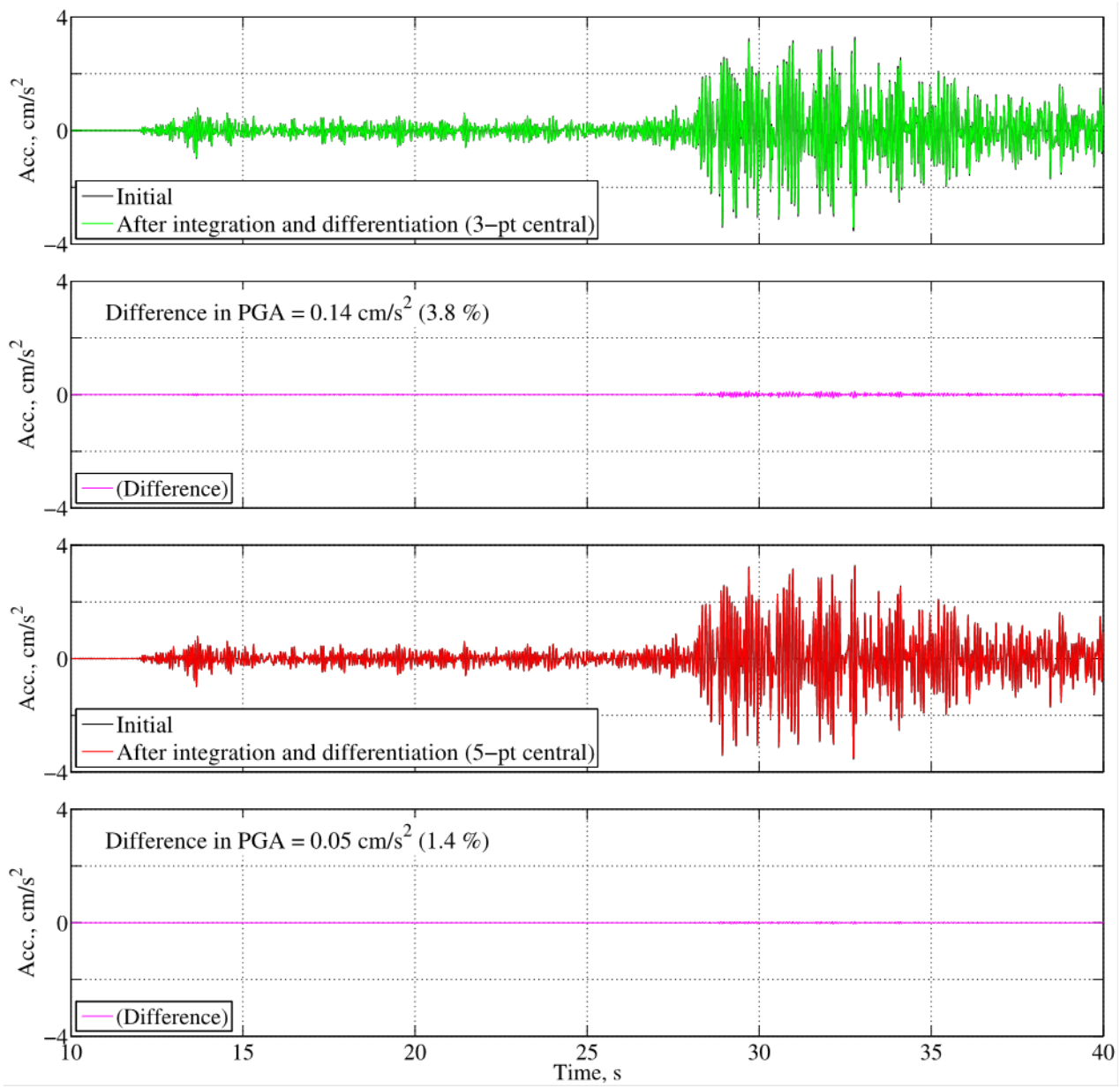


Figure 3. Graphs showing reduction in numerical error (difference in time series) resulting from differentiation produced by interpolating input motion to 200 samples-per-second (sps) prior to differentiation and then downsampling to 100 sps. Using a 5-point central difference operator reduces error in peak ground acceleration (PGA) by 2.4 percent. acc., acceleration; cm/s$^2$, centimeters per second squared; PGA, peak ground acceleration; pt, point; s, seconds.

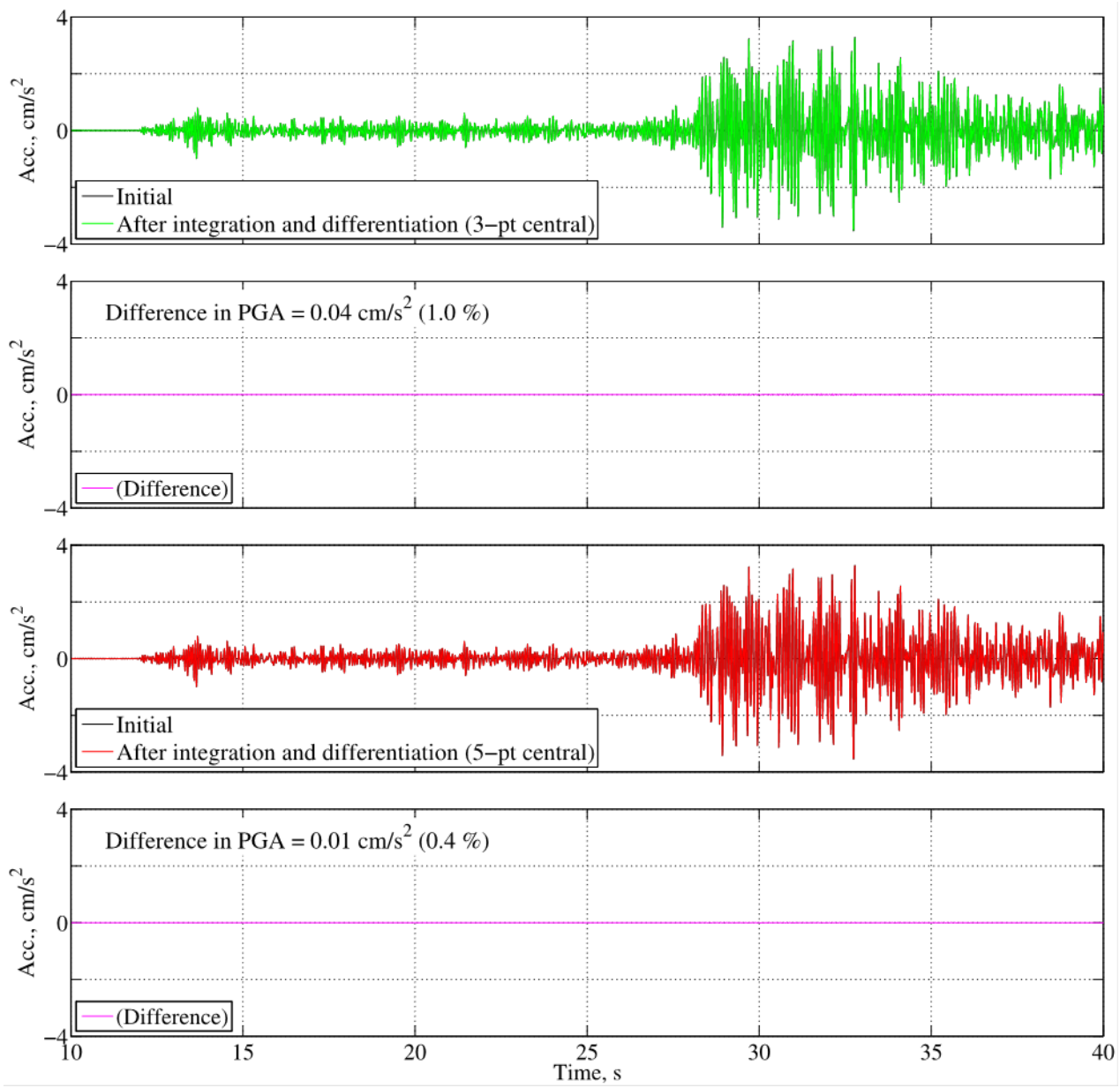


Figure 4. Graphs showing reduction in numerical error (difference in time series) resulting from differentiation produced by interpolating input motion to 400 samples-per-second (sps) prior to differentiation and then downsampling to 100 sps. Using a 5-point central difference operator reduces error in peak ground acceleration (PGA) by 0.6 percent. acc., acceleration; cm/s$^2$, centimeters per second squared; PGA, peak ground acceleration; pt, point; s, seconds.

## Measuring Time-Series Similarities

The similarities among time series processed by using PRISM, BAP, and CSMIP were measured in four ways: first, by comparing peak amplitudes in acceleration, velocity, and displacement (these are peak ground acceleration [PGA], peak ground velocity [PGV], and peak ground displacement [PGD]); second, by computing coherence, cross spectrum phase and cross correlation of the time series; third, by comparing Fourier amplitude spectrum (FAS) of acceleration, velocity, and displacement time series; and fourth, by computing and comparing spectrograms of the power spectrum.

The spectral coherence is used here as a metric to identify frequency-domain correlation between two signals (Stoica and Moses, 2005). The magnitude-squared coherence values tending toward 1 indicate that corresponding frequency $(f)$ components are well correlated, whereas values tending toward 0 indicate that corresponding frequency components are uncorrelated. The magnitude-squared coherence is a function of the power spectral densities, $P_{xx}(f)$ and $P_{yy}(f)$, of signals *x* and *y*, and of the cross power spectral density, $P_{xy}(f)$, of *x* and *y* as

$$C_{xy}(f) = \frac{|P_{xy}(f)|^2}{P_{xx}(f)P_{yy}(f)} \tag{1}$$

To reduce the finite size effect, arising in calculations made on short duration intervals of time series data, the power spectral density (PSD) was calculated by averaging over the estimated periodograms for subintervals of equal length (see Welch's method, Welch, 1967).

At frequencies where spectral coherence is high, the relative phase $\theta_{xy}(f)$ between correlated components can be estimated directly from the complex-valued $P_{xy}(f)$. It should be noted that the phase estimates are only meaningful where significant frequency-domain correlation exists. If the two signals do not have the same phase relationship for the two wave numbers averaged together, then the coherence will diminish. Measurement of $\theta_{xy}(f)$ enables one to determine the time delay $\tau_0$ between the two windowed signals by noting that $\theta_{xy}(f)$ is a linear function of $f$ with a slope of $2\pi\tau_0$ (Bendat and Piersol, 2010).

Cross correlation is another method for estimating phase delays between two signals. In the time domain, the normalized cross-correlation sequence, $R_{xx}$, of signals *x* and *y* at delay *d* is defined as (Buck and others, 2002)

$$R_{xy}(d) = \frac{\sum_{i=1}^{N}[(x(i)-mx)*(y(i-d)-my)]}{\sqrt{\sum_{i=1}^{N}(x(i)-mx)^2}\sqrt{\sum_{i=1}^{N}(y(i-d)-my)^2}} \tag{2}$$

where *mx* and *my* are the mean of signals *x* and *y*, respectively; *N* is number of data points.

If equation (2) is computed for all delays (lags) d = 0, 1, 2,…*N*−1 then it results in a cross correlation series of twice the length of the original signal. The denominator in equation (2) serves to normalize the correlation coefficients to quantify the lag between two signals, which has value of 1 at 0 lag (delay) if the two signals are fully correlated.

Lastly, signal similarities are measured by performing time-frequency analysis, where a time series is segmented into short, overlapping intervals, and then estimating the power spectrum over sliding windows. This fast Fourier transform (FFT)-based spectral estimate of each sliding window helps one to visualize how the frequency content of the signal changes over time. The time series are divided into segments with 50 percent overlap. Prior to computing the PSD, each segment is weighted with a Hamming window (Hamming, 1989). Here, spectrograms of PSD values are plotted using a logarithmic frequency scale. The unit of spectrogram is the decibel (dB/Hz); the number of decibels is ten times the logarithm to base 10 of the ratio of the power in the two windows.

## PRISM Versus BAP Processing

PRISM and BAP processing are compared first by using the record from the station IU.AFI (Afiamalu, Samoa) acquired from the Incorporated Research Institutions for Seismology (IRIS) Data Center (http://ds.iris.edu/ds/nodes/dmc/; last accessed November 2016) for a body-wave magnitude ($m_b$) 5.0 earthquake that occurred on September 15, 2015, at 19:35 Universal Time (UT) about 170 km to the southwest at a depth of 21 km. The original record was sampled at 100 sps. This record was chosen because of a large discrepancy observed in high-frequency acceleration between BAP and development version of PRISM (fig. 5). This figure also shows the differences between acceleration, velocity, and displacement. Although the velocity and displacement time series match closely, the lower amplitudes in the acceleration waveform are quite noticeable. These differences are attributed to computational inaccuracies introduced as a result of the low sampling rate (100 sps) of the recording.

The record was re-processed using PRISM, and the comparison with BAP is shown in figure 6. Except in the final few seconds of the processed records, the differences are very small. The difference in PGA relative to BAP is reduced from 11.5 percent to 0.1 percent. There is no difference in PGV of time series, and the difference in PGD is 0.1 percent.

Figure 7 shows frequency and time domain metrics used to measure signal similarities. Products from PRISM and BAP have high coherence with near zero phase difference within the filter passband. Signals do not show any lag as evident from the normalized cross-correlation measure (NCCM) plots.

In figure 8, FAS plots for acceleration, velocity, and displacement time series are superimposed. Frequency contents of the acceleration, velocity, and displacement waveforms agree well within the passband (0.3–40 Hz), defined as between the corner frequencies of the low-cut (high-pass) and high-cut (low-pass) filters used in the processing. We attribute small differences at higher frequencies near the low-pass filter corner to fundamental dissimilarities in the shape of the transfer functions for the Butterworth filter used in PRISM (with n=4) and the cosine taper used in BAP (fig. 9).

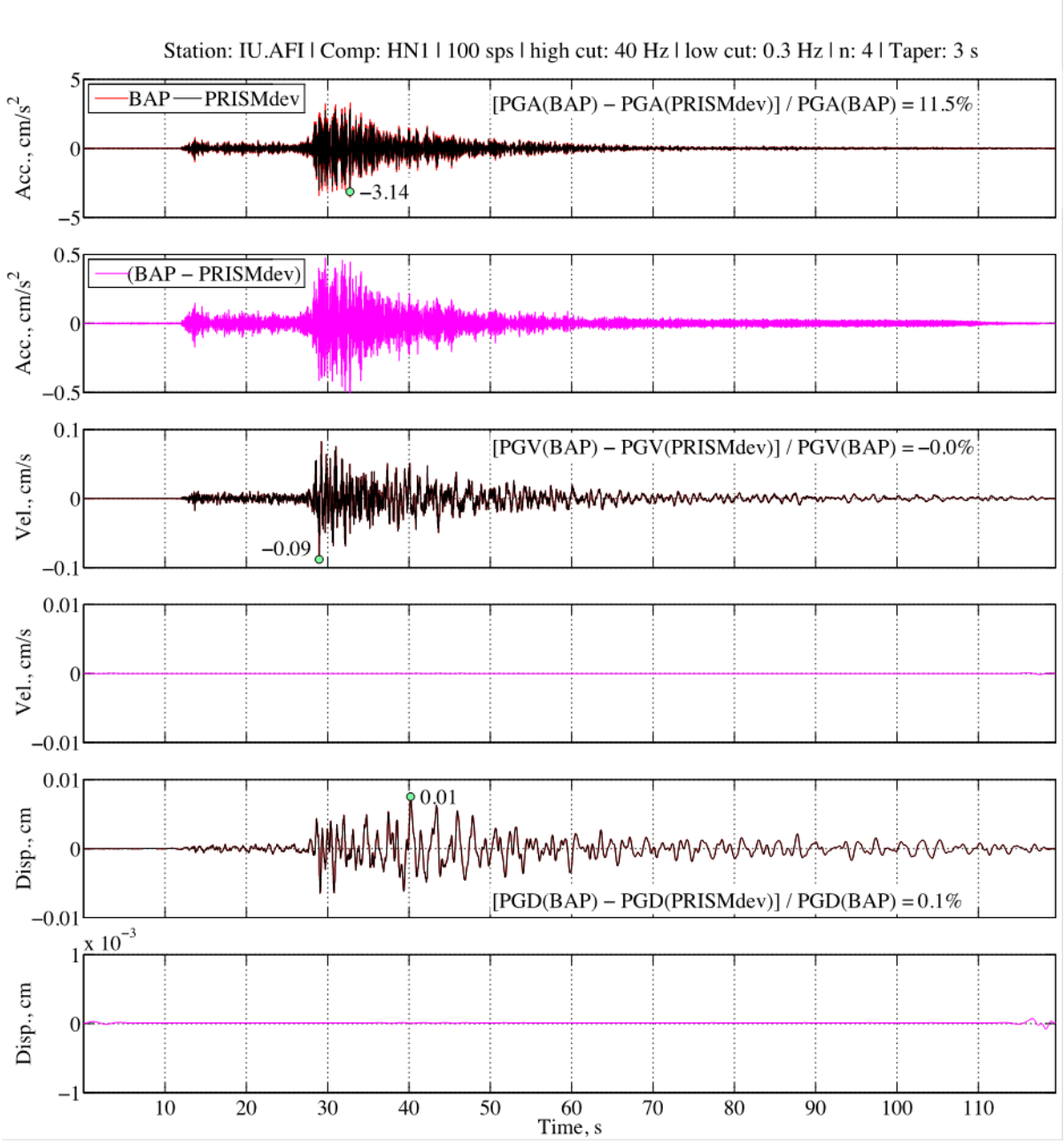


Figure 5. Graphs comparing acceleration (acc.), velocity (vel.), and displacement (disp.) time series obtained by using development version of Processing and Review Interface for Strong Motion data (PRISMdev) and Basic Strong-Motion Accelerogram Processing Software (BAP) to process component (comp) HN1 of station IU.AFI record from the 2015 $m_b$5.0 earthquake in Afiamalu, Samoa. The record processed in PRISMdev (black lines) overlies the BAP version (red lines). Percent differences in peak ground acceleration (PGA), peak ground velocity (PGV), and peak ground displacement (PGD) are shown. Note differences in scaling used to enhance visibility for each pair of physical motion plots. Green circles indicate peak values of PRISMdev processing. cm, centimeters; cm/s, centimeters per second; cm/s$^2$, centimeters per second squared; Hz, hertz; n, Butterworth filter order; s, seconds; sps, samples-per-second.

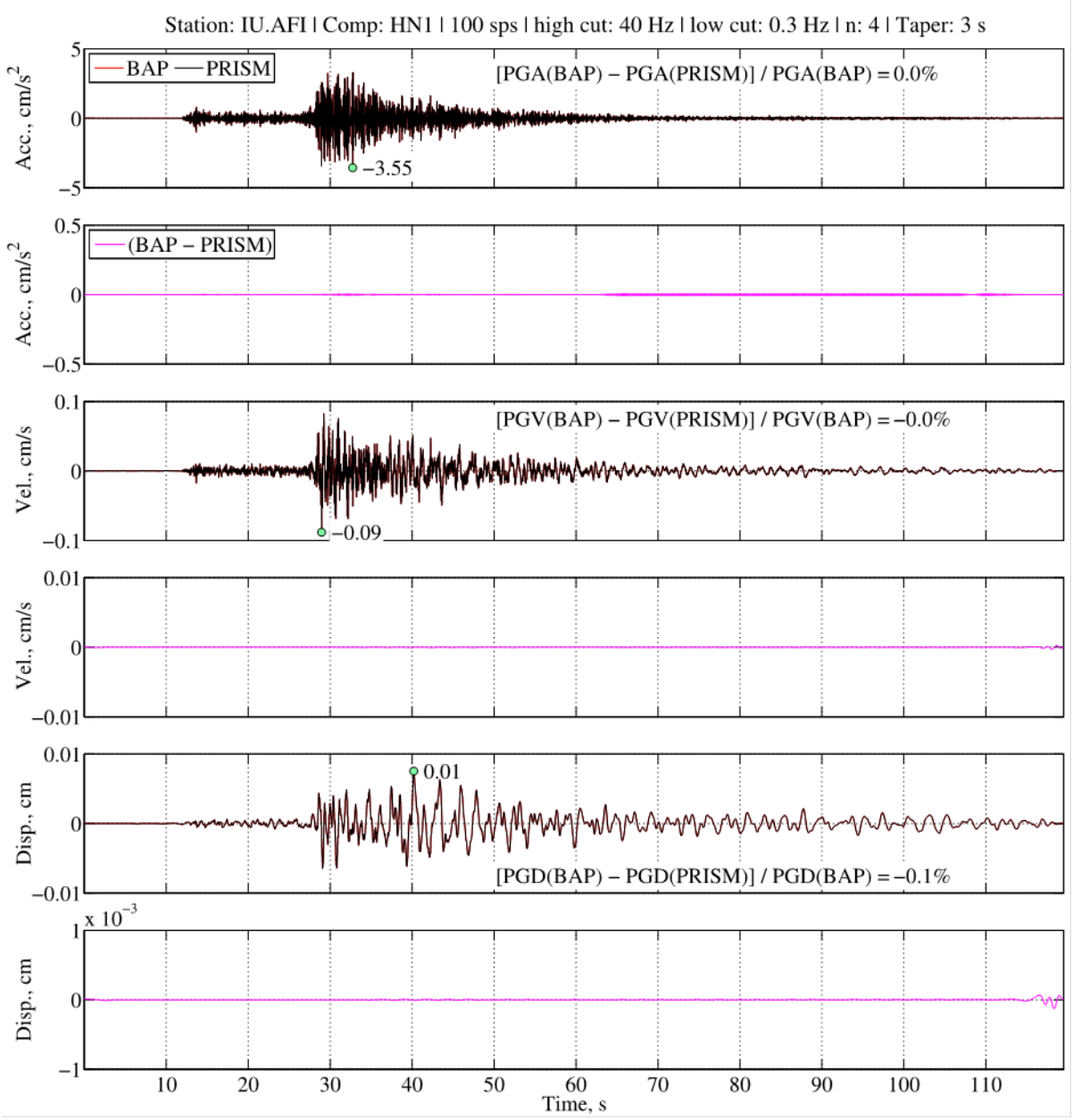


Figure 6. Graphs comparing acceleration (acc.), velocity (vel.), and displacement (disp.) time series obtained by using Processing and Review Interface for Strong Motion data (PRISM) and Basic Strong-Motion Accelerogram Processing Software (BAP) to process component (comp) HN1 of station IU.AFI record from the 2015 $m_b$5.0 earthquake in Afiamalu, Samoa. The record processed in PRISM (black lines) overlies the BAP version (red lines). Percent differences in peak ground acceleration (PGA), peak ground velocity (PGV), and peak ground displacement (PGD) are shown. Note differences in scaling used to enhance visibility for each pair of physical motion plots. Green circles indicate peak values of PRISM processing. cm, centimeters; cm/s, centimeters per second; cm/s$^2$, centimeters per second squared; Hz, hertz; n, Butterworth filter order; s, seconds; sps, samples-per-second.

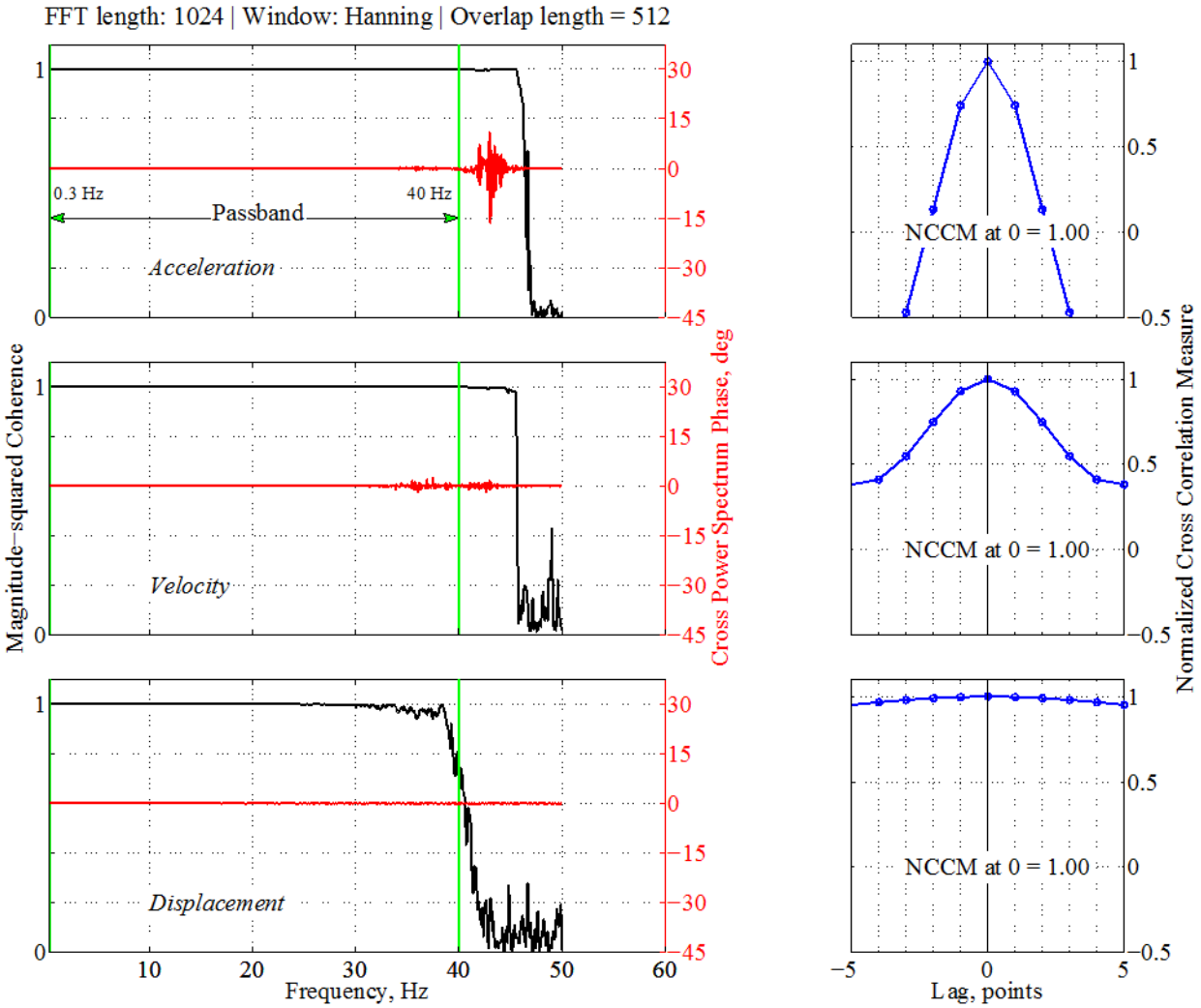


Figure 7. Graphs showing magnitude-squared coherence, cross spectrum phase in degrees, and normalized cross-correlation measure (NCCM) used to measure frequency and time domain similarities between acceleration, velocity, and displacement time series processed by Processing and Review Interface for Strong Motion data (PRISM) and Basic Strong-Motion Accelerogram Processing Software (BAP). Vertical green lines show corners of bandpass filter. Data correspond to component HN1 of station IU.AFI record from the 2015 $m_b$5.0 earthquake in Afiamalu, Samoa. FFT, fast Fourier transform; Hz, hertz.

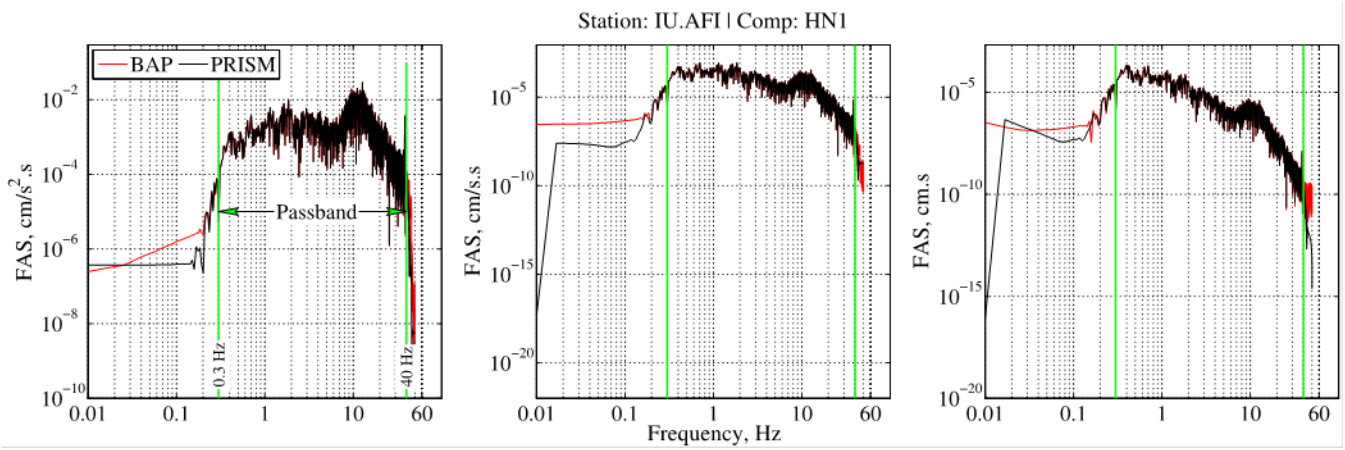


Figure 8. Graphs showing Fourier amplitude spectra (FAS) of acceleration, velocity, and displacement time series obtained by using Processing and Review Interface for Strong Motion data (PRISM) and Basic Strong-Motion Accelerogram Processing Software (BAP) to process component (comp) HN1 of station IU.AFI record from the 2015 $m_b$5.0 earthquake in Afiamalu, Samoa. The record processed in PRISM (black lines) overlies the BAP version (red lines). Vertical green lines show corners of bandpass filter. cm·s, centimeters second; cm/s·s, centimeters per second second; cm/s²·s, centimeters per second squared second; Hz, hertz.

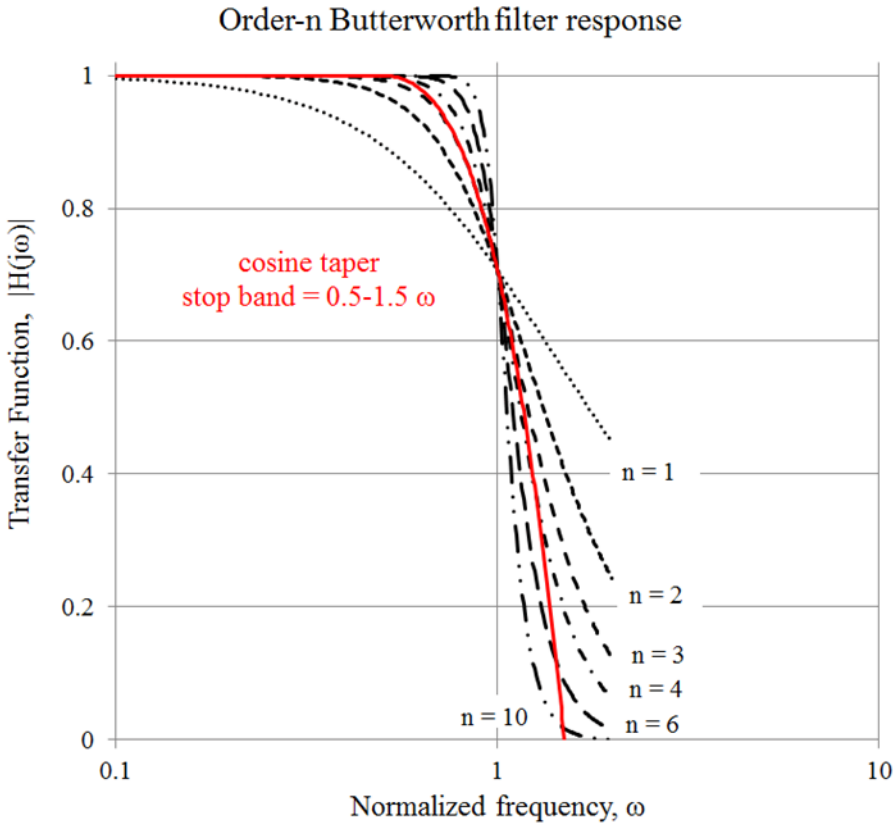


Figure 9. Graphs showing frequency responses of order-n Butterworth low-pass filter (black lines) and cosine taper approximation (red line).

Next, PRISM and BAP processing are compared by using two additional ground-motion records sampled at 200 sps. The first record, from CSMIP station CE.57444, is for the 2015 moment magnitude (*M*) 3.6 San Ramon earthquake at an epicenter distance of 2.4 km. The PGA of this record is small (1.2 percent gravitational acceleration [g]), but the record is selected because it represents a near-field ground motion of a small magnitude event with significant high-frequency content. The second record, from CSMIP station CE.68150, is for the 2014 *M*6.0 South Napa earthquake, with a closest-to-fault distance of 4.5 km (CESMD) and a PGA of 37.5 percent g. This strong-motion record was chosen because of the long-period content and proximity to the source. The uncorrected (V1) and the corrected (V2) waveforms processed by CSMIP were obtained from the Center for Engineering Strong Motion Data (CESMD; http://strongmotioncenter.org; last accessed November 2016). The V1 time series were input into PRISM and BAP to generate V2, where the bandpass filter corners and tapering were matched as closely as possible to those used by CSMIP in generating V2. Figure 10 compares the acceleration, velocity, and displacement time series of component HNN of CE.57444 record. Differences in PGA, PGV, and PGD, as compared with corresponding BAP values, are essentially zero, as is the difference between the time series.

In figure 11, the magnitude-squared coherence, cross spectrum phase, and NCCM are presented. Within the passband (0.3–40 Hz), acceleration, velocity, and displacement waveforms have coherence values equal or close to 1. The NCCM results are consistent with the zero lag inferred from phase angles between the two signals.

In figure 12 FAS are overlaid to demonstrate that frequency contents of signals are comparable within the filter passband. The spectrograms (frequency and energy over time) of acceleration, velocity, and displacement time series are shown in figure 13, where spectrogram colors encode frequency power levels ranging from 0 to 50 Hz. Red indicates frequency content with higher power; blue colors indicate frequency content with very low power; and differences between windowed PSD results are plotted. The signals have a broad range of frequency content, and earthquake energy arrives suddenly with the sharp (impulsive) onset of the P-phase, denoted by a vertical line. Overall, the frequency content of the records is comparable for the earthquake signal following the P-phase arrival; these results indicate that signals processed by PRISM and BAP match well.

Figures 14 through figure 21 show similar plots for components HNE and HNZ of the CE.57444 record, demonstrating that BAP and PRISM results are nearly identical for these two components. Maximum discrepancies in PGA, PGV, and PGD are within 0.3 percent for component HNZ; there is essentially no difference for the other horizontal component.

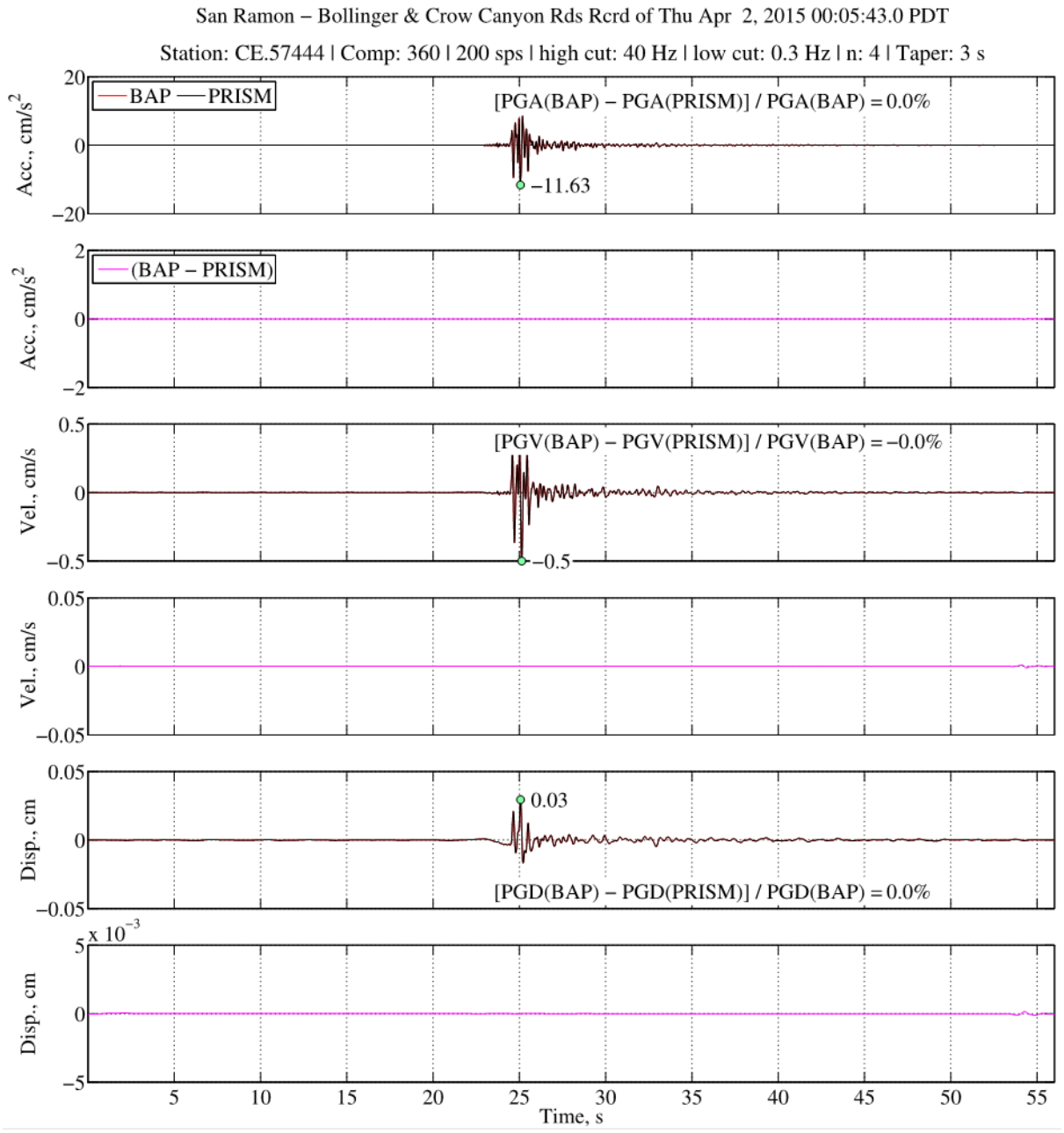


Figure 10. Graphs comparing acceleration (acc.), velocity (vel.), and displacement (disp.) time series obtained by using Processing and Review Interface for Strong Motion data (PRISM) and Basic Strong-Motion Accelerogram Processing Software (BAP) to process component (comp) HNN of station CE.57444 record from the 2015 *M*3.6 San Ramon earthquake in California. The record processed in PRISM (black lines) overlies the BAP version (red lines). Percent differences in peak ground acceleration (PGA), peak ground velocity (PGV), and peak ground displacement (PGD) are shown. Note differences in scaling used to enhance visibility for each pair of physical motion plots. Green circles indicate peak values of PRISM processing. cm, centimeters; cm/s, centimeters per second; cm/s$^2$, centimeters per second squared; Hz, hertz; n, Butterworth filter order; PDT, Pacific daylight time; s, seconds; sps, samples-per-second.

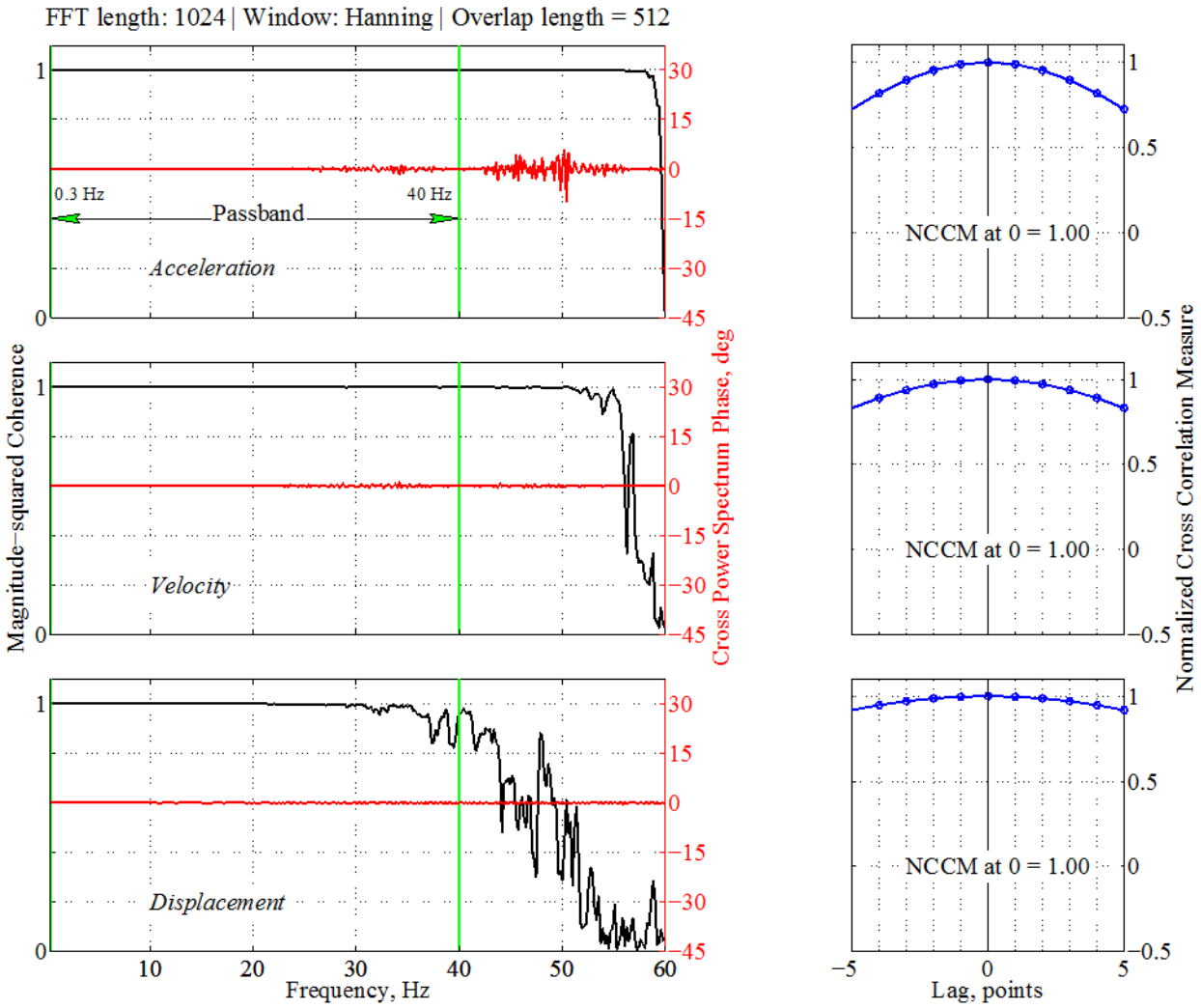


Figure 11. Graphs showing magnitude-squared coherence, cross spectrum phase in degrees, and normalized cross-correlation measure (NCCM) used to measure frequency and time domain similarities between acceleration, velocity, and displacement time series processed by Processing and Review Interface for Strong Motion data (PRISM) and Basic Strong-Motion Accelerogram Processing Software (BAP). Vertical green lines show corners of bandpass filter. Data correspond to component HNN of station CE.57444 record from the 2015 *M*3.6 San Ramon earthquake in California. FFT, fast Fourier transform; Hz, hertz.

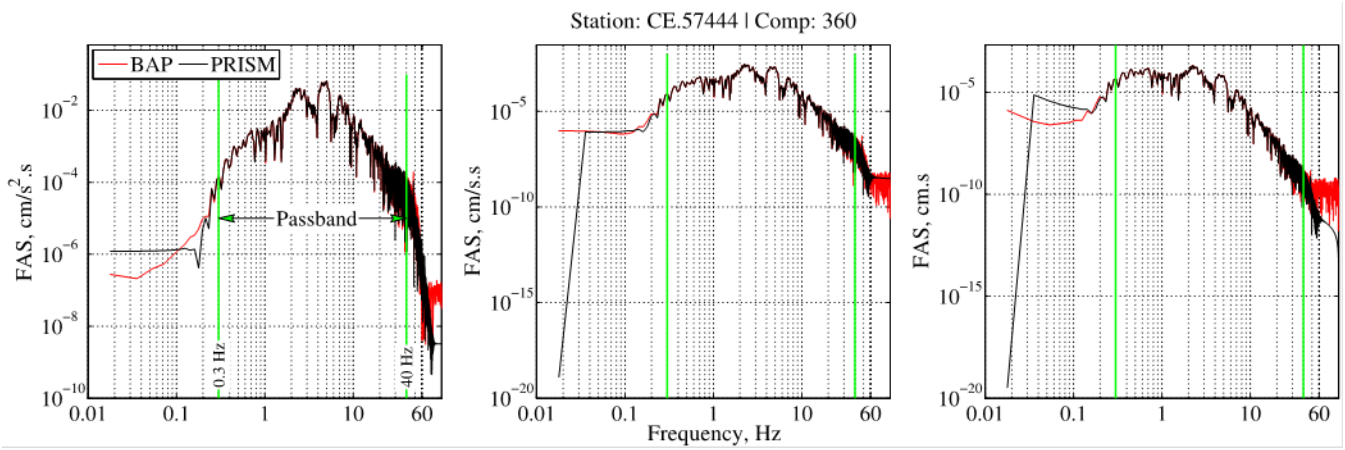


Figure 12. Graphs showing Fourier amplitude spectra (FAS) of acceleration, velocity, and displacement time series obtained by using Processing and Review Interface for Strong Motion data (PRISM) and Basic Strong-Motion Accelerogram Processing Software (BAP) to process component (comp) HNN of station CE.57444 record from the 2015 *M*3.6 San Ramon earthquake in California. The record processed in PRISM (black lines) overlies the BAP version (red lines). Vertical green lines show corners of bandpass filter. cm·s, centimeters second; cm/s·s, centimeters per second second; cm/s²·s, centimeters per second squared second; Hz, hertz.

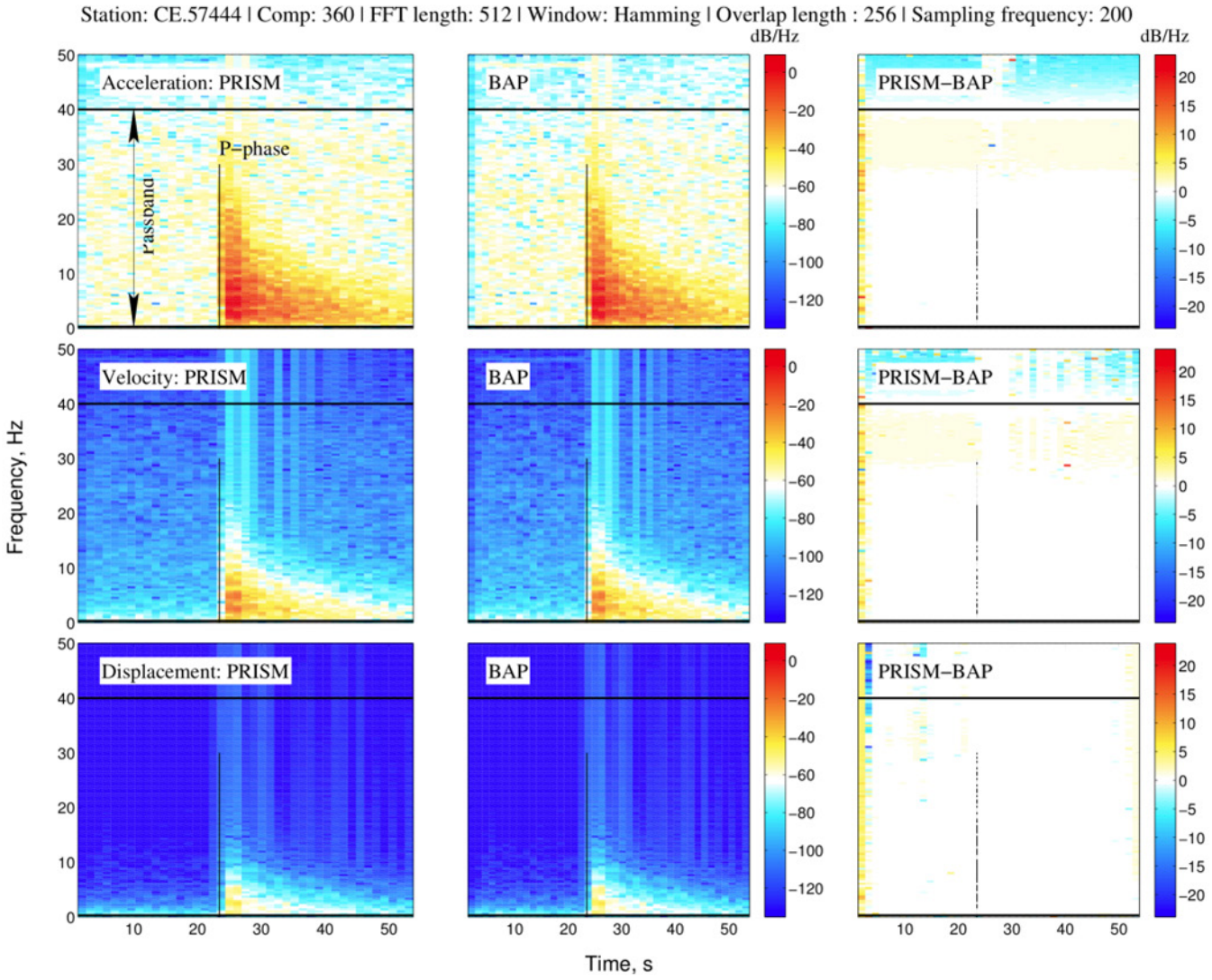


Figure 13. Spectrograms of acceleration, velocity, and displacement time series obtained by using Processing and Review Interface for Strong Motion data (PRISM) and Basic Strong-Motion Accelerogram Processing Software (BAP) to process component (comp) HNN of station CE.57444 record from the 2015 *M*3.6 San Ramon earthquake in California. Differences in power spectral densities are plotted in right column. Color indicates strength of time series at a range of frequencies over time. Horizontal lines show corners of bandpass filter; vertical black lines denote P-phase arrival time. dB/Hz, decibel per hertz; FFT, fast Fourier transform; Hz, hertz; s, seconds.

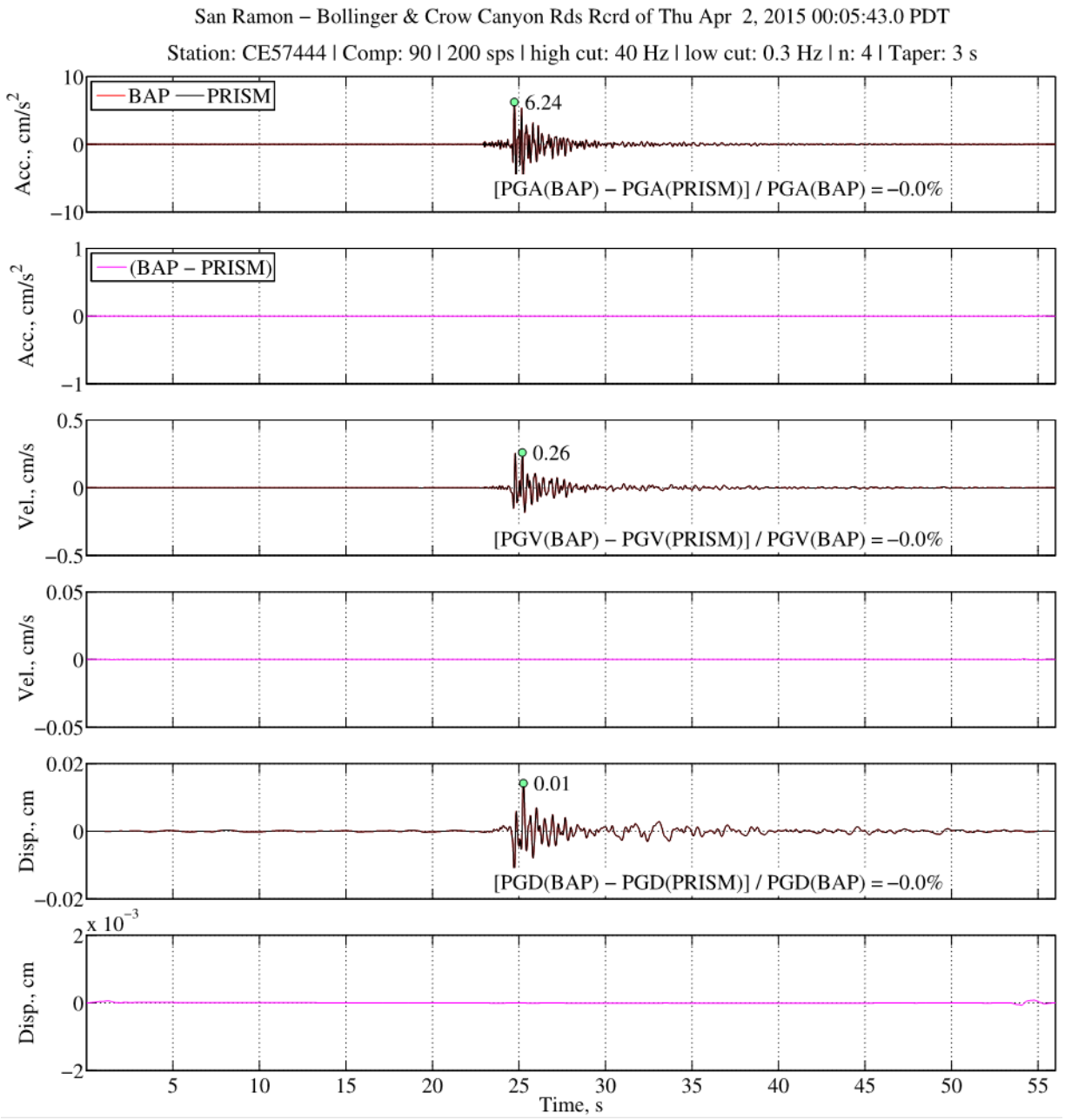


Figure 14. Graphs comparing acceleration (acc.), velocity (vel.), and displacement (disp.) time series obtained by using Processing and Review Interface for Strong Motion data (PRISM) and Basic Strong-Motion Accelerogram Processing Software (BAP) to process component (comp) HNE of station CE.57444 record from the 2015 *M*3.6 San Ramon earthquake in California. The record processed in PRISM (black lines) overlies the BAP version (red lines). Percent differences in peak ground acceleration (PGA), peak ground velocity (PGV), and peak ground displacement (PGD) are shown. Note differences in scaling used to enhance visibility for each pair of physical motion plots. Green circles indicate peak values of PRISM processing. cm, centimeters; cm/s, centimeters per second; cm/s$^2$, centimeters per second squared; Hz, hertz; n, Butterworth filter order; PDT, Pacific daylight time; s, seconds; sps, samples-per-second.

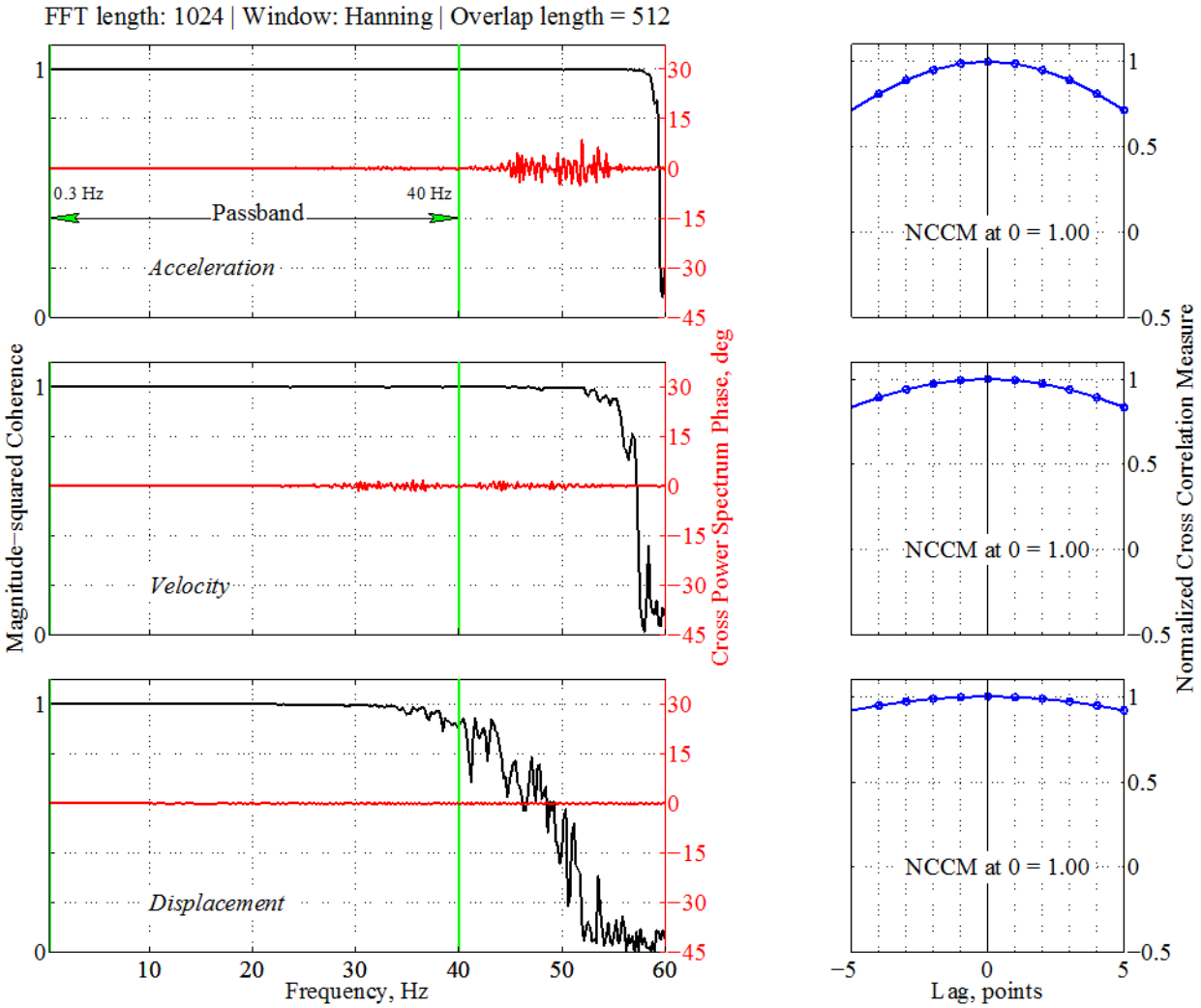


Figure 15. Graphs showing magnitude-squared coherence, cross spectrum phase in degrees, and normalized cross-correlation measure (NCCM) used to measure frequency and time domain similarities between acceleration, velocity, and displacement time series processed by Processing and Review Interface for Strong Motion data (PRISM) and Basic Strong-Motion Accelerogram Processing Software (BAP). Vertical green lines show corners of bandpass filter. Data correspond to component HNE of station CE.57444 record from the 2015 *M*3.6 San Ramon earthquake in California. FFT, fast Fourier transform; Hz, hertz.

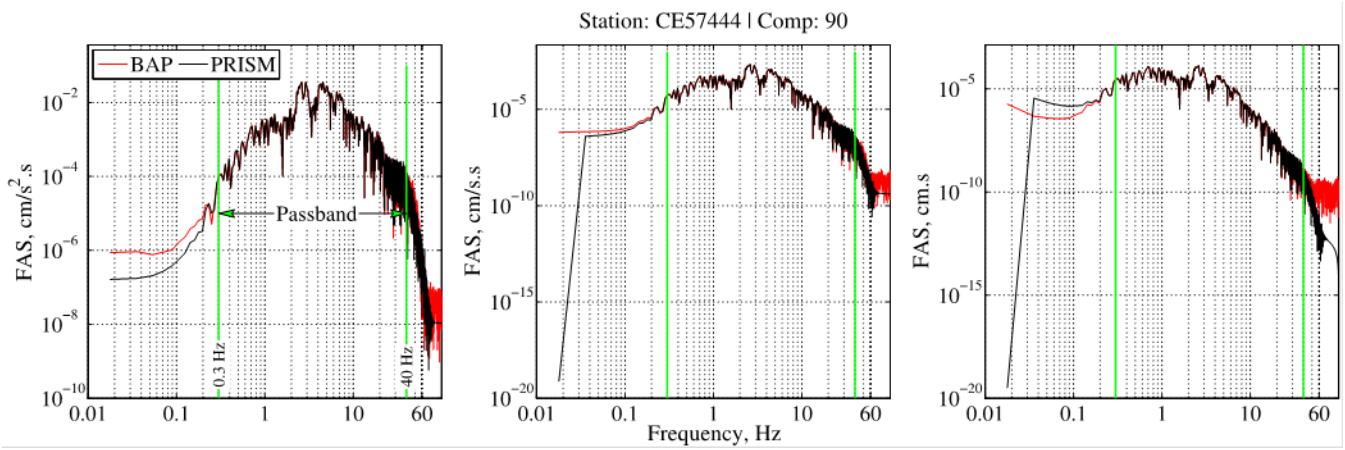


Figure 16. Graphs showing Fourier amplitude spectra (FAS) of acceleration, velocity, and displacement time series obtained by using Processing and Review Interface for Strong Motion data (PRISM) and Basic Strong-Motion Accelerogram Processing Software (BAP) to process component (comp) HNE of station CE.57444 record from the 2015 *M*3.6 San Ramon earthquake in California. The record processed in PRISM (black lines) overlies the BAP version (red lines). Vertical green lines show corners of bandpass filter. cm·s, centimeters second; cm/s·s, centimeters per second second; cm/s²·s, centimeters per second squared second; Hz, hertz.

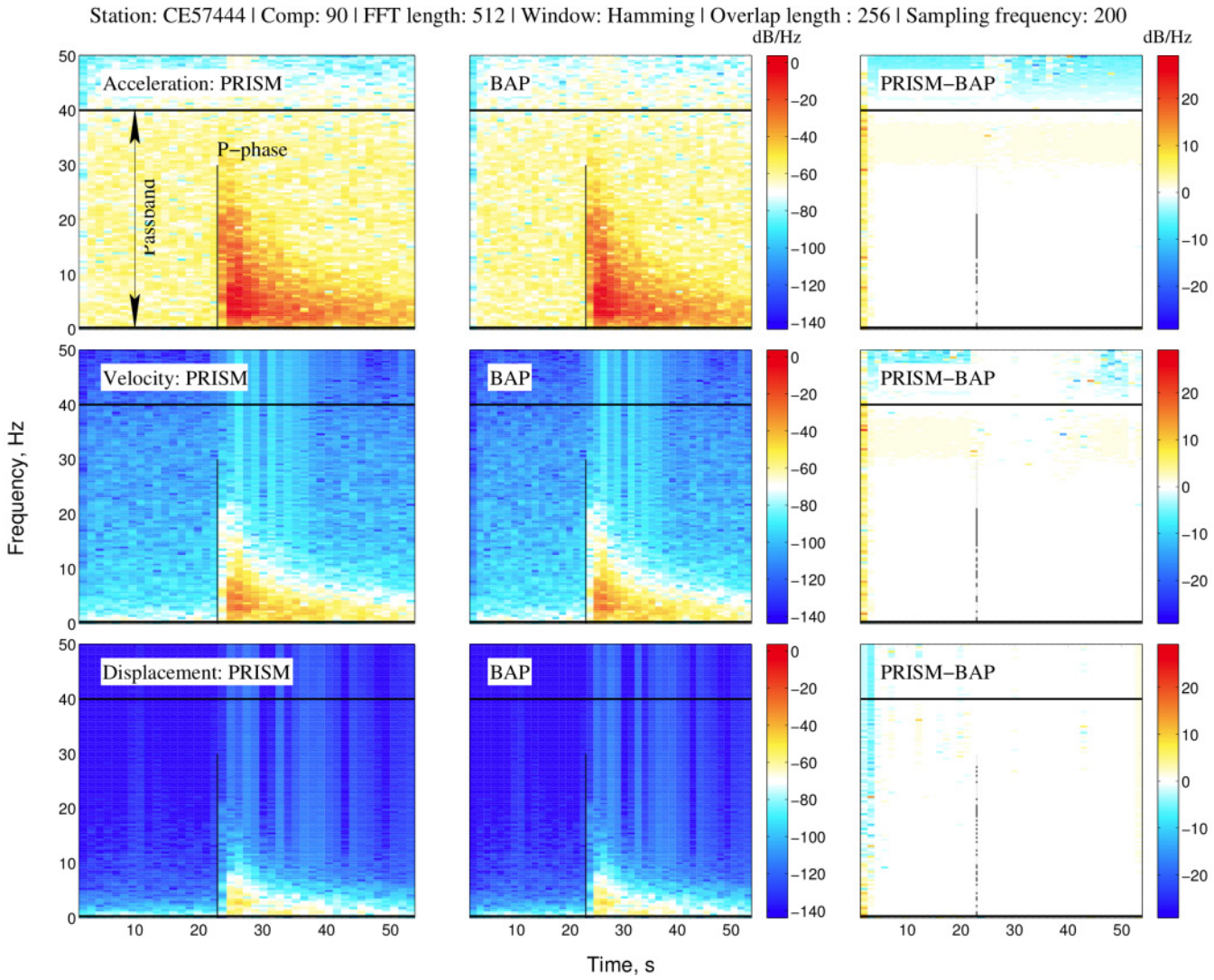


Figure 17. Spectrograms of acceleration, velocity, and displacement time series obtained by using Processing and Review Interface for Strong Motion data (PRISM) and Basic Strong-Motion Accelerogram Processing Software (BAP) to process component (comp) HNE of station CE.57444 record from the 2015 *M*3.6 San Ramon earthquake in California. Differences in power spectral densities are plotted in right column. Color indicates strength of time series at a range of frequencies over time. Horizontal lines show corners of bandpass filter; vertical black lines denote P-phase arrival time. dB/Hz, decibel per hertz; FFT, fast Fourier transform; Hz, hertz; s, seconds.

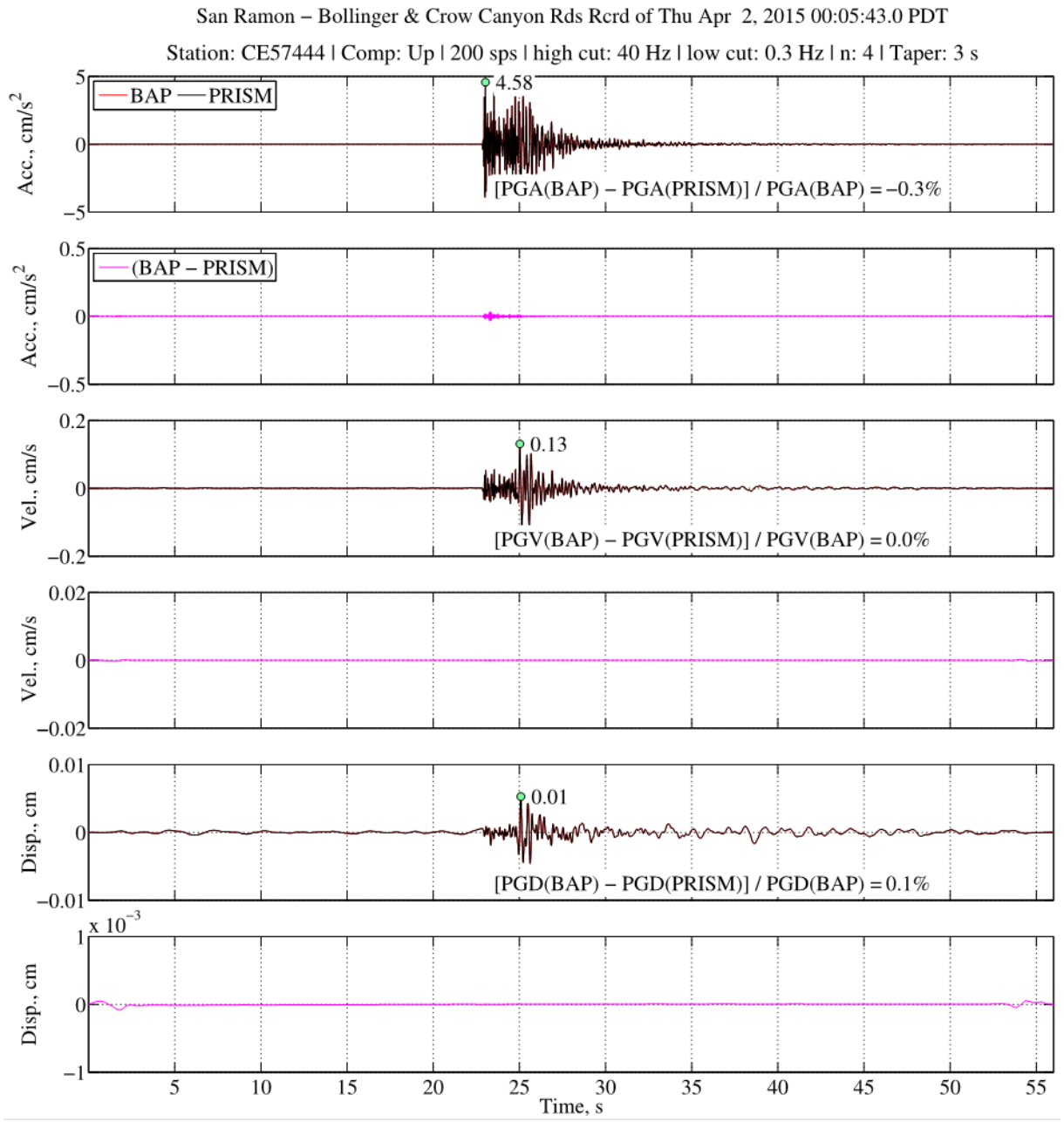


Figure 18. Graphs comparing acceleration (acc.), velocity (vel.), and displacement (disp.) time series obtained by using Processing and Review Interface for Strong Motion data (PRISM) and Basic Strong-Motion Accelerogram Processing Software (BAP) to process component (comp) HNZ of station CE.57444 record from the 2015 *M*3.6 San Ramon earthquake in California. The record processed in PRISM (black lines) overlies the BAP version (red lines). Percent differences in peak ground acceleration (PGA), peak ground velocity (PGV), and peak ground displacement (PGD) are shown. Note differences in scaling used to enhance visibility for each pair of physical motion plots. Green circles indicate peak values of PRISM processing. cm, centimeters; cm/s, centimeters per second; cm/s$^2$, centimeters per second squared; Hz, hertz; n, Butterworth filter order; PDT, Pacific daylight time; s, seconds; sps, samples-per-second.

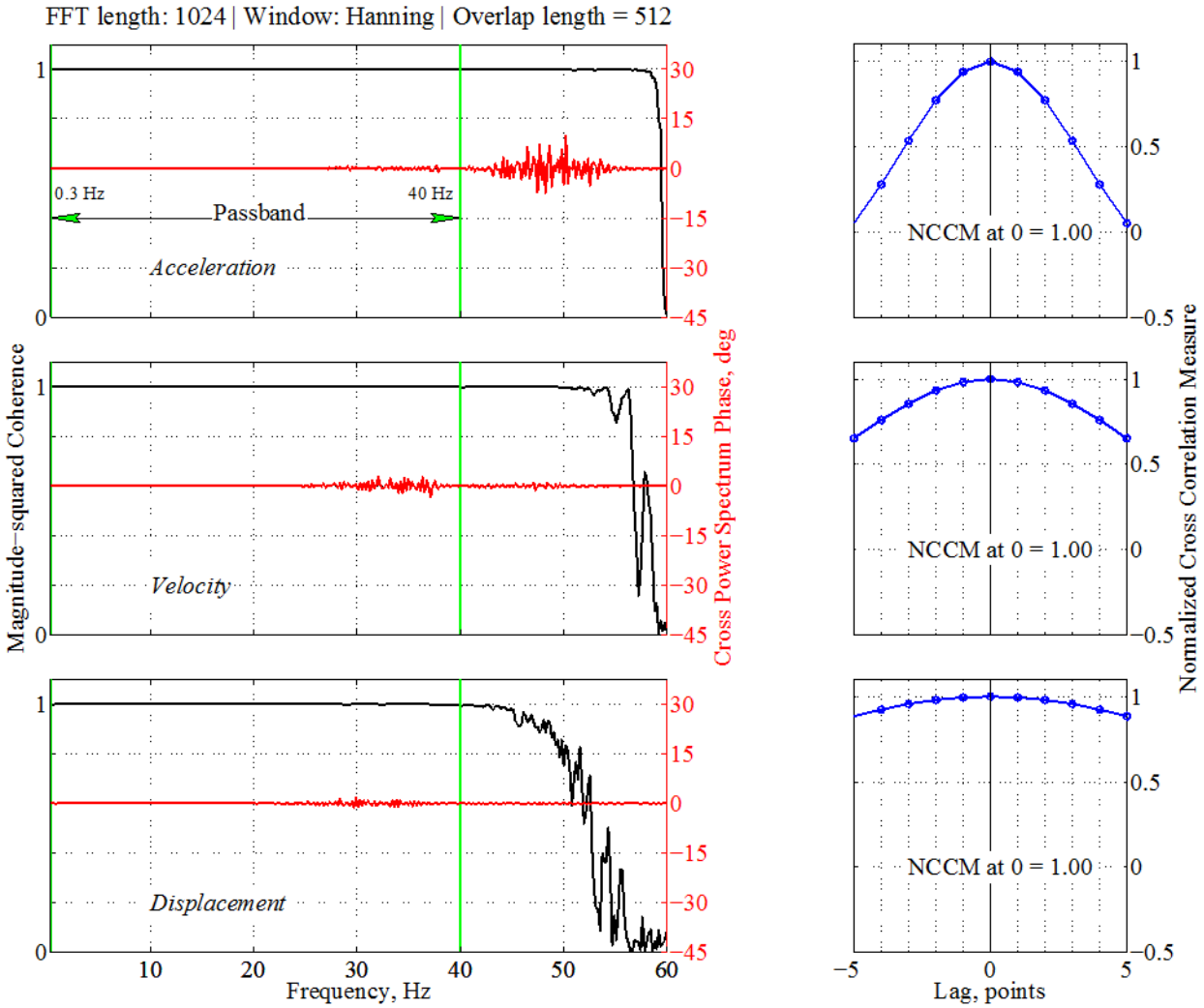


Figure 19. Graphs showing magnitude-squared coherence, cross spectrum phase in degrees, and normalized cross-correlation measure (NCCM) used to measure frequency and time domain similarities between acceleration, velocity, and displacement time series processed by Processing and Review Interface for Strong Motion data (PRISM) and Basic Strong-Motion Accelerogram Processing Software (BAP). Vertical green lines show corners of bandpass filter. Data correspond to component HNZ of station CE.57444 record from the 2015 *M*3.6 San Ramon earthquake in California. FFT, fast Fourier transform; Hz, hertz.

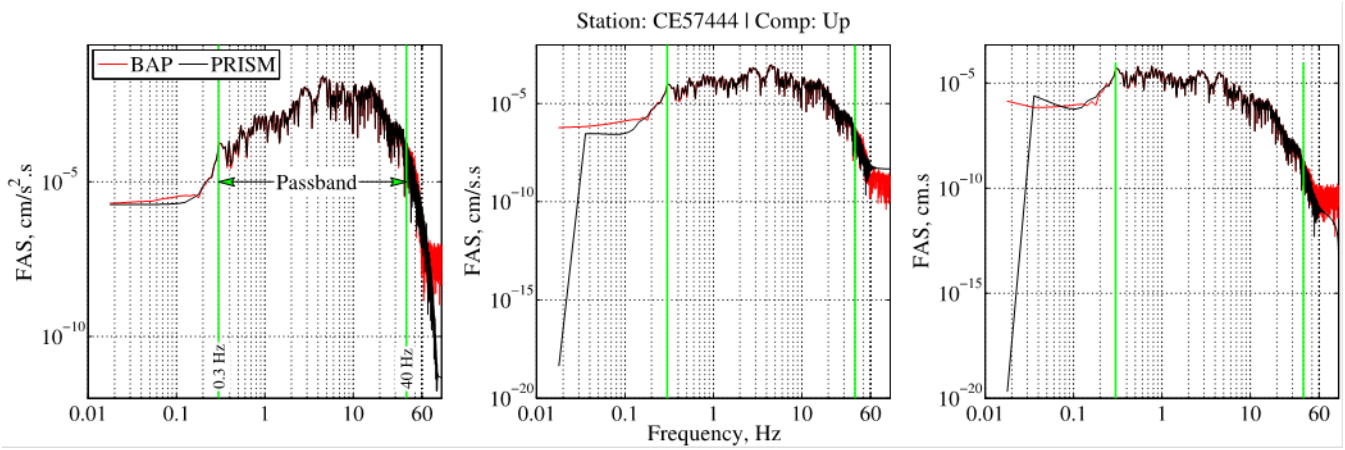


Figure 20. Graphs showing Fourier amplitude spectra (FAS) of acceleration, velocity, and displacement time series obtained by using Processing and Review Interface for Strong Motion data (PRISM) and Basic Strong-Motion Accelerogram Processing Software (BAP) to process component (comp) HNZ of station CE.57444 record from the 2015 *M*3.6 San Ramon earthquake in California. The record processed in PRISM (black lines) overlies the BAP version (red lines). Vertical green lines show corners of bandpass filter. cm·s, centimeters second; cm/s·s, centimeters per second second; cm/s²·s, centimeters per second squared second; Hz, hertz.

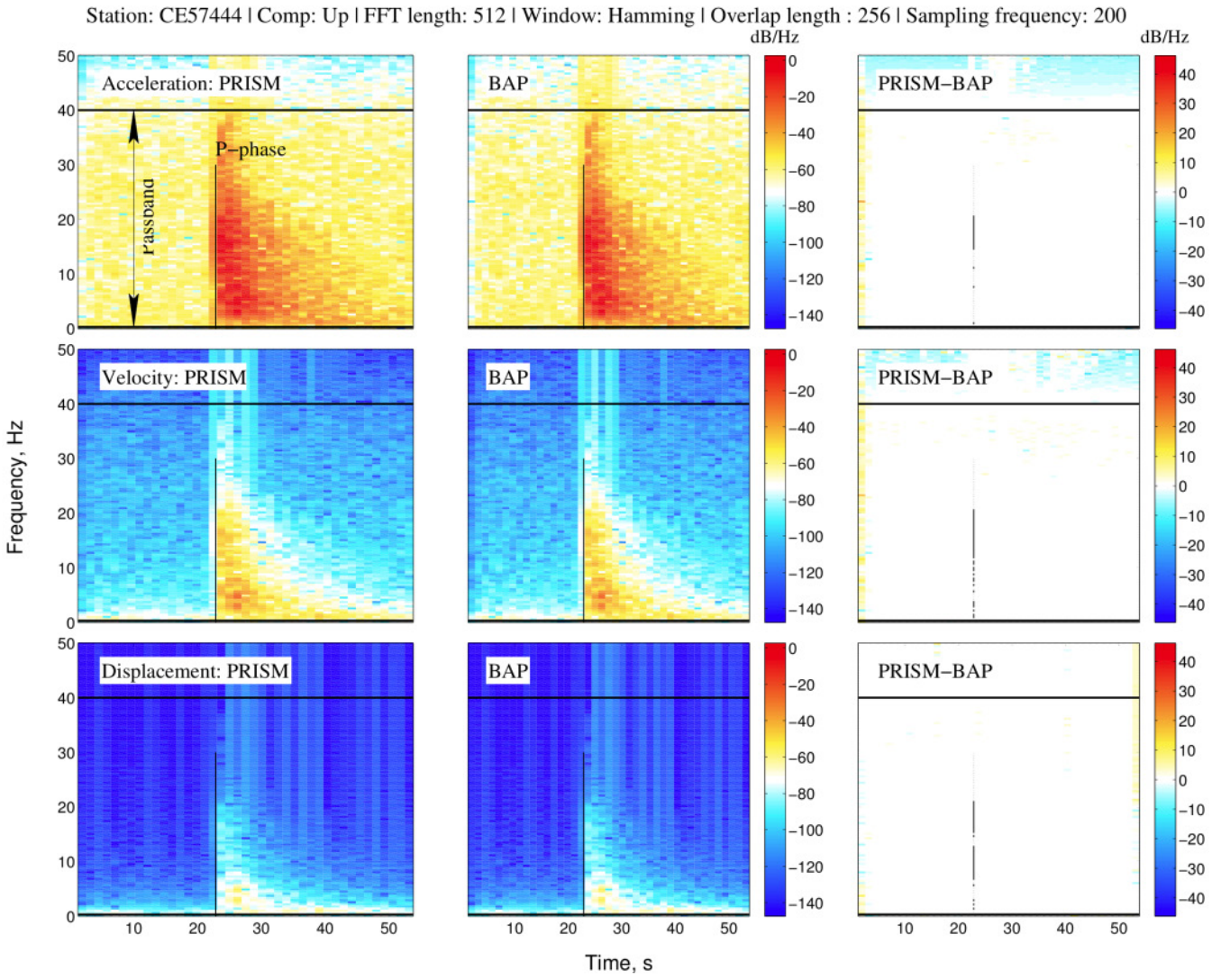


Figure 21. Spectrograms of acceleration, velocity, and displacement time series obtained by using Processing and Review Interface for Strong Motion data (PRISM) and Basic Strong-Motion Accelerogram Processing Software (BAP) to process component (comp) HNZ of station CE.57444 record from the 2015 *M*3.6 San Ramon earthquake in California. Differences in power spectral densities are plotted in right column. Color indicates strength of time series at a range of frequencies over time. Horizontal lines show corners of bandpass filter; vertical black lines denote P-phase arrival time. dB/Hz, decibel per hertz; FFT, fast Fourier transform; Hz, hertz; s, seconds.

In figures 22 through 33, analogous comparisons are presented between PRISM and BAP processing for three components of the CE.68150 record of Napa College. The maximum observed discrepancy in peak values is 0.1 percent for the acceleration and displacement waveforms of component HNZ. For other components, there is no difference in PGV and PGD, and the largest difference in PGA is 0.1 percent. The metrics used to quantify signal similarities indicate that the PRISM and BAP processed waveforms are in coherence; zero-slope of phase angles and NCCM results manifest that there are no time delays. FAS plots and spectrograms match well within the bandpass corner frequencies. The differences in FAS plots for displacement waveforms of components HNN and HNE at high frequencies result from very small variations between the two signals, but these differences have very low energy. This is shown in figure 34, where the narrowband filtered (between 15 and 40 Hz) displacement waveforms are compared for components HNN and HNE of the record. The differences in time domain are less than $5\times10^{-4}$ cm. Comparisons of spectrograms (figs. 25 and 29) show near zero energy within the passband consistent with the time series comparisons. In these figures, the energy jump after 80 s indicates the aftershock.

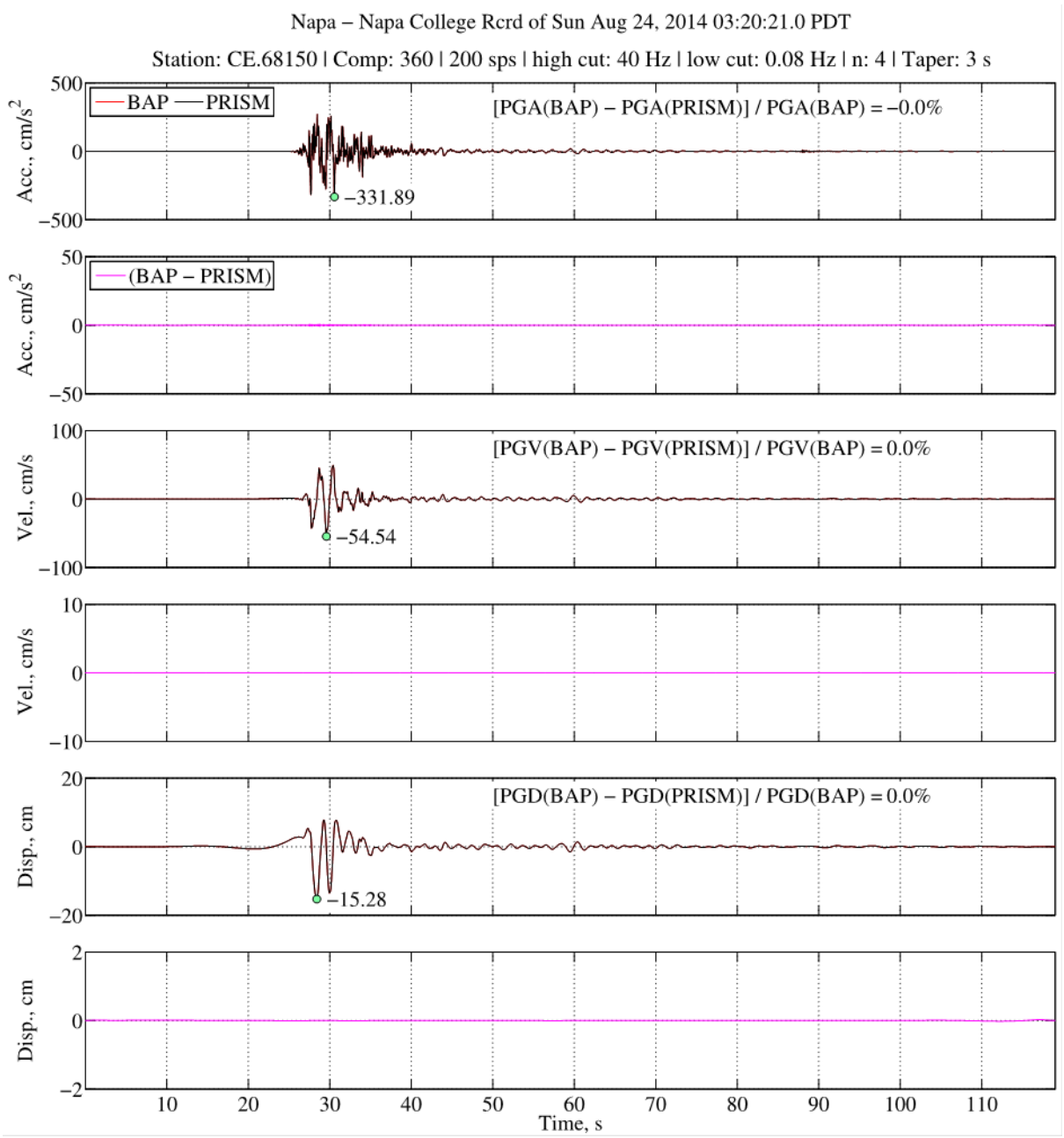


Figure 22. Graphs comparing acceleration (acc.), velocity (vel.), and displacement (disp.) time series obtained by using Processing and Review Interface for Strong Motion data (PRISM) and Basic Strong-Motion Accelerogram Processing Software (BAP) to process component (comp) HNN of station CE.68150 record from the 2014 *M*6.0 South Napa earthquake in California. The record processed in PRISM (black lines) overlies the BAP version (red lines). Percent differences in peak ground acceleration (PGA), peak ground velocity (PGV), and peak ground displacement (PGD) are shown. Note differences in scaling used to enhance visibility for each pair of physical motion plots. Green circles indicate peak values of PRISM processing. cm, centimeters; cm/s, centimeters per second; cm/s$^2$, centimeters per second squared; Hz, hertz; n, Butterworth filter order; PDT, Pacific daylight time; s, seconds; sps, samples-per-second.

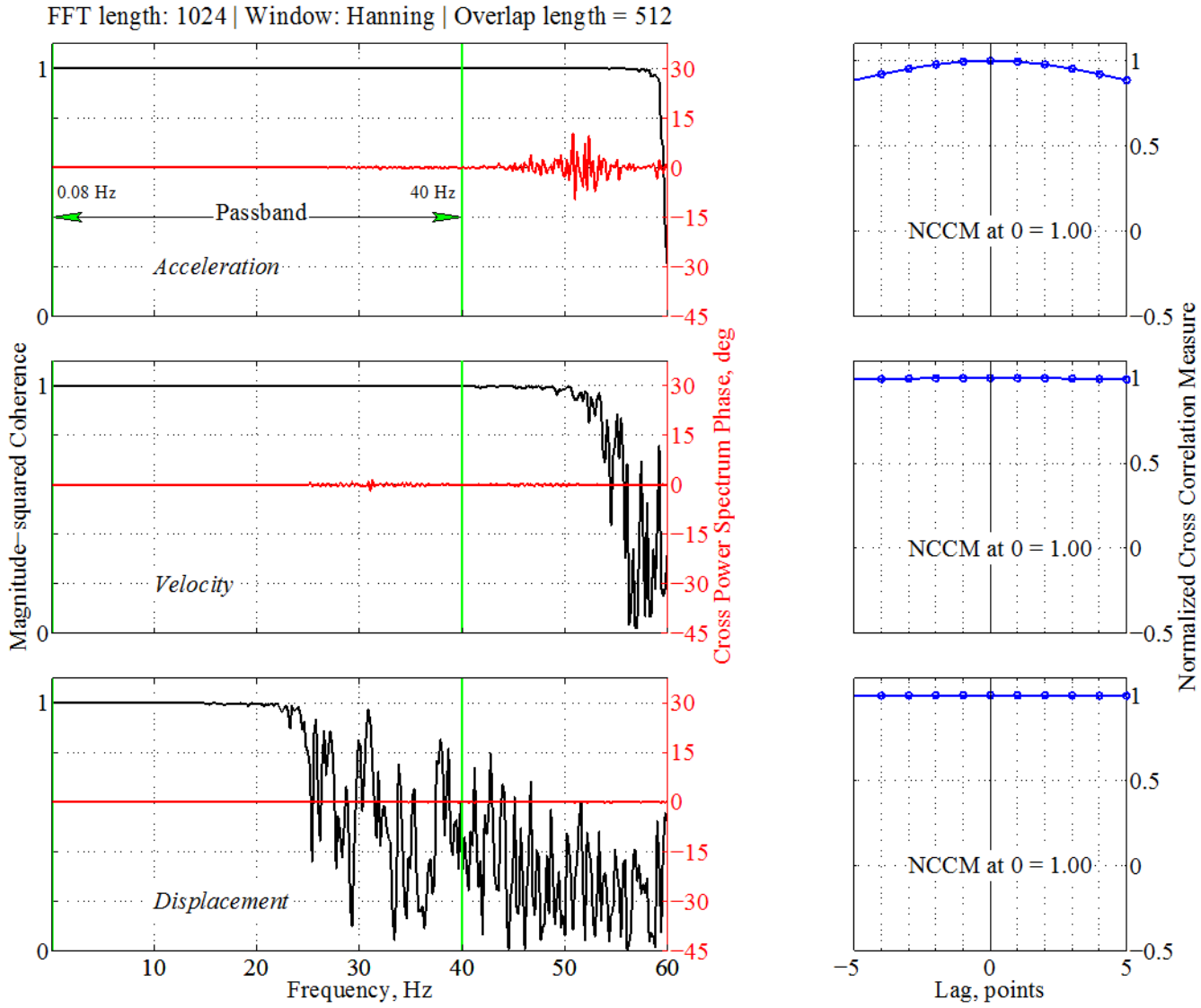


Figure 23. Graphs showing magnitude-squared coherence, cross spectrum phase in degrees, and normalized cross-correlation measure (NCCM) used to measure frequency and time domain similarities between acceleration, velocity, and displacement time series processed by Processing and Review Interface for Strong Motion data (PRISM) and Basic Strong-Motion Accelerogram Processing Software (BAP). Vertical green lines show corners of bandpass filter. Data correspond to component HNN of station CE.68150 record from the 2014 *M*6.0 South Napa earthquake in California. FFT, fast Fourier transform; Hz, hertz.

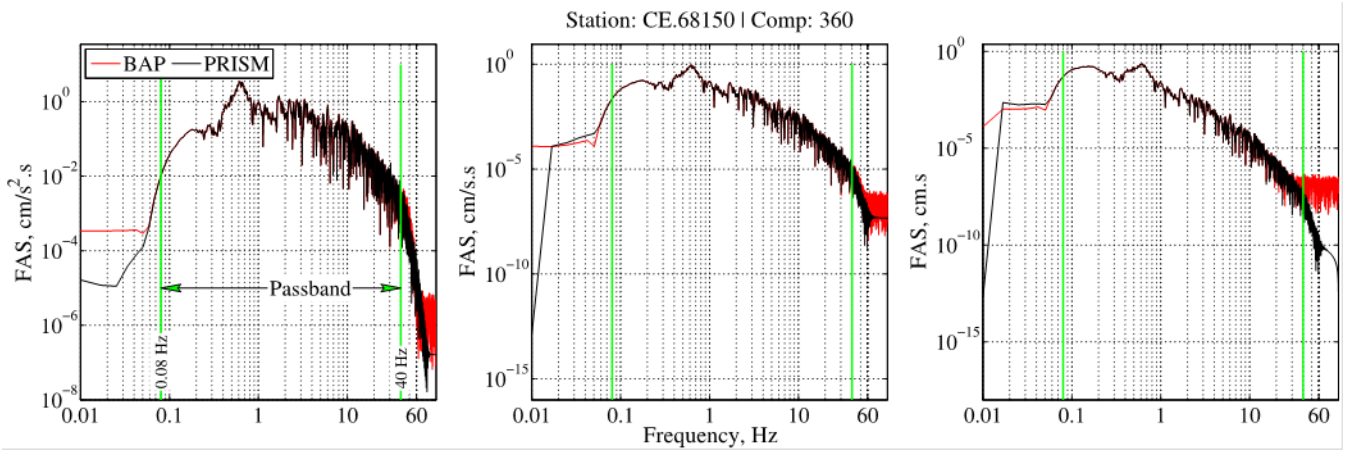


Figure 24. Graphs showing Fourier amplitude spectra (FAS) of acceleration, velocity, and displacement time series obtained by using Processing and Review Interface for Strong Motion data (PRISM) and Basic Strong-Motion Accelerogram Processing Software (BAP) to process component (comp) HNN of station CE.68150 record from the 2014 *M*6.0 South Napa earthquake in California. The record processed in PRISM (black lines) overlies the BAP version (red lines). Vertical green lines show corners of bandpass filter. cm·s, centimeters second; cm/s·s, centimeters per second second; cm/s²·s, centimeters per second squared second; Hz, hertz.

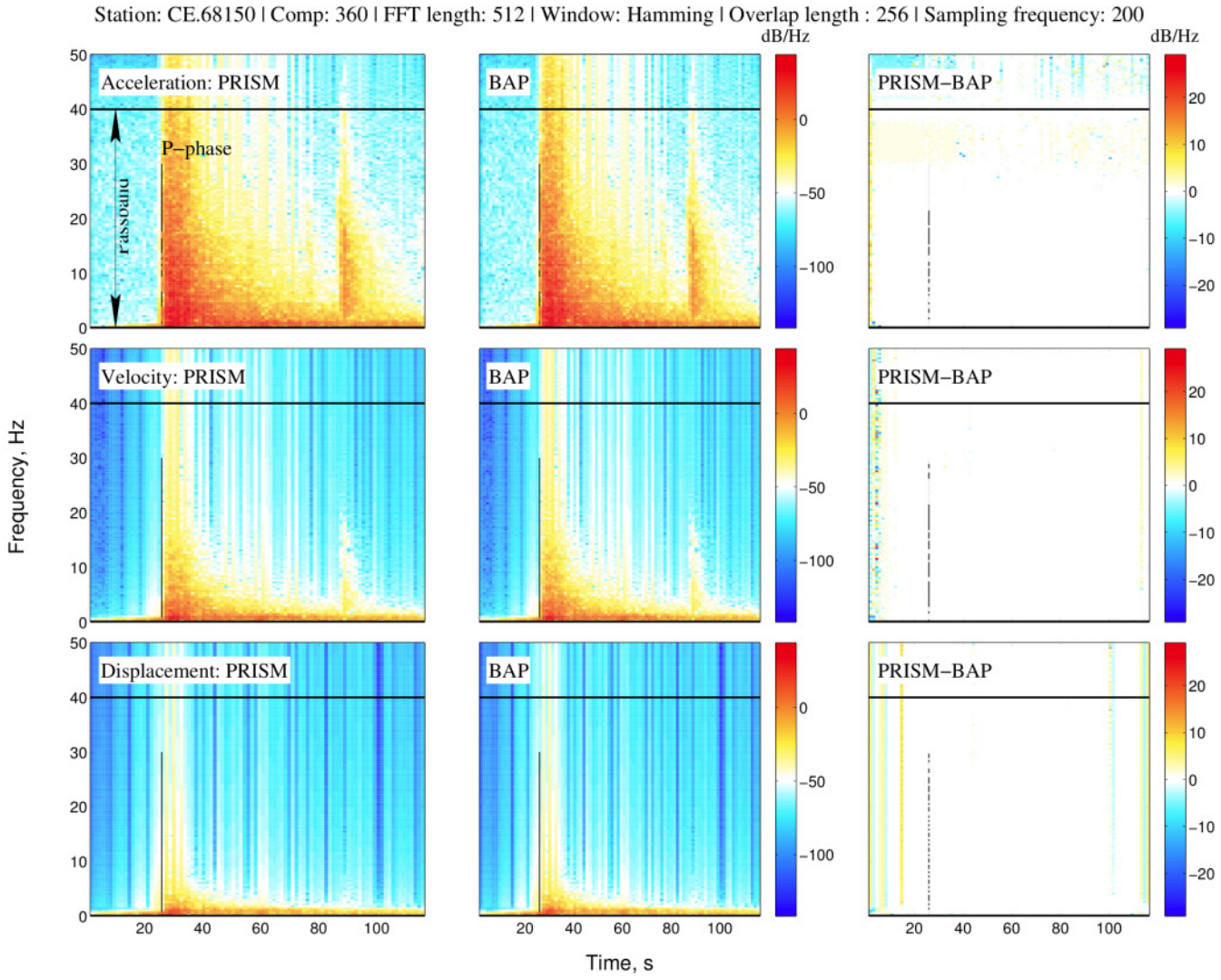


Figure 25. Spectrograms of acceleration, velocity, and displacement time series obtained by using Processing and Review Interface for Strong Motion data (PRISM) and Basic Strong-Motion Accelerogram Processing Software (BAP) to process component (comp) HNN of station CE.68150 record from the 2014 *M*6.0 South Napa earthquake in California. Differences in power spectral densities are plotted in right column. Color indicates strength of time series at a range of frequencies over time. Horizontal lines show corners of bandpass filter; vertical black lines denote P-phase arrival time. dB/Hz, decibel per hertz; FFT, fast Fourier transform; Hz, hertz; s, seconds.

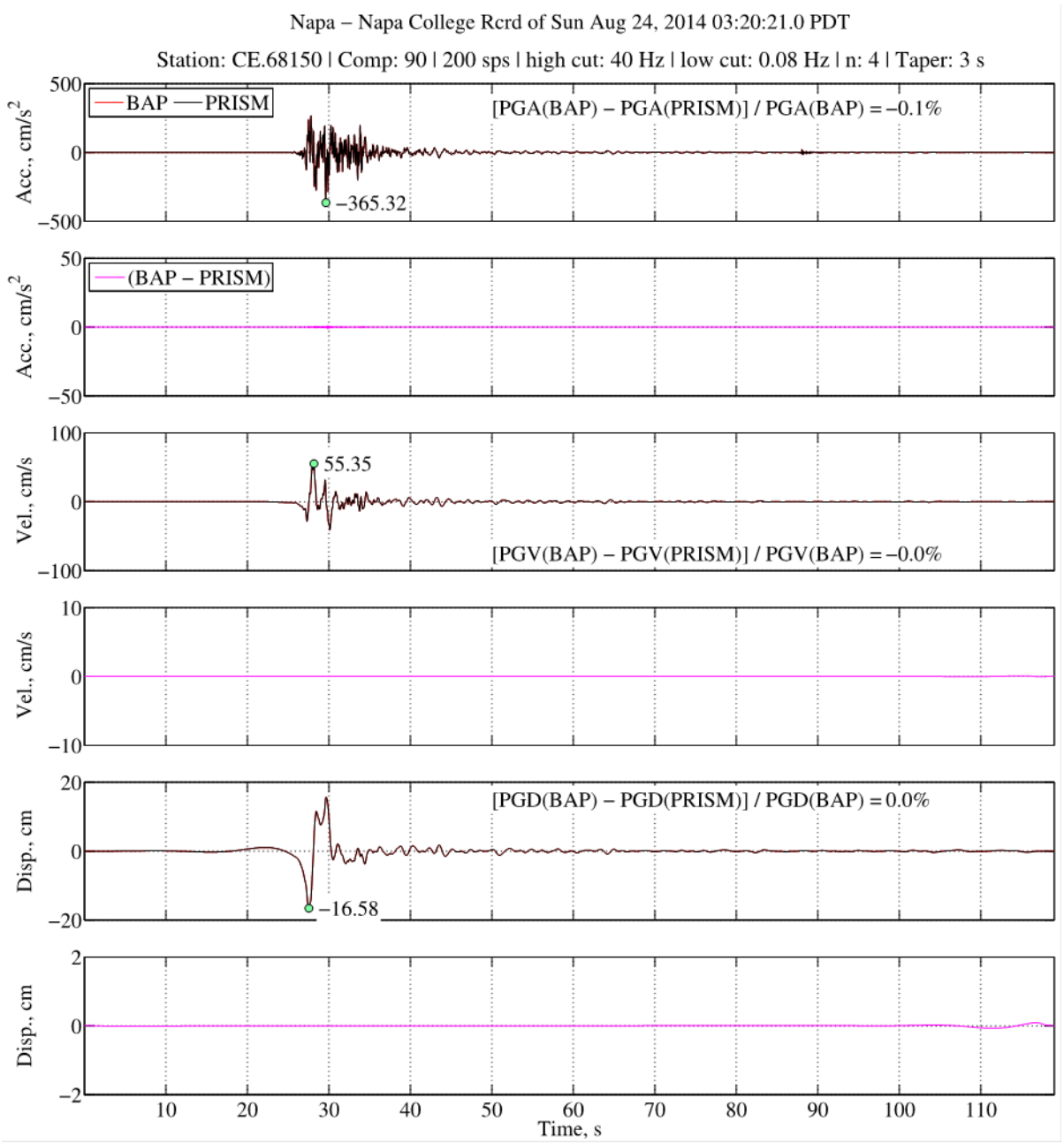


Figure 26. Graphs comparing acceleration (acc.), velocity (vel.), and displacement (disp.) time series obtained by using Processing and Review Interface for Strong Motion data (PRISM) and Basic Strong-Motion Accelerogram Processing Software (BAP) to process component (comp) HNE of station CE.68150 record from the 2014 *M*6.0 South Napa earthquake in California. The record processed in PRISM (black lines) overlies the BAP version (red lines); percent differences in peak ground acceleration (PGA), peak ground velocity (PGV), and peak ground displacement (PGD) are shown. Note differences in scaling used to enhance visibility for each pair of physical motion plots. Green circles indicate peak values of PRISM processing. cm, centimeter; cm/s, centimeters per second; cm/s$^2$, centimeters per second squared; Hz, hertz; n, Butterworth filter order; PDT, Pacific daylight time; s, seconds; sps, samples-per-second.

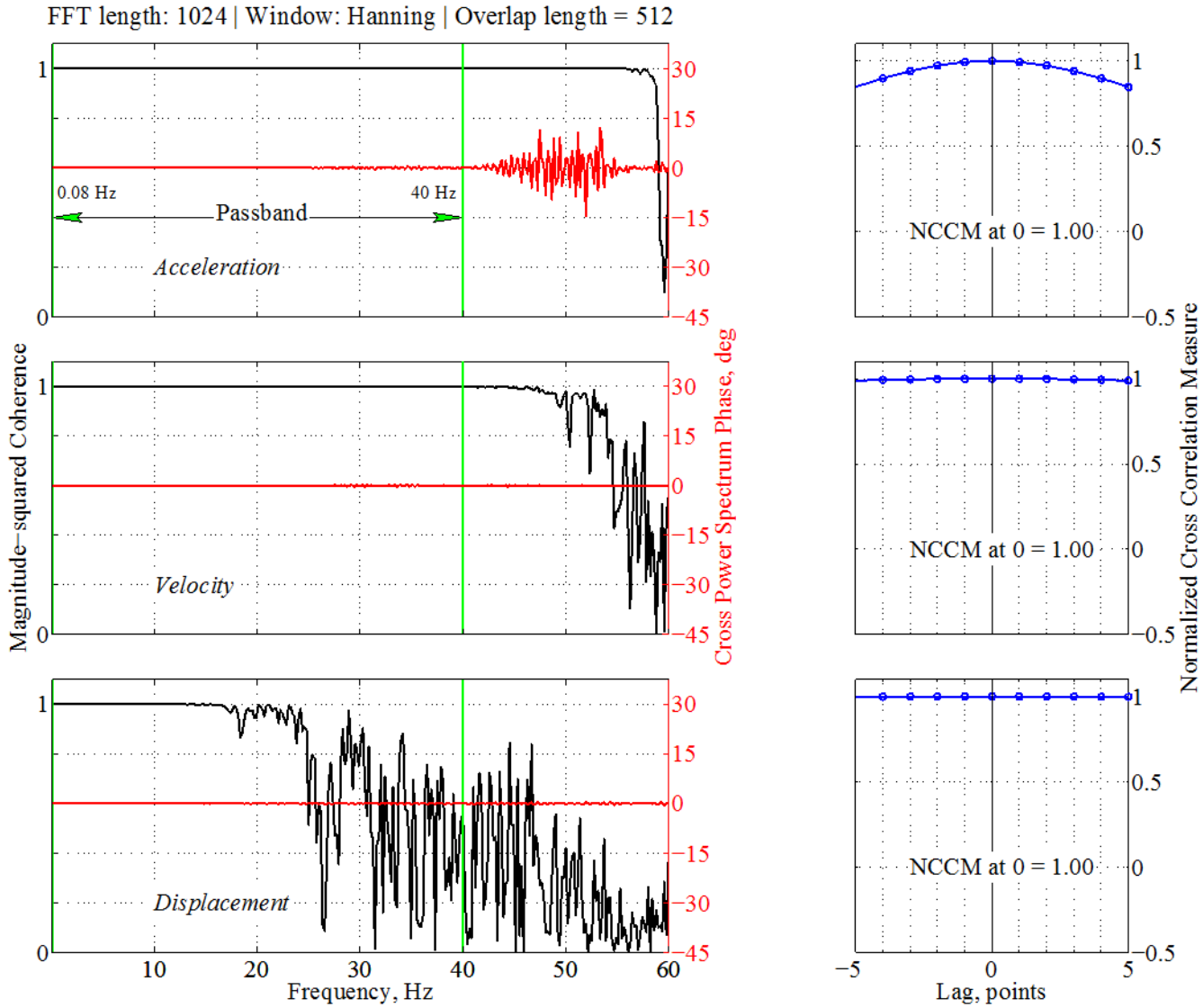


Figure 27. Graphs showing magnitude-squared coherence, cross spectrum phase in degrees, and normalized cross-correlation measure (NCCM) used to measure frequency and time domain similarities between acceleration, velocity, and displacement time series processed by Processing and Review Interface for Strong Motion data (PRISM) and Basic Strong-Motion Accelerogram Processing Software (BAP). Vertical green lines show corners of bandpass filter. Data correspond to component HNE of station CE.68150 record from the 2014 *M*6.0 South Napa earthquake in California. FFT, fast Fourier transform; Hz, hertz.

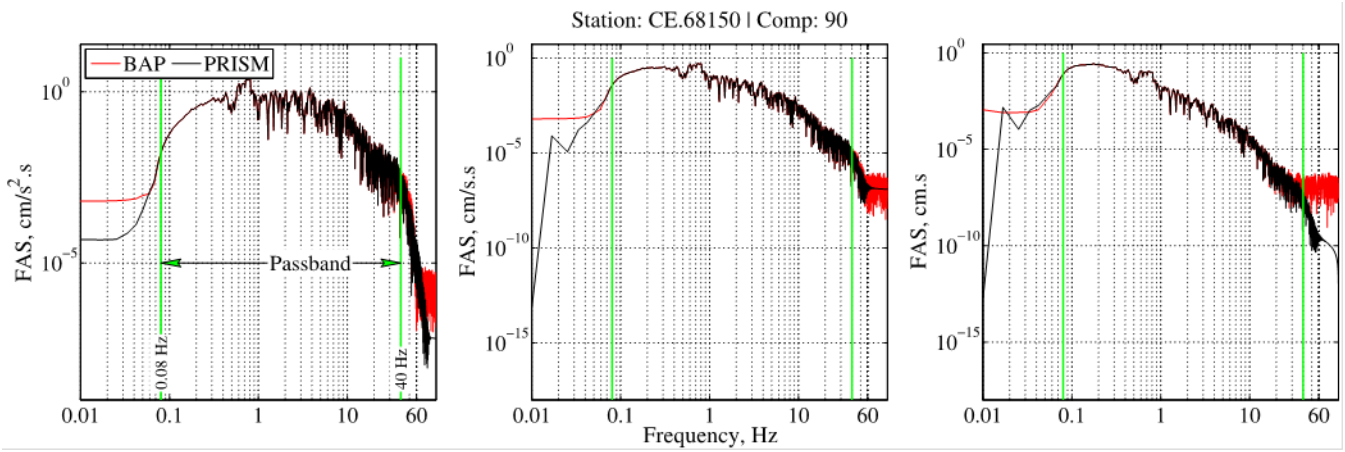


Figure 28. Graphs showing Fourier amplitude spectra (FAS) of acceleration, velocity, and displacement time series obtained by using Processing and Review Interface for Strong Motion data (PRISM) and Basic Strong-Motion Accelerogram Processing Software (BAP) to process component (comp) HNE of station CE.68150 record from the 2014 *M*6.0 South Napa earthquake in California. The record processed in PRISM (black lines) overlies the BAP version (red lines). Vertical green lines show corners of bandpass filter. cm·s, centimeters second; cm/s·s, centimeters per second second; cm/s²·s, centimeters per second squared second; Hz, hertz.

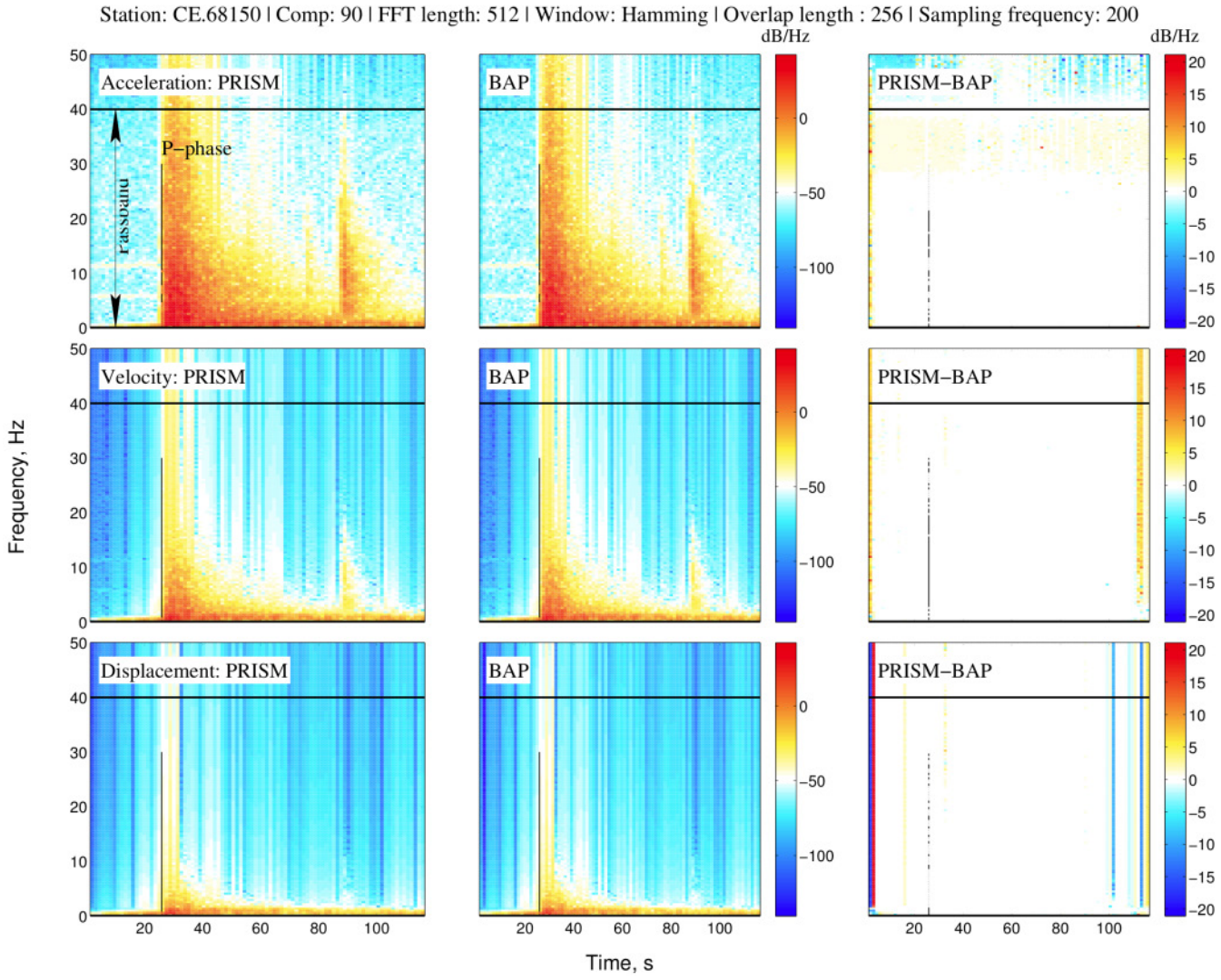


Figure 29. Spectrograms of acceleration, velocity, and displacement time series obtained by using Processing and Review Interface for Strong Motion data (PRISM) and Basic Strong-Motion Accelerogram Processing Software (BAP) to process component (comp) HNE of station CE.68150 record from the 2014 *M*6.0 South Napa earthquake in California. Differences in power spectral densities are plotted in right column. Color indicates strength of time series at a range of frequencies over time. Horizontal lines show corners of bandpass filter; vertical black lines denote P-phase arrival time. dB/Hz, decibel per hertz; FFT, fast Fourier transform; Hz, hertz; s, seconds.

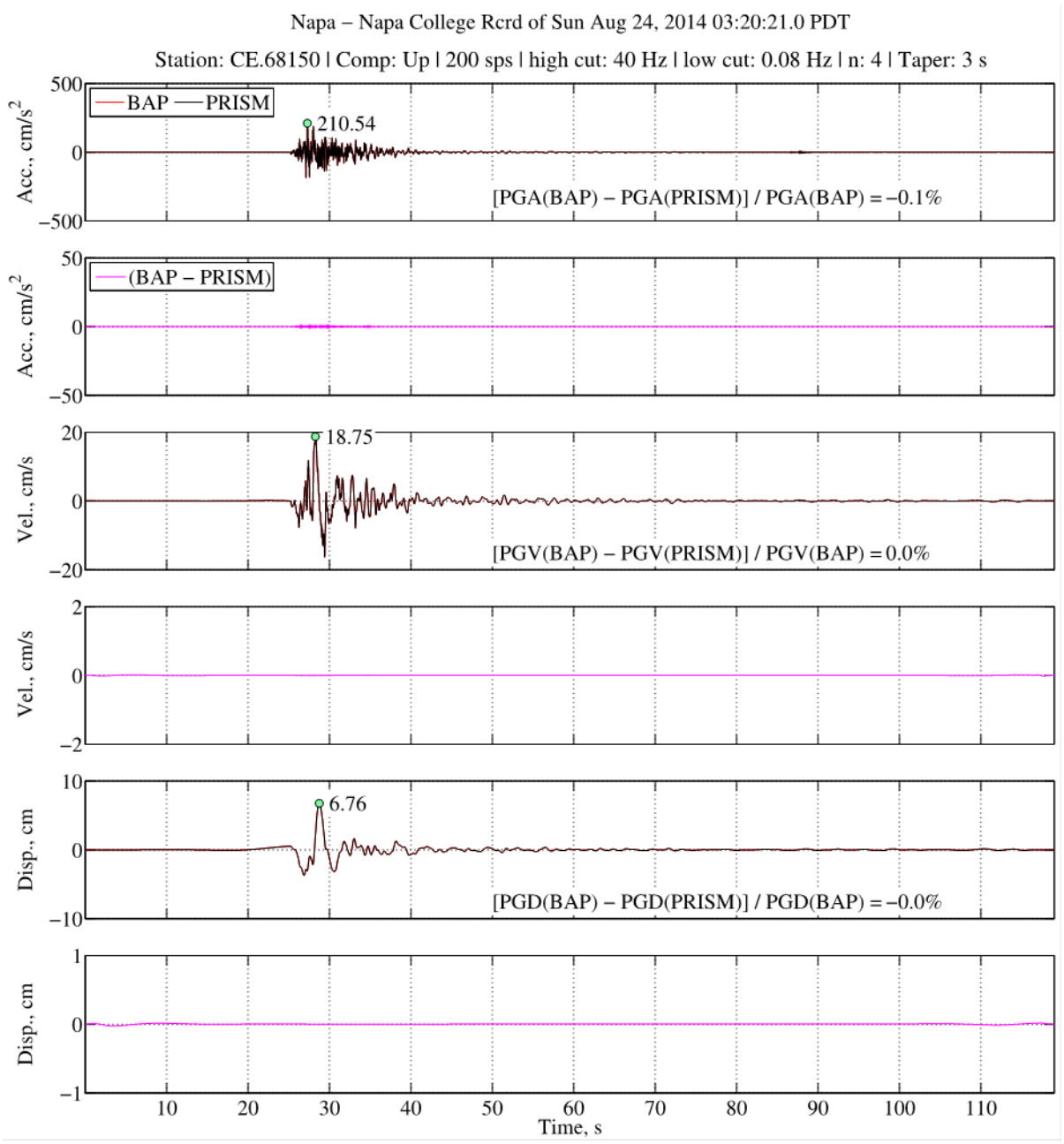


Figure 30. Graphs comparing acceleration (acc.), velocity (vel.), and displacement (disp.) time series obtained by using Processing and Review Interface for Strong Motion data (PRISM) and Basic Strong-Motion Accelerogram Processing Software (BAP) to process component (comp) HNZ of station CE.68150 record from the 2014 *M*6.0 South Napa earthquake in California. The record processed in PRISM (black lines) overlies the BAP version (red lines). Percent differences in peak ground acceleration (PGA), peak ground velocity (PGV), and peak ground displacement (PGD) are shown. Note differences in scaling used to enhance visibility for each pair of physical motion plots. Green circles indicate peak values of PRISM processing. cm, centimeters; cm/s, centimeters per second; cm/s$^2$, centimeters per second squared; Hz, hertz; n, Butterworth filter order; PDT, Pacific daylight time; s, seconds; sps, samples-per-second. Note difference in y-axis scale.

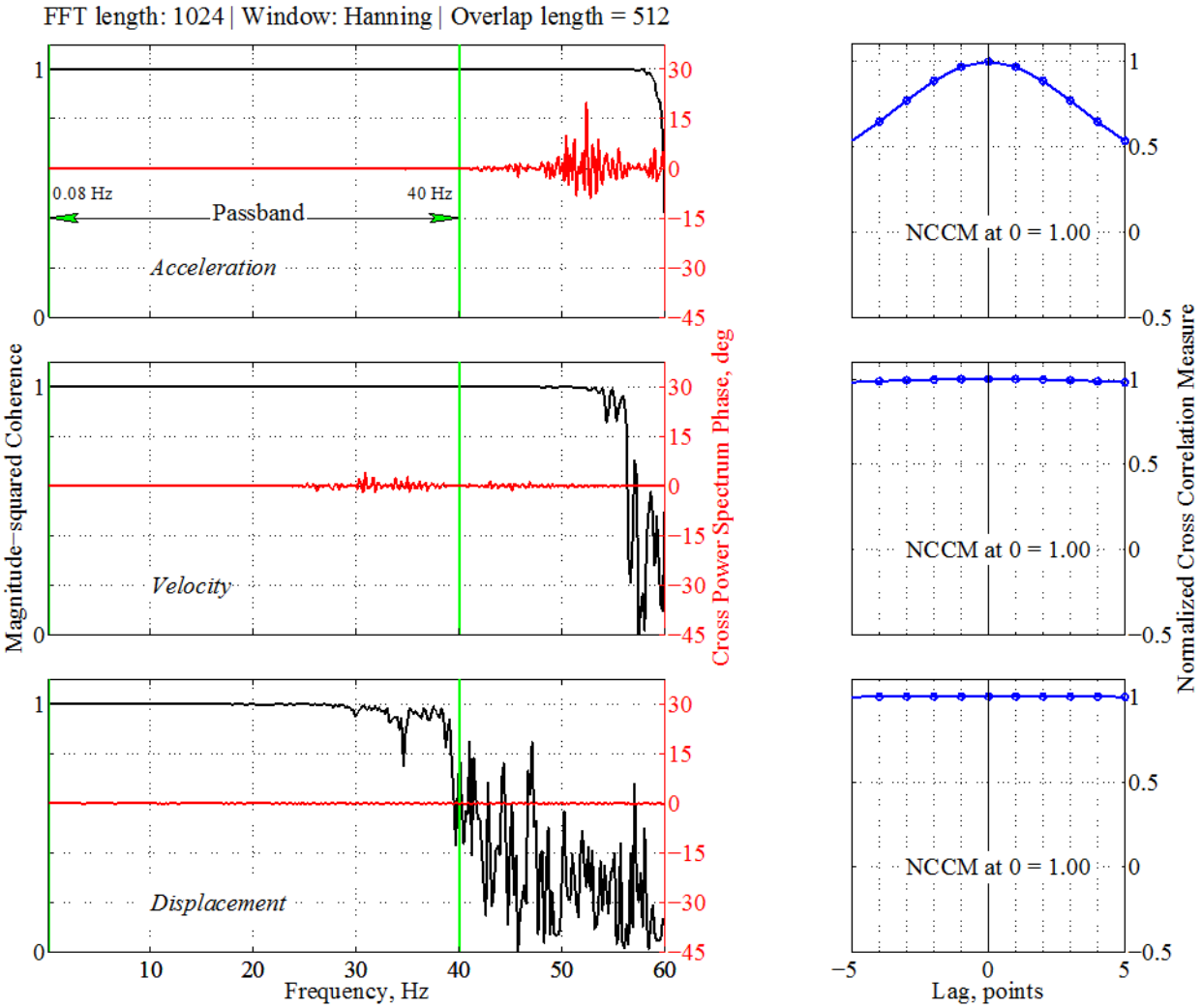


Figure 31. Graphs showing magnitude-squared coherence, cross spectrum phase in degrees, and normalized cross-correlation measure (NCCM) used to measure frequency and time domain similarities between acceleration, velocity, and displacement time series processed by Processing and Review Interface for Strong Motion data (PRISM) and Basic Strong-Motion Accelerogram Processing Software (BAP). Vertical green lines show corners of bandpass filter. Data correspond to component HNZ of station CE.68150 record from the 2014 *M*6.0 South Napa earthquake in California. FFT, fast Fourier transform; Hz, hertz.

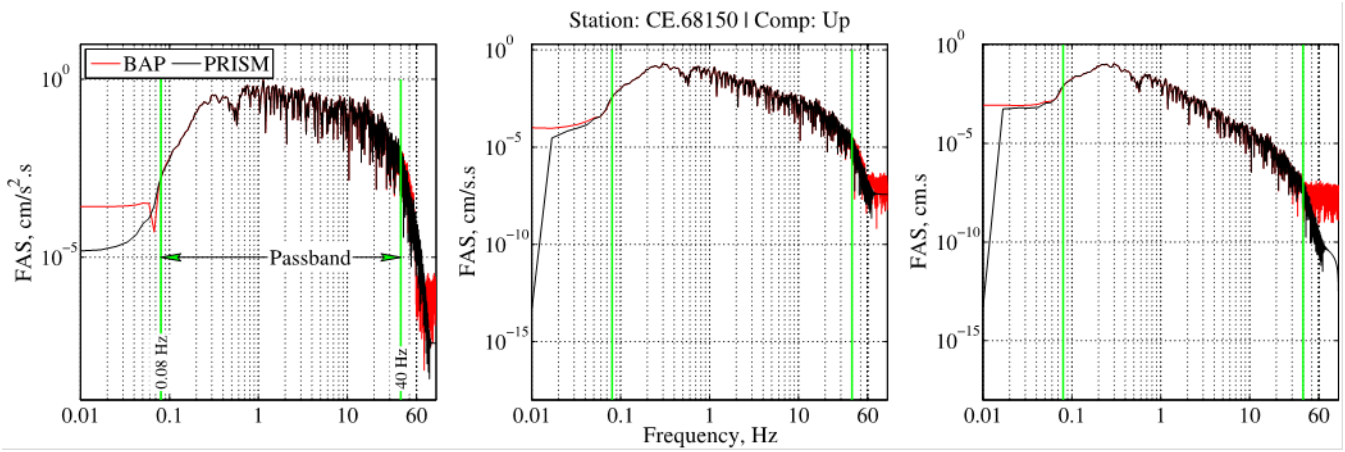


Figure 32. Graphs showing Fourier amplitude spectra (FAS) of acceleration, velocity, and displacement time series obtained by using Processing and Review Interface for Strong Motion data (PRISM) and Basic Strong-Motion Accelerogram Processing Software (BAP) to process component (comp) HNZ of station CE.68150 record from the 2014 *M*6.0 South Napa earthquake in California. The record processed in PRISM (black lines) overlies the BAP version (red lines). Vertical green lines show corners of bandpass filter. cm·s, centimeters second; cm/s·s, centimeters per second second; cm/s$^2$·s, centimeters per second squared second; Hz, hertz.

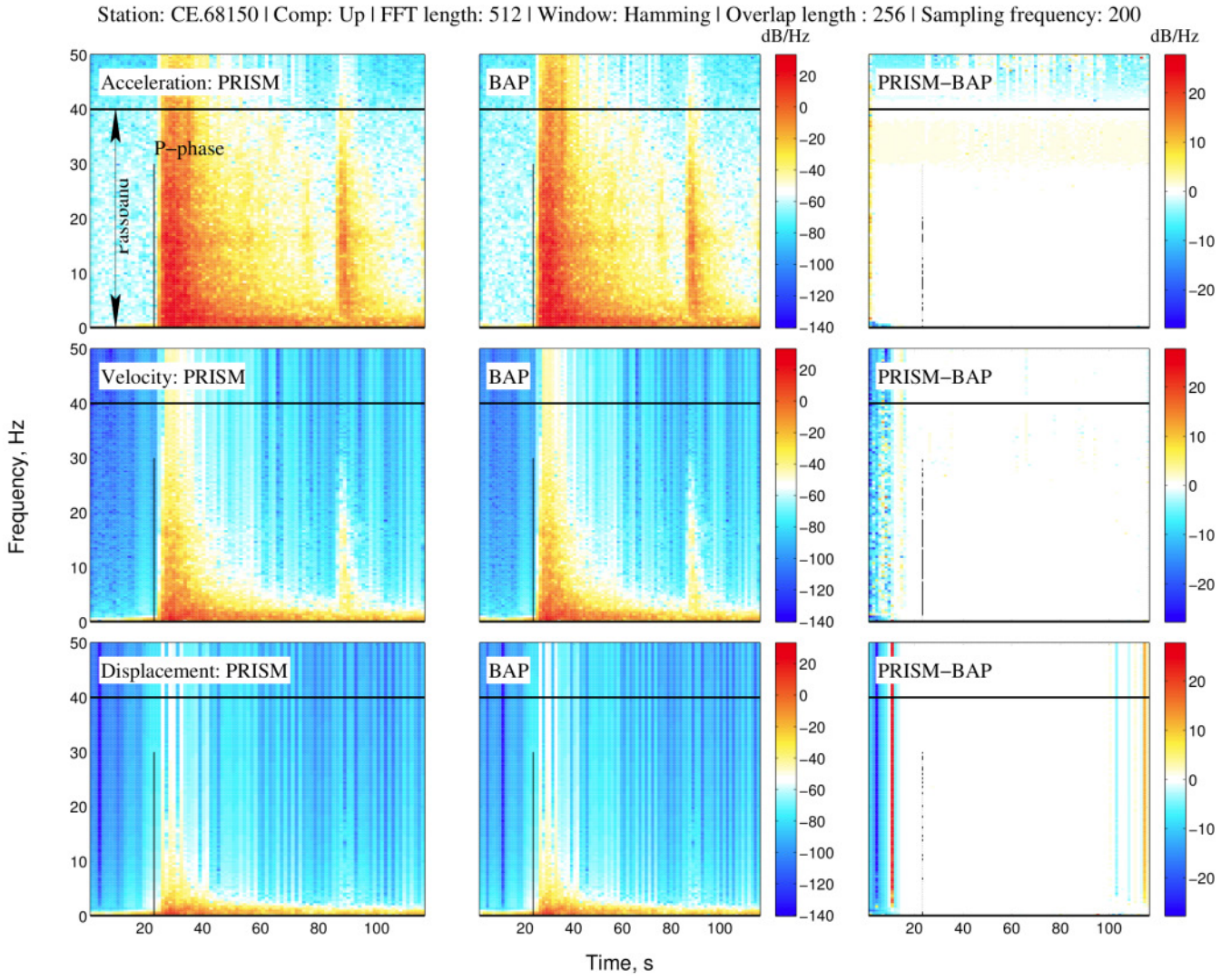


Figure 33. Spectrograms of acceleration, velocity, and displacement time series obtained by using Processing and Review Interface for Strong Motion data (PRISM) and Basic Strong-Motion Accelerogram Processing Software (BAP) to process component (comp) HNZ of station CE.68150 record from the 2014 *M*6.0 South Napa earthquake in California. Differences in power spectral densities are plotted in right column. Color indicates strength of time series at a range of frequencies over time. Horizontal lines show corners of bandpass filter; vertical black lines denote P-phase arrival time. dB/Hz, decibel per hertz; FFT, fast Fourier transform; Hz, hertz; s, seconds.

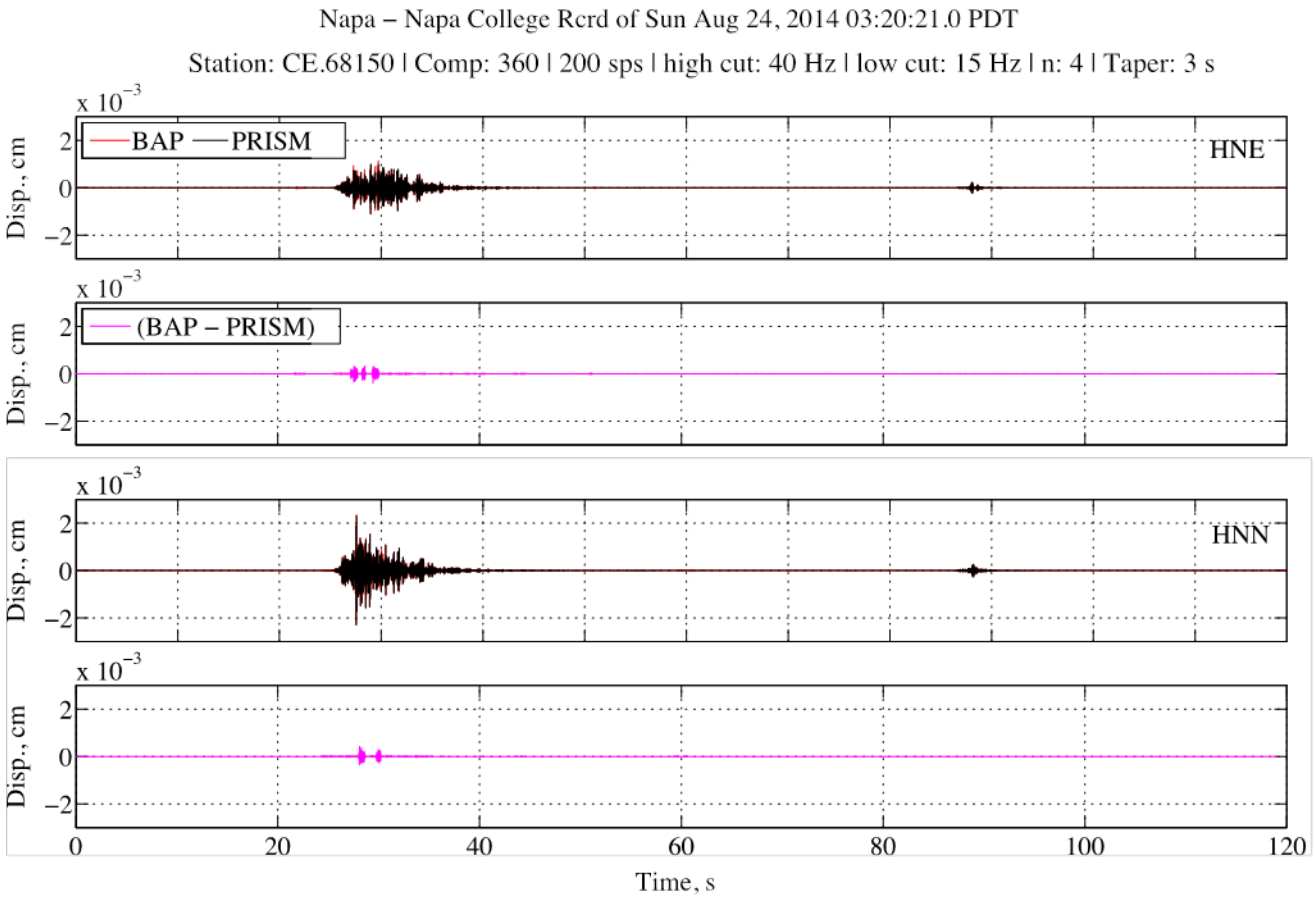


Figure 34. Graphs comparing narrow band (15-40 Hz) filtered displacement (disp.) time series obtained by using Processing and Review Interface for Strong Motion data (PRISM) and Basic Strong-Motion Accelerogram Processing Software (BAP) to process components (comp) HNE and HNN of station CE.68150 record from the 2014 *M*6.0 South Napa earthquake in California. The record processed in PRISM (black lines) overlies the BAP version (red lines); time series differences are shown. Green circles indicate peak values of PRISM processing. cm, centimeters; Hz, hertz; n, Butterworth filter order; PDT, Pacific daylight time; s, seconds; sps, samples-per-second.

## PRISM Versus CSMIP Processing

Whereas the details of record-processing procedures and software platforms may differ for PRISM and for CSMIP, data users can expect minor differences in waveform products within the frequency passband common to both processing procedures. To elucidate this point, we present examples comparing PRISM to CSMIP processing results using two CSMIP records (CE.57444 and CE.68150). Figures 35 through 46 show time series evaluations, signal similarity measures, FAS, and spectrogram comparisons for CE.57444. In general, the resulting waveforms compare well. Peak motion values are within 0.2 percent for horizontal components, and within 4 percent for the vertical component. Small differences at the leading and trailing sections of time series (in particular for displacement) result from different taper implementation. In figure 36, and subsequently in figures 40 and 44, the phases of the complex-valued cross-power spectrum of acceleration, velocity, and displacement all have a linear trend starting at the origin and extending to about 10–20 Hz. This trend indicates a small time delay, which can be estimated by fitting a line between 0 and 10 Hz. The largest delay is computed to be 1.0 millisecond, which is consistent with the normalized cross-correlation measures that show a lag of no more than 1 sample. FAS plots and spectrograms generally match well within the bandpass corner frequencies.

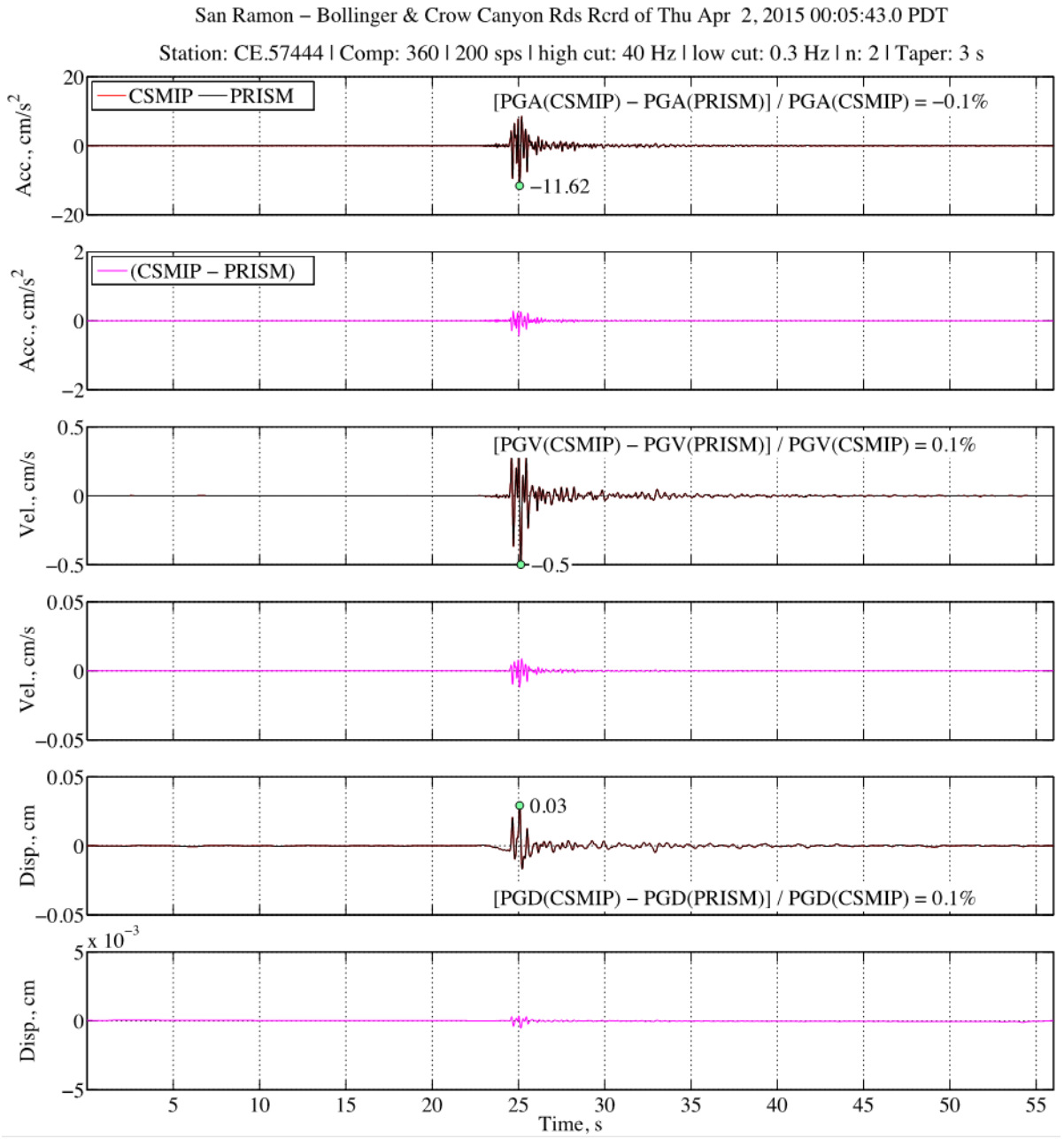


Figure 35. Graphs comparing acceleration (acc.), velocity (vel.), and displacement (disp.) time series obtained by using Processing and Review Interface for Strong Motion data (PRISM) and California Strong Motion Instrumentation Program (CSMIP) to process component (comp) HNN of station CE.57444 record from the 2015 *M*3.6 San Ramon earthquake in California. The record processed in PRISM (black lines) overlies the CSMIP version (red lines). Percent differences in peak ground acceleration (PGA), peak ground velocity (PGV), and peak ground displacement (PGD) are shown. Note differences in scaling used to enhance visibility for each pair of physical motion plots. Green circles indicate peak values of PRISM processing. cm, centimeters; cm/s, centimeters per second; cm/s$^2$, centimeters per second squared; Hz, hertz; n, Butterworth filter order; PDT, Pacific daylight time; s, seconds; sps, samples-per-second.

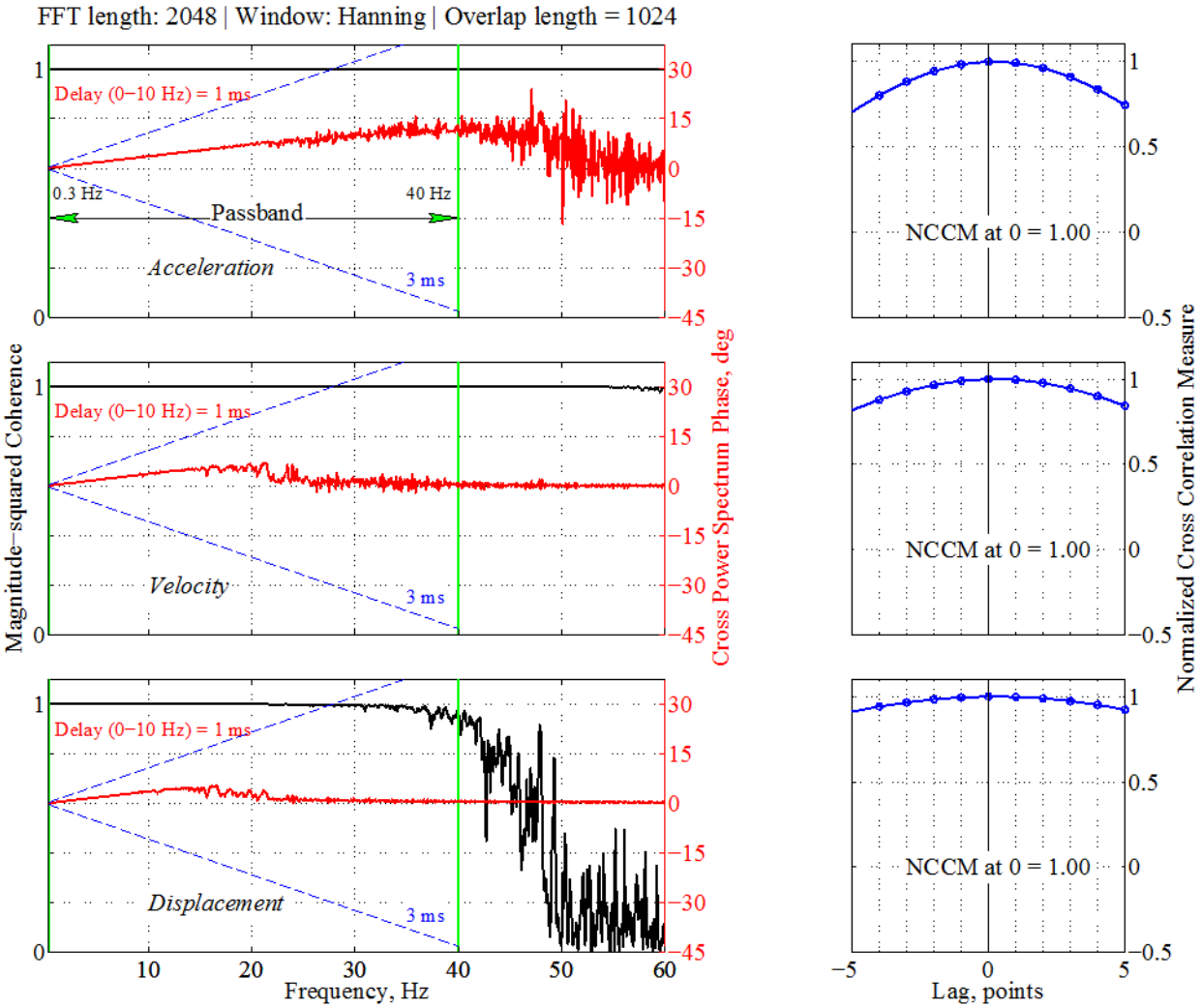


Figure 36. Graphs showing magnitude-squared coherence, cross spectrum phase in degrees, and normalized cross-correlation measure (NCCM) used to measure frequency and time domain similarities between acceleration, velocity, and displacement time series processed by Processing and Review Interface for Strong Motion data (PRISM) and California Strong Motion Instrumentation Program (CSMIP). Vertical green lines show corners of bandpass filter. Time delay, in milliseconds (ms), computed based on phase spectrum between 0 and 10 hertz (Hz) is marked; dashed blue lines denote ±3 ms time delay. Data correspond to component HNN of station CE.57444 record from the 2015 *M*3.6 San Ramon earthquake in California. FFT, fast Fourier transform.

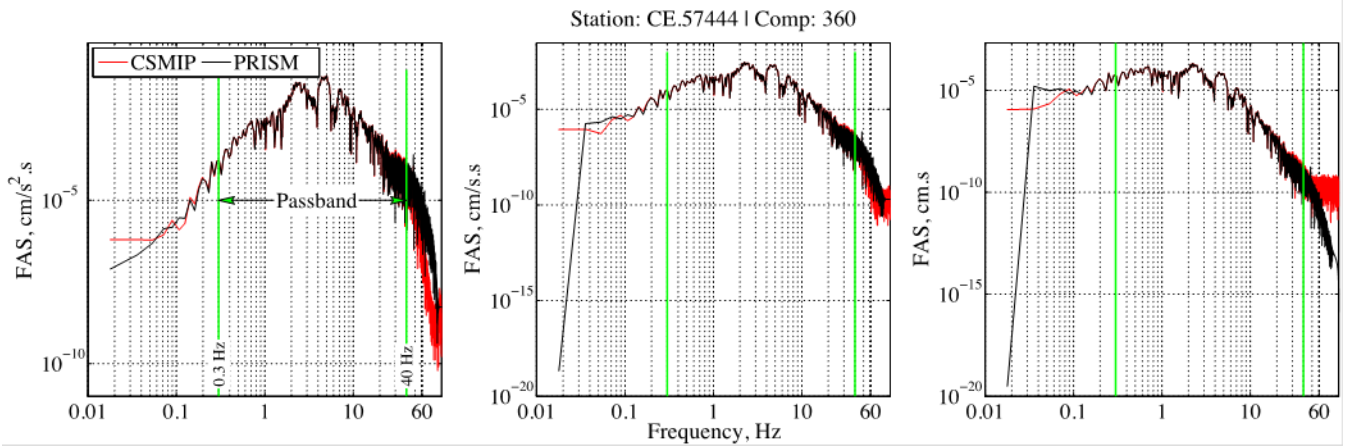


Figure 37. Graphs showing Fourier amplitude spectra (FAS) of acceleration, velocity, and displacement time series obtained by using Processing and Review Interface for Strong Motion data (PRISM) and California Strong Motion Instrumentation Program (CSMIP) to process component (comp) HNN of station CE.57444 record from the 2015 *M*3.6 San Ramon earthquake in California. The record processed in PRISM (black lines) overlies the CSMIP version (red lines). Vertical green lines show corners of bandpass filter. cm·s, centimeters second; cm/s·s, centimeters per second second; cm/s²·s, centimeters per second squared second; Hz, hertz.

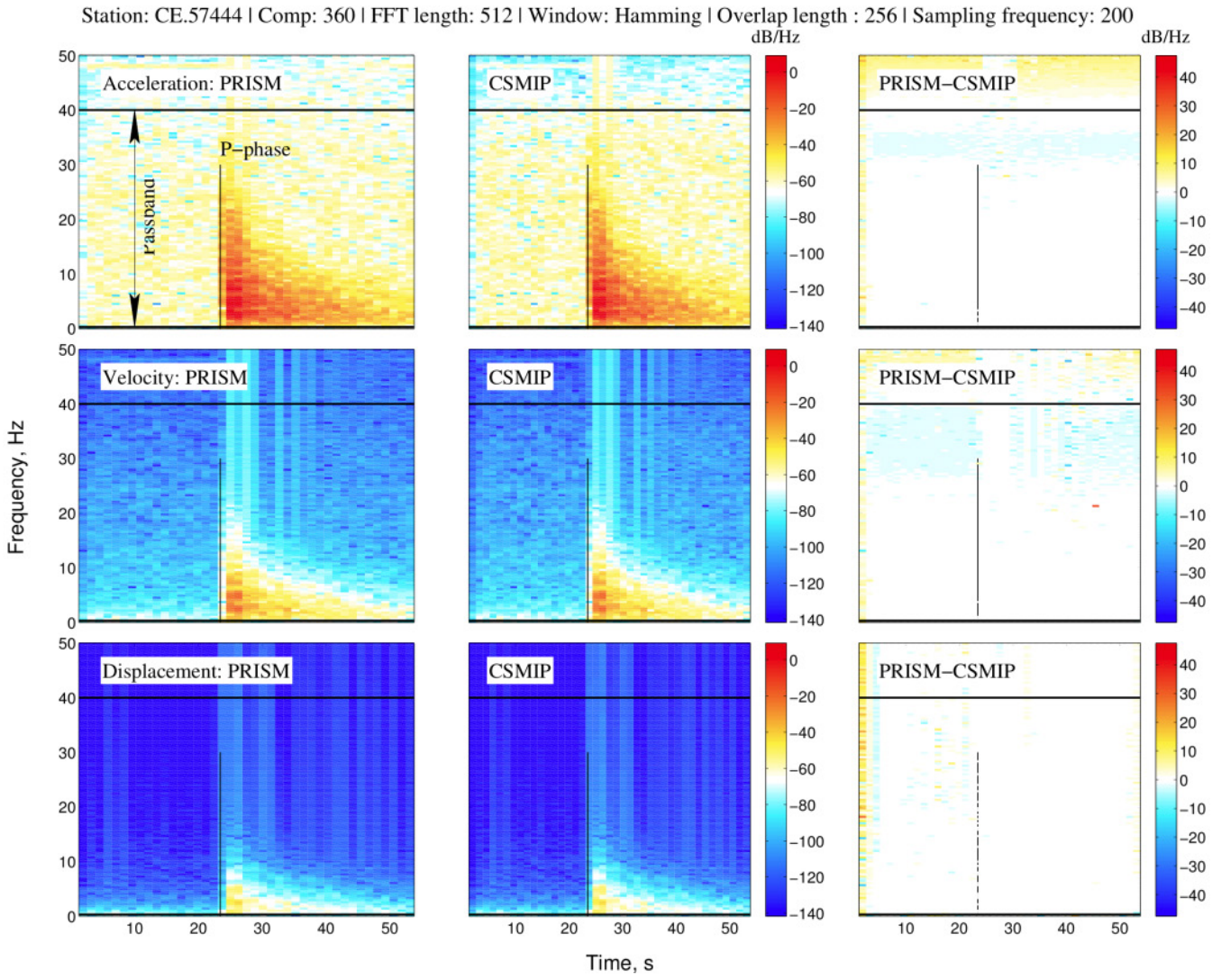


Figure 38. Spectrograms of acceleration, velocity, and displacement time series obtained by using Processing and Review Interface for Strong Motion data (PRISM) and California Strong Motion Instrumentation Program (CSMIP) to process component (comp) HNN of station CE.57444 record from the 2015 *M*3.6 San Ramon earthquake in California. Differences in power spectral densities are plotted in right column. Color indicates strength of time series at a range of frequencies over time. Horizontal lines show corners of bandpass filter; vertical black lines denote P-phase arrival time. dB/Hz, decibel per hertz; FFT, fast Fourier transform; Hz, hertz; s, seconds.

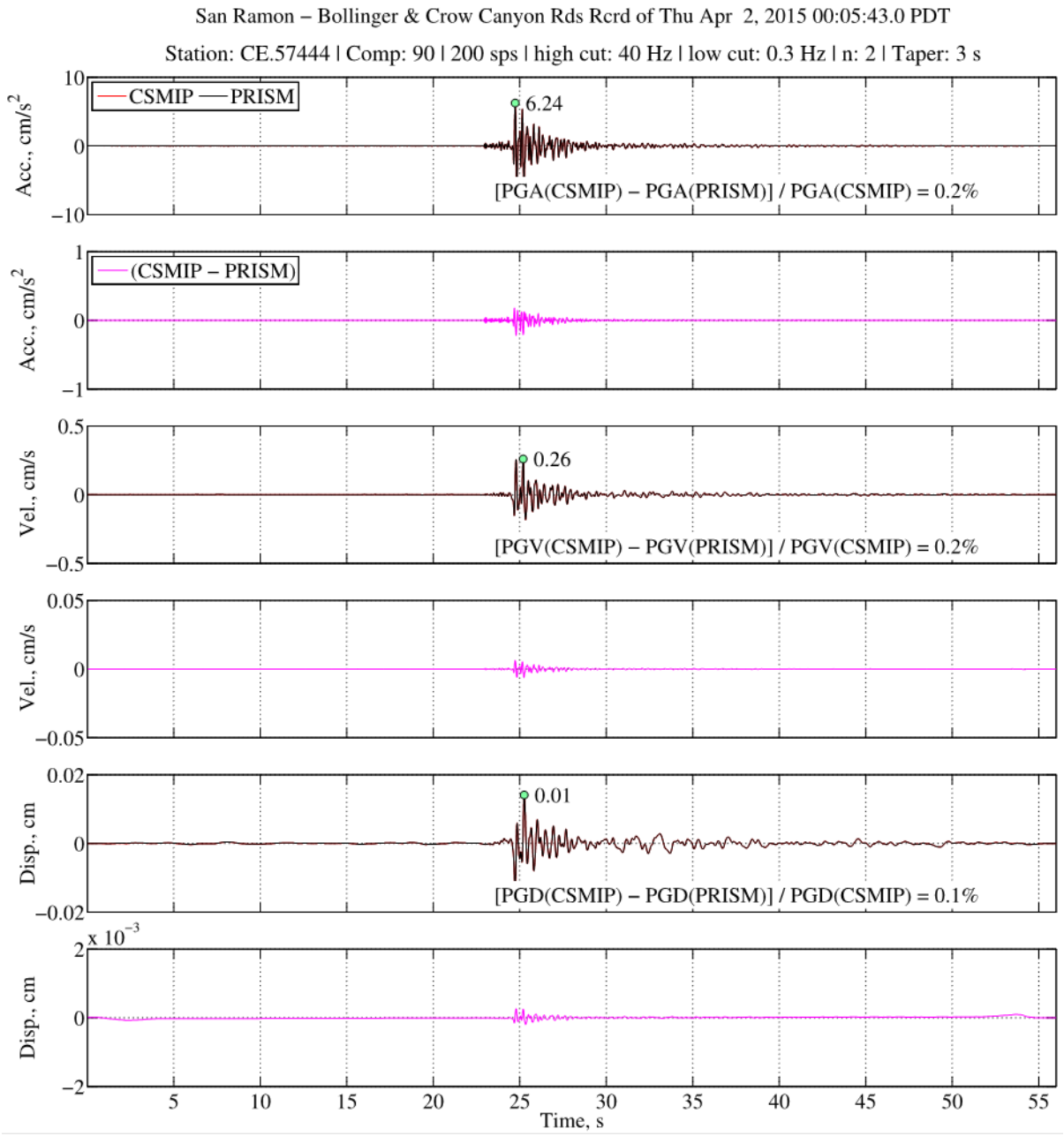


Figure 39. Graphs comparing acceleration (acc.), velocity (vel.), and displacement (disp.) time series obtained by using Processing and Review Interface for Strong Motion data (PRISM) and California Strong Motion Instrumentation Program (CSMIP) to process component (comp) HNE of station CE.57444 record from the 2015 *M*3.6 San Ramon earthquake in California. The record processed in PRISM (black lines) overlies the CSMIP version (red lines). Percent differences in peak ground acceleration (PGA), peak ground velocity (PGV), and peak ground displacement (PGD) are shown. Note differences in scaling used to enhance visibility for each pair of physical motion plots. Green circles indicate peak values of PRISM processing. cm, centimeters; cm/s, centimeters per second; cm/s$^2$, centimeters per second squared; Hz, hertz; n, Butterworth filter order; PDT, Pacific daylight time; s, seconds; sps, samples-per-second.

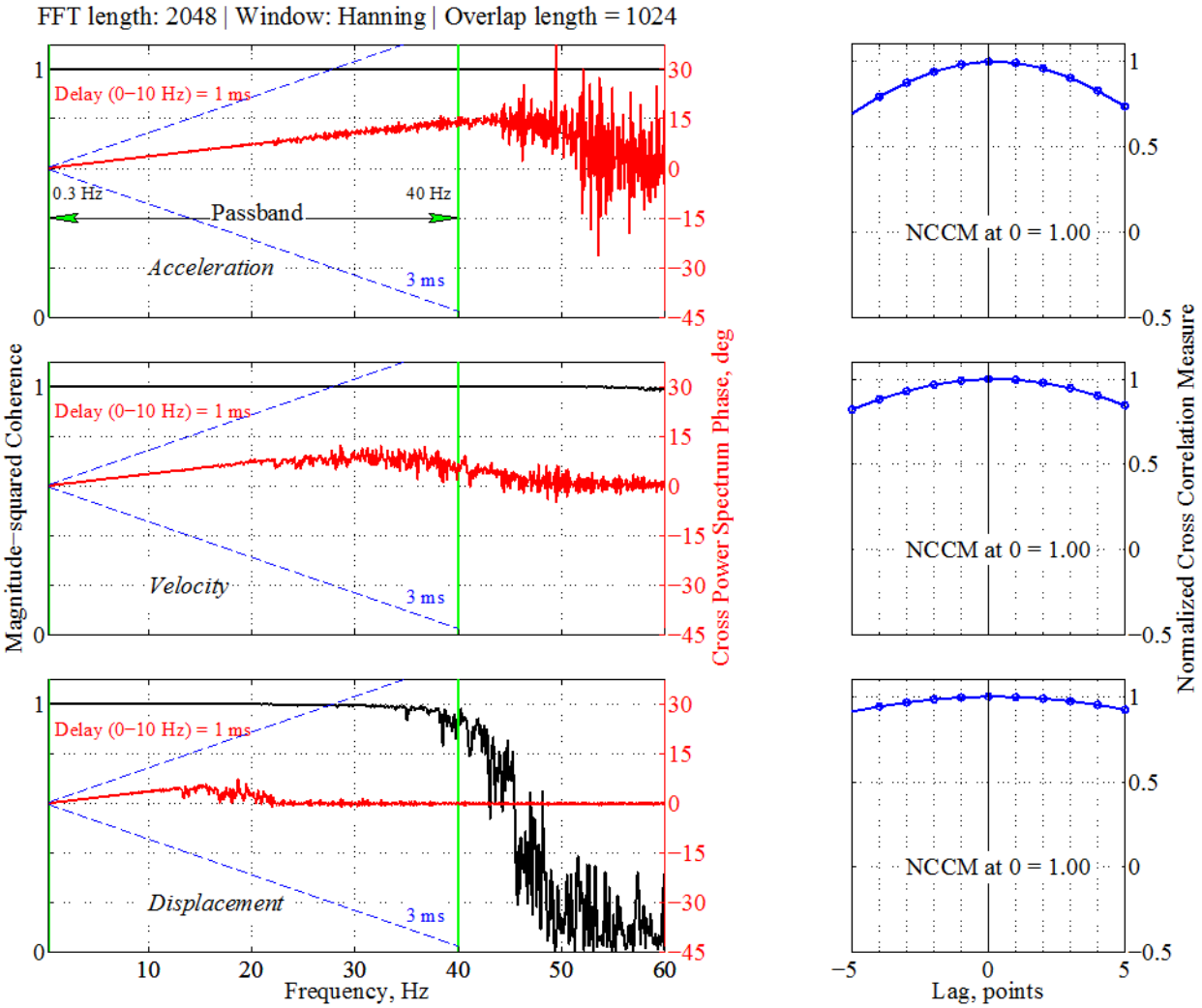


Figure 40. Graphs showing magnitude-squared coherence, cross spectrum phase in degrees, and normalized cross-correlation measure (NCCM) used to measure frequency and time domain similarities between acceleration, velocity, and displacement time series processed by Processing and Review Interface for Strong Motion data (PRISM) and California Strong Motion Instrumentation Program (CSMIP). Time delay in milliseconds (ms) computed based on phase spectrum between 0 and 10 hertz (Hz) is marked; dashed blue lines denote ±3 ms time delay. Vertical green lines show corners of bandpass filter. Data correspond to component HNE of station CE.57444 record from the 2015 *M*3.6 San Ramon earthquake in California. FFT, fast Fourier transform.

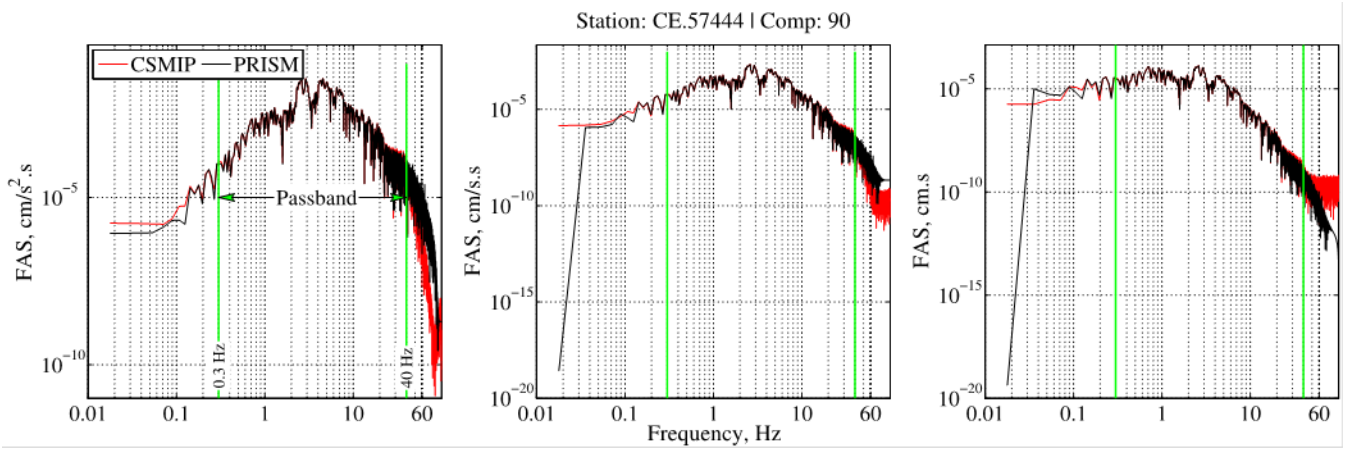


Figure 41. Graphs showing Fourier amplitude spectra (FAS) of acceleration, velocity, and displacement time series obtained by using Processing and Review Interface for Strong Motion data (PRISM) and California Strong Motion Instrumentation Program (CSMIP) to process component (comp) HNE of station CE.57444 record from the 2015 *M*3.6 San Ramon earthquake in California. The record processed in PRISM (black lines) overlies the CSMIP version (red lines). Vertical green lines show corners of bandpass filter. cm·s, centimeters second; cm/s·s, centimeters per second second; cm/s$^2$·s, centimeters per second squared second; Hz, hertz.

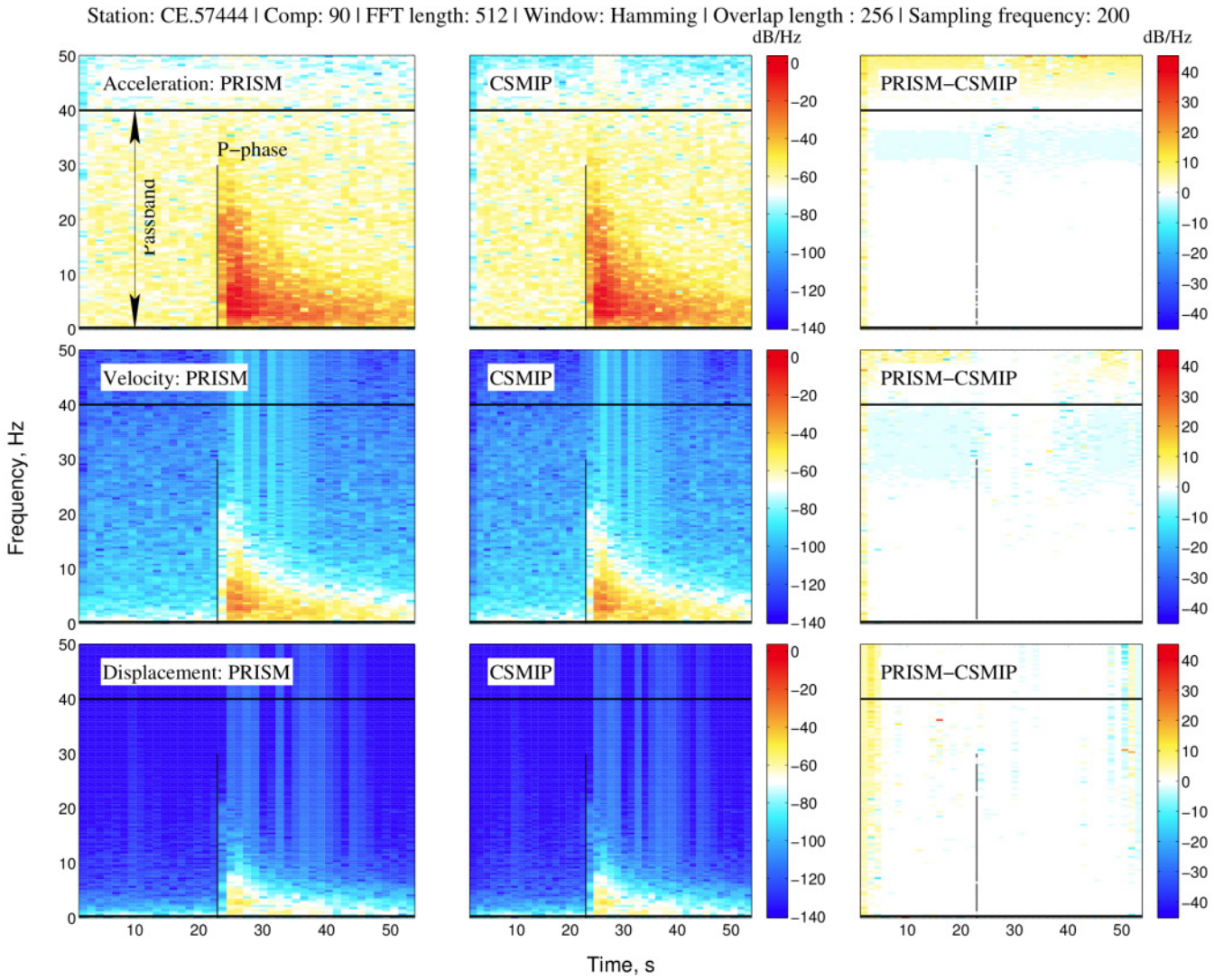


Figure 42. Spectrograms of acceleration, velocity, and displacement time series obtained by using Processing and Review Interface for Strong Motion data (PRISM) and California Strong Motion Instrumentation Program (CSMIP) to process component HNE of station CE.57444 record from the 2015 *M*3.6 San Ramon earthquake in California. Differences in power spectral densities are plotted in right column. Color indicates strength of signal at a range of frequencies over time. Horizontal lines show corners of bandpass filter; vertical black lines denote P-phase arrival time. dB/Hz, decibel per hertz; FFT, fast Fourier transform; Hz, hertz; s, seconds.

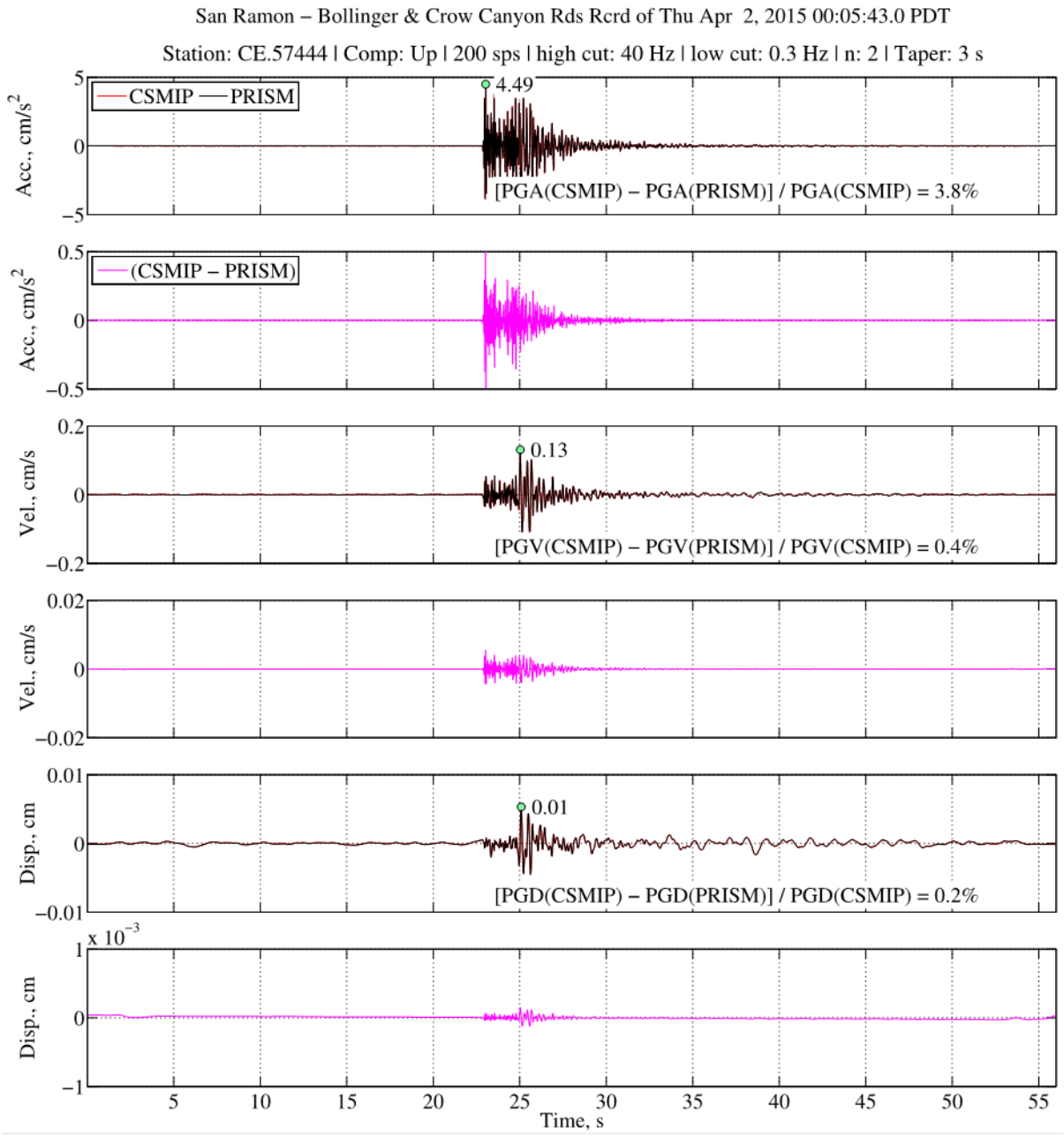


Figure 43. Graphs comparing acceleration (acc.), velocity (vel.), and displacement (disp.) time series obtained by using Processing and Review Interface for Strong Motion data (PRISM) and California Strong Motion Instrumentation Program (CSMIP) to process component (comp) HNZ of station CE.57444 record from the 2015 *M*3.6 San Ramon earthquake in California. The record processed in PRISM (black lines) overlies the CSMIP version (red lines). Percent differences in peak ground acceleration (PGA), peak ground velocity (PGV), and peak ground displacement (PGD) are shown. Note differences in scaling used to enhance visibility for each pair of physical motion plots. Green circles indicate peak values of PRISM processing. cm, centimeters; cm/s, centimeters per second; cm/s$^2$, centimeters per second squared; Hz, hertz; n, Butterworth filter order; PDT, Pacific daylight time; s, seconds; sps, samples-per-second.

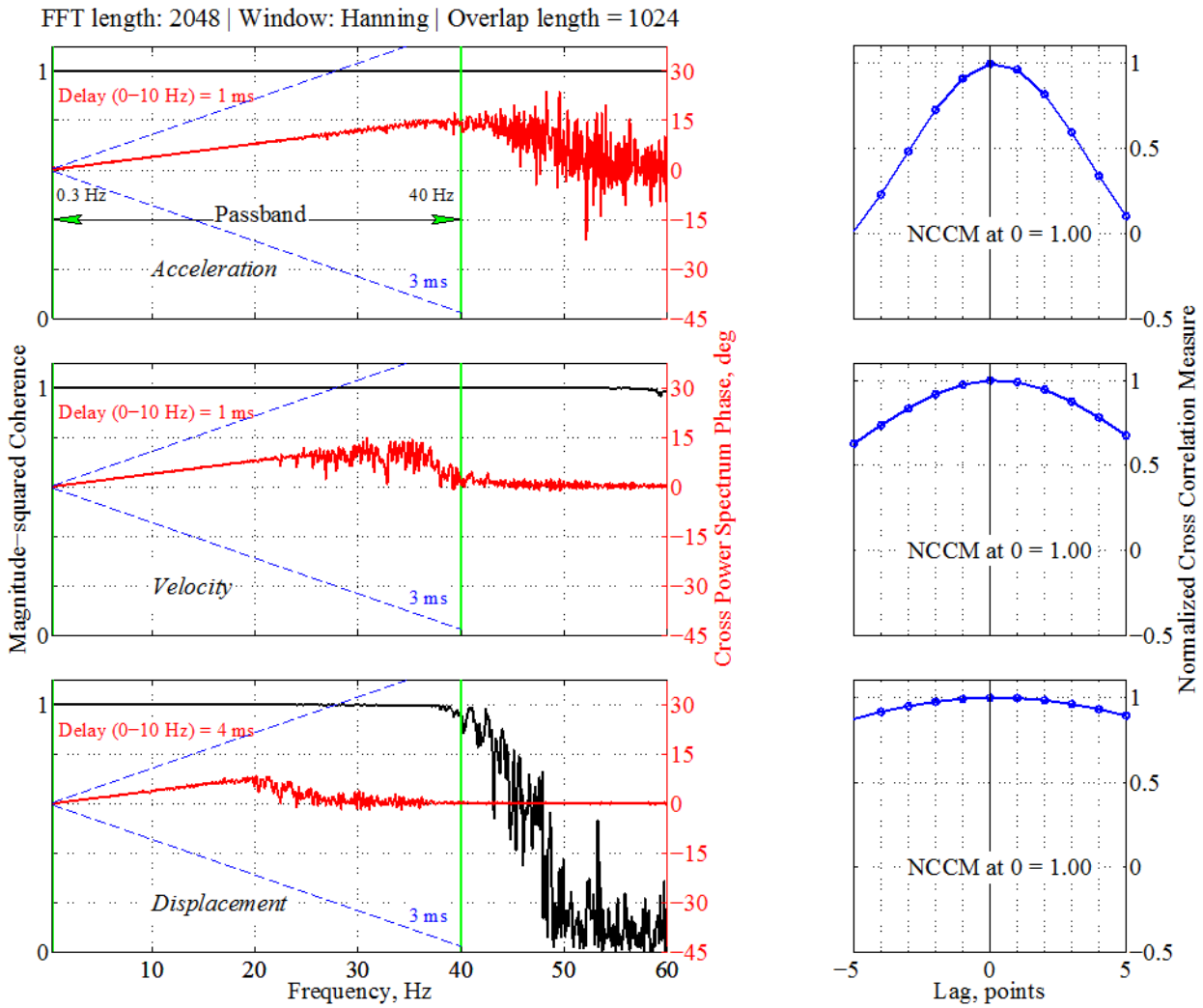


Figure 44. Graphs showing magnitude-squared coherence, cross spectrum phase in degrees, and normalized cross-correlation measure (NCCM) used to measure frequency and time domain similarities between acceleration, velocity, and displacement time series processed by Processing and Review Interface for Strong Motion data (PRISM) and California Strong Motion Instrumentation Program (CSMIP). Vertical green lines show corners of bandpass filter. Time delay in milliseconds (ms) computed based on phase spectrum between 0 and 10 hertz (Hz) is marked; dashed blue lines denote ±3 ms time delay. Data correspond to component HNZ of station CE.57444 record from the 2015 *M*3.6 San Ramon earthquake in California. FFT, fast Fourier transform.

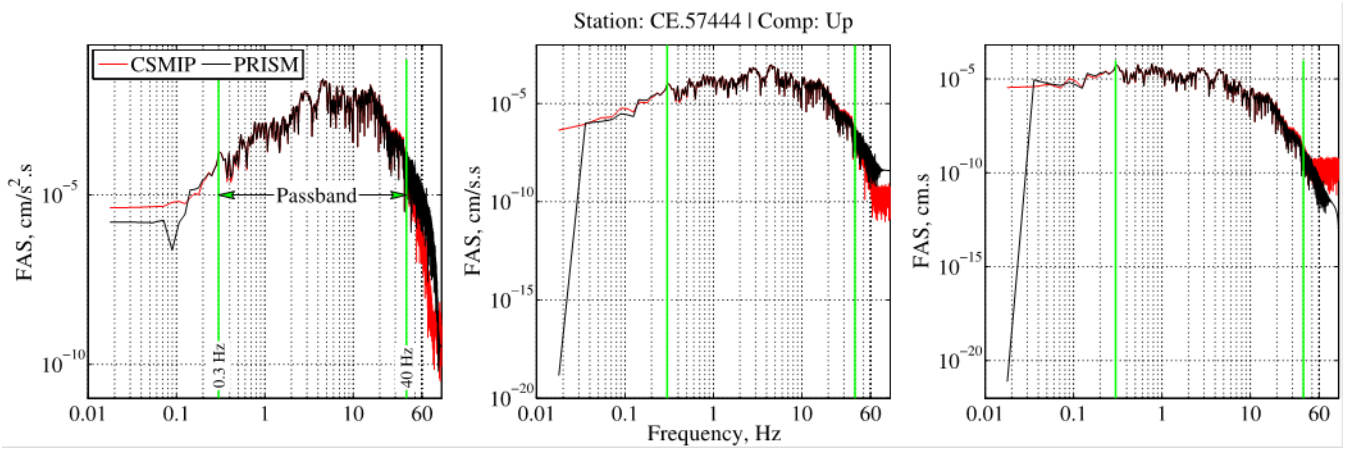


Figure 45. Graphs showing Fourier amplitude spectra (FAS) of acceleration, velocity, and displacement time series obtained by using Processing and Review Interface for Strong Motion data (PRISM) and California Strong Motion Instrumentation Program (CSMIP) to process component (comp) HNZ of station CE.57444 record from the 2015 *M*3.6 San Ramon earthquake in California. The record processed in PRISM (black lines) overlies the CSMIP version (red lines). Vertical green lines show corners of bandpass filter. cm·s, centimeters second; cm/s·s, centimeters per second second; cm/s$^2$·s, centimeters per second squared second; Hz, hertz.

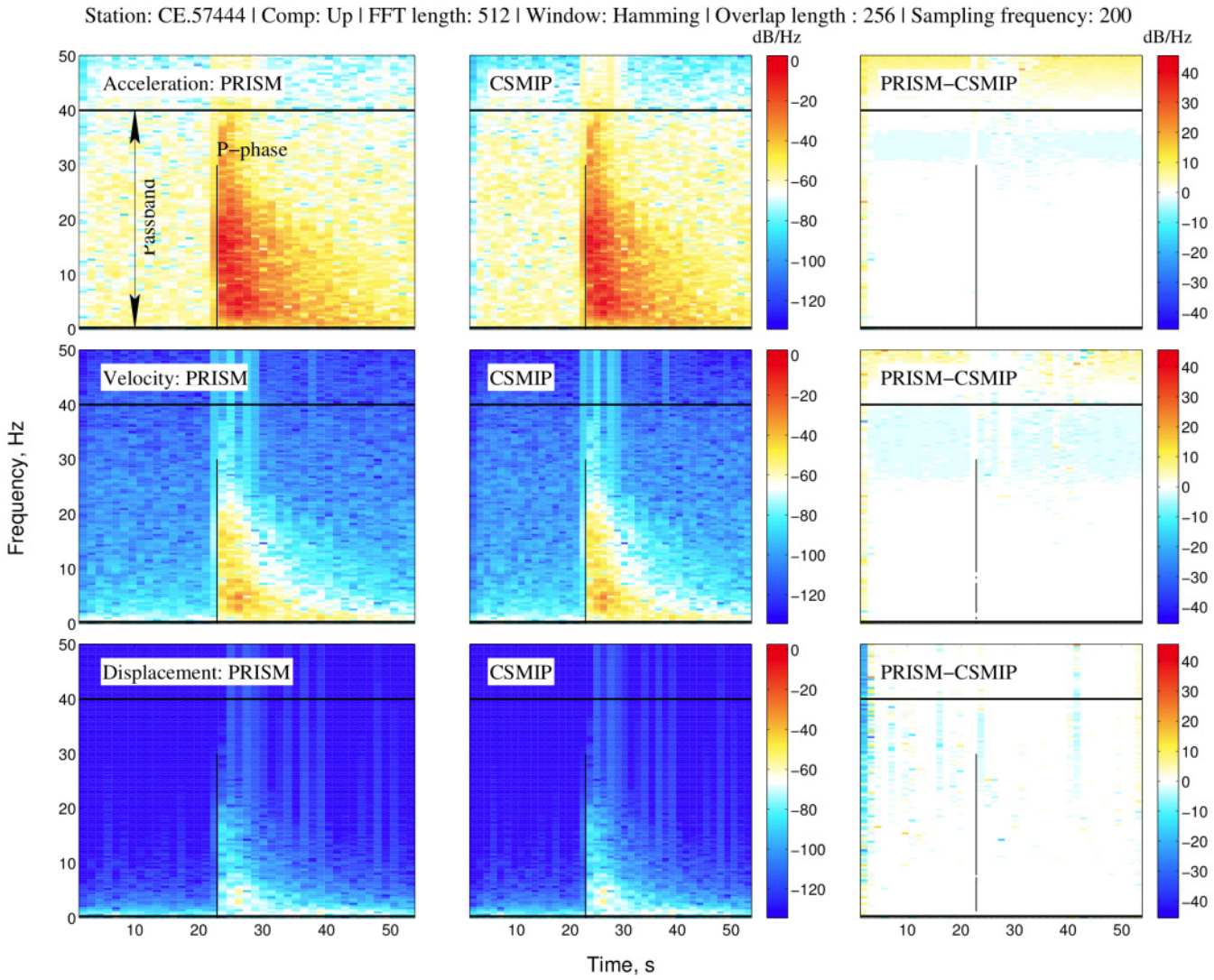


Figure 46. Spectrograms of acceleration, velocity, and displacement time series obtained by using Processing and Review Interface for Strong Motion data (PRISM) and California Strong Motion Instrumentation Program (CSMIP) to process component (comp) HNZ of station CE.57444 record from the 2015 *M*3.6 San Ramon earthquake in California. Differences in power spectral densities are plotted in right column. Color indicates strength of time series at a range of frequencies over time. Horizontal lines show corners of bandpass filter; vertical black lines denote P-phase arrival time. dB/Hz, decibel per hertz; FFT, fast Fourier transform; Hz, hertz; s, seconds.

In figures 47 through 58 time series, signal similarity measures, FAS, and spectrograms are compared for CE.68150. To ensure compatibility in sampling rates of CSMIP and PRISM V2 for performing coherence, phase, and cross correlation analyses, PRISM V2 data were down-sampled from 200 to 100 sps. The resampling procedure applies an anti-aliasing (low-pass) FIR filter to the signal during the resampling process (Parks and Burrus, 1987). Note that PRISM-processed waveforms are down-sampled to 100 sps only in figures 48, 52, and 56 where metrics for signal similarities are exhibited. Time series comparisons are based on original sampling rates of signals.

Despite any differences between PRISM and CSMIP processing, the resultant waveforms generally match well. The PGA, PGV, and PGD values are very similar between the two processing procedures, with the largest observed discrepancy on the order of 1 percent. A time delay of 2.0 milliseconds is apparent in all three components because of a small phase shift. In normalized cross-correlation measures, peak values are at or close to 1. Comparisons of FAS and spectrograms display an overall good match.

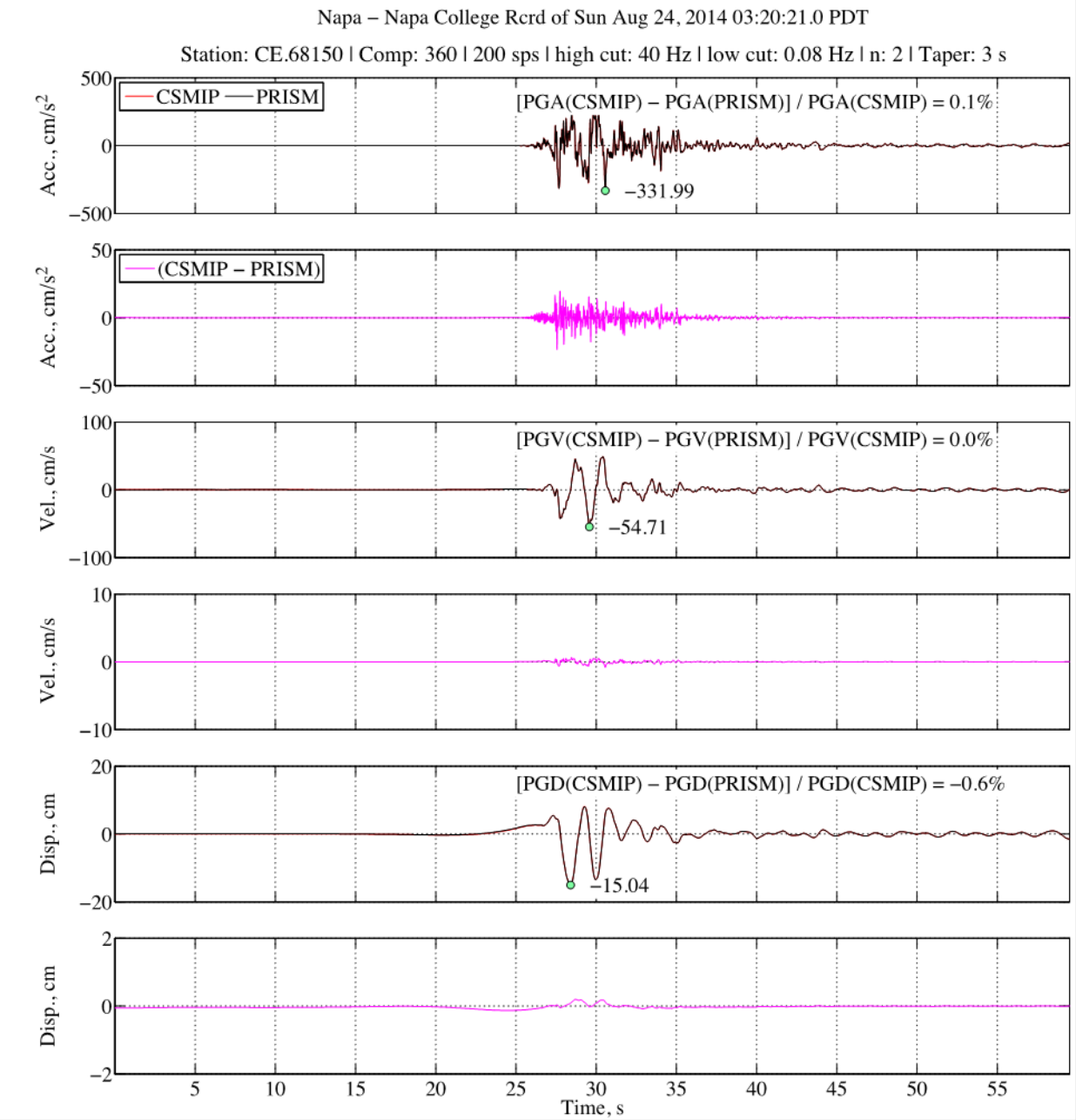


Figure 47. Graphs comparing acceleration (acc.), velocity (vel.), and displacement (disp.) time series obtained by using Processing and Review Interface for Strong Motion data (PRISM) and California Strong Motion Instrumentation Program (CSMIP) to process component (comp) HNN of station CE.68150 record from the 2014 *M*6.0 South Napa earthquake in California. The record processed in PRISM (black lines) overlies the CSMIP version (red lines). Percent differences in peak ground acceleration (PGA), peak ground velocity (PGV), and peak ground displacement (PGD) are shown. CSMIP processed record is at 100 samples-per-second (sps); whereas PRISM processed record is at 200 sps. Green circles indicate peak values of PRISM processing. cm, centimeters; cm/s, centimeters per second; cm/s$^2$, centimeters per second squared; Hz, hertz; n, Butterworth filter order; PDT, Pacific daylight time; s, seconds; sps, samples-per-second.

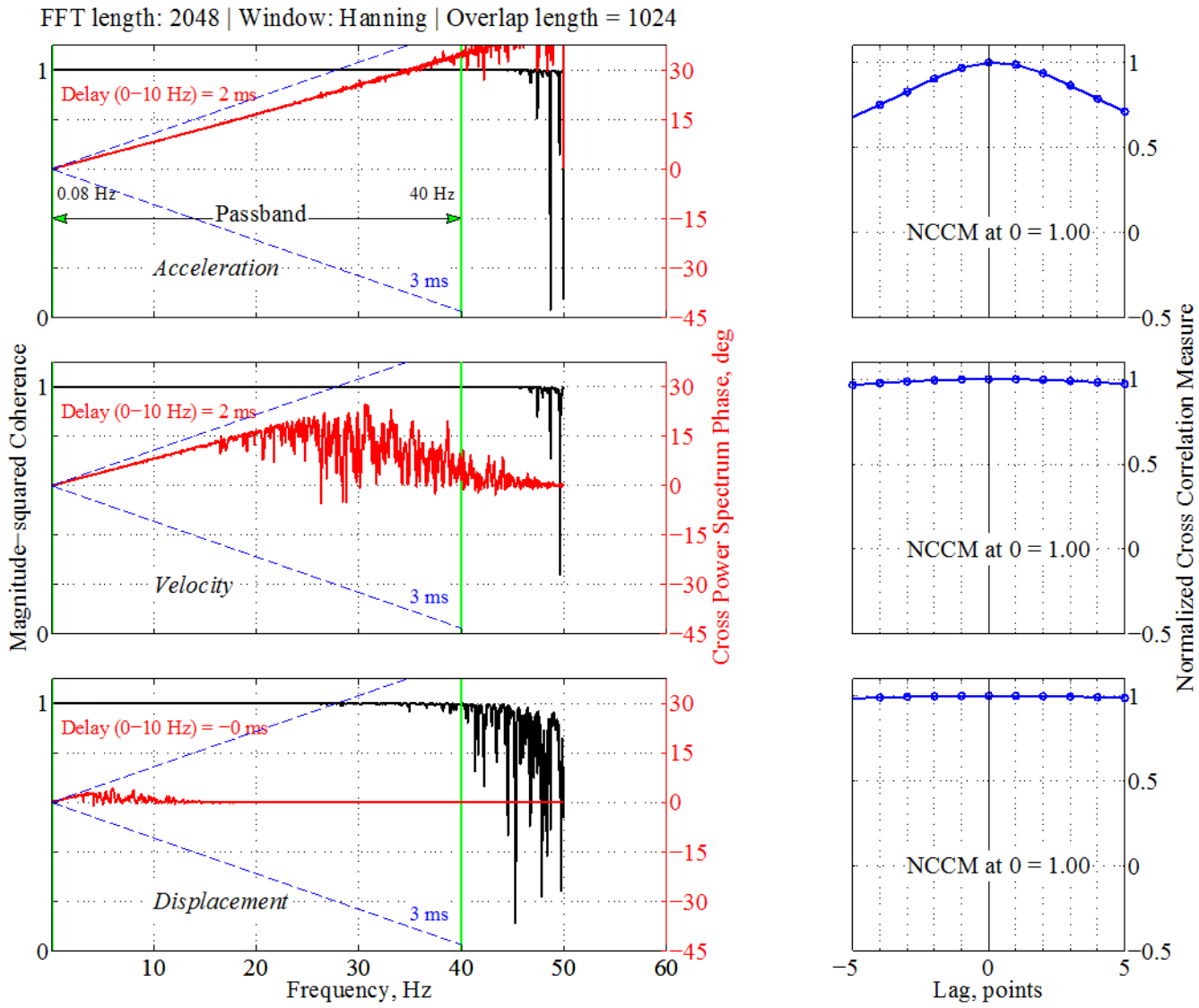


Figure 48. Graphs showing magnitude-squared coherence, cross spectrum phase in degrees, and normalized cross-correlation measure (NCCM) used to measure frequency and time domain similarities between acceleration, velocity, and displacement time series processed by Processing and Review Interface for Strong Motion data (PRISM) and California Strong Motion Instrumentation Program (CSMIP). Vertical green lines show corners of bandpass filter. Time delay in milliseconds (ms) computed based on phase spectrum between 0 and 10 hertz (Hz) is marked; dashed blue lines denote ±3 ms time delay. Data correspond to component HNN of station CE.68150 record from the 2014 *M*6.0 South Napa earthquake in California. FFT, fast Fourier transform.

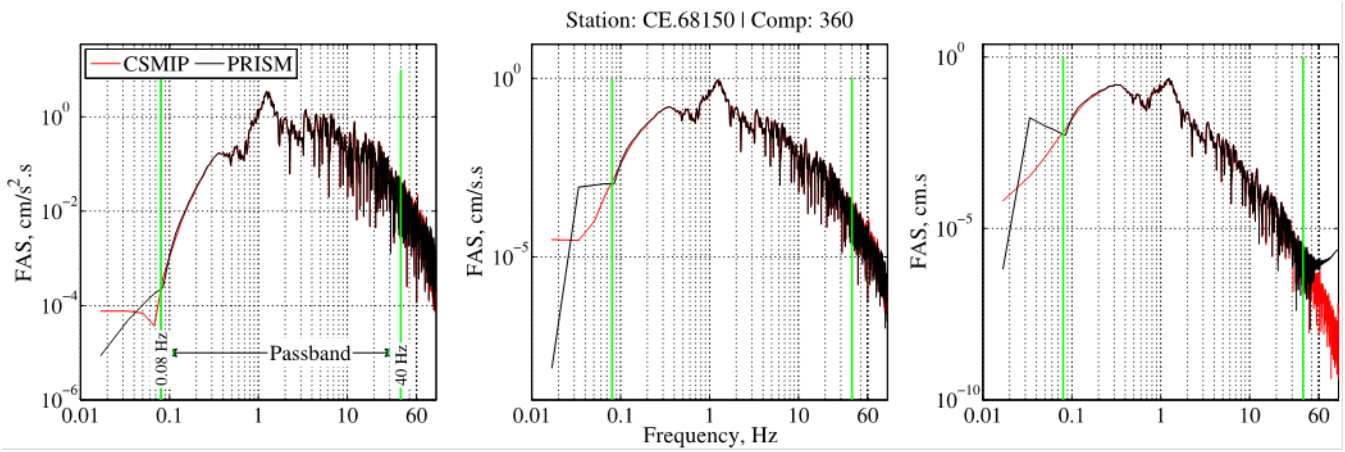


Figure 49. Graphs showing Fourier amplitude spectra (FAS) of acceleration, velocity, and displacement time series obtained by using Processing and Review Interface for Strong Motion data (PRISM) and California Strong Motion Instrumentation Program (CSMIP) to process component (comp) HNN of station CE.68150 record from the 2014 *M*6.0 South Napa earthquake in California. The record processed in PRISM (black lines) overlies the CSMIP version (red lines). Vertical green lines show corners of bandpass filter; vertical black lines denote P-phase arrival time. cm·s, centimeters second; cm/s·s, centimeters per second second; cm/s$^2$·s, centimeters per second squared second; Hz, hertz.

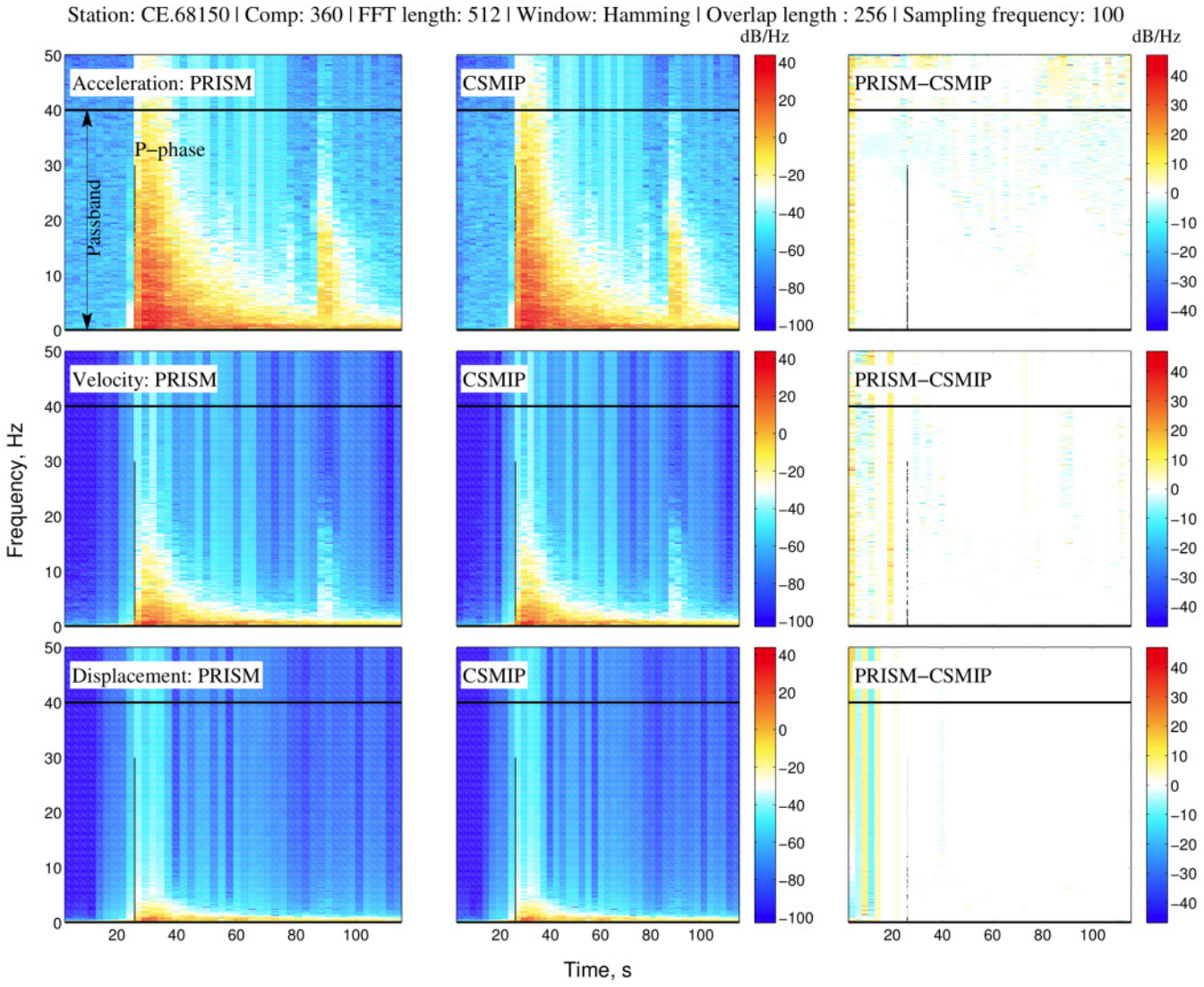


Figure 50. Spectrograms of acceleration, velocity, and displacement time series obtained by using Processing and Review Interface for Strong Motion data (PRISM) and California Strong Motion Instrumentation Program (CSMIP) to process component (comp) HNE of station CE.68150 record from the 2014 *M*6.0 South Napa earthquake in California. Differences in power spectral densities are plotted in right column. Color indicates strength of time series at a range of frequencies over time. Horizontal lines show corners of bandpass filter; vertical black lines denote P-phase arrival time. dB/Hz, decibel per hertz; FFT, fast Fourier transform; Hz, hertz; s, seconds.

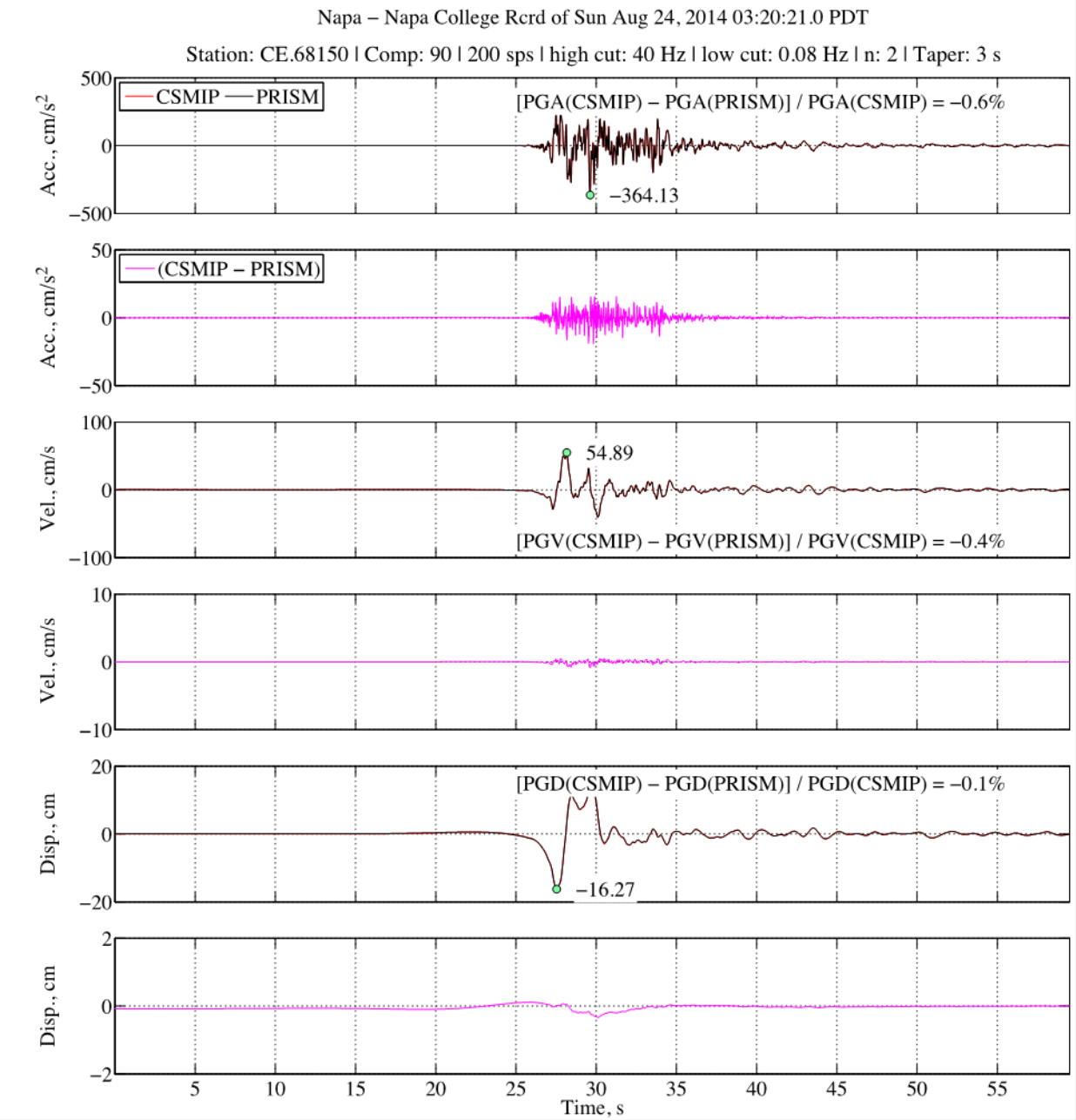


Figure 51. Graphs comparing acceleration (acc.), velocity (vel.), and displacement (disp.) time series obtained by using Processing and Review Interface for Strong Motion data (PRISM) and California Strong Motion Instrumentation Program (CSMIP) to process component (comp) HNE of station CE.68150 record from the 2014 *M*6.0 South Napa earthquake in California. The record processed in PRISM (black lines) overlies the CSMIP version (red lines). Percent differences in peak ground acceleration (PGA), peak ground velocity (PGV), and peak ground displacement (PGD) are shown. CSMIP processed record is at 100 samples-per-second (sps); whereas PRISM processed record is at 200 sps. Green circles indicate peak values of PRISM processing. cm, centimeters; cm/s, centimeters per second; cm/s$^2$, centimeters per second squared; Hz, hertz; n, Butterworth filter order; PDT, Pacific daylight time; s, seconds; sps, samples-per-second.

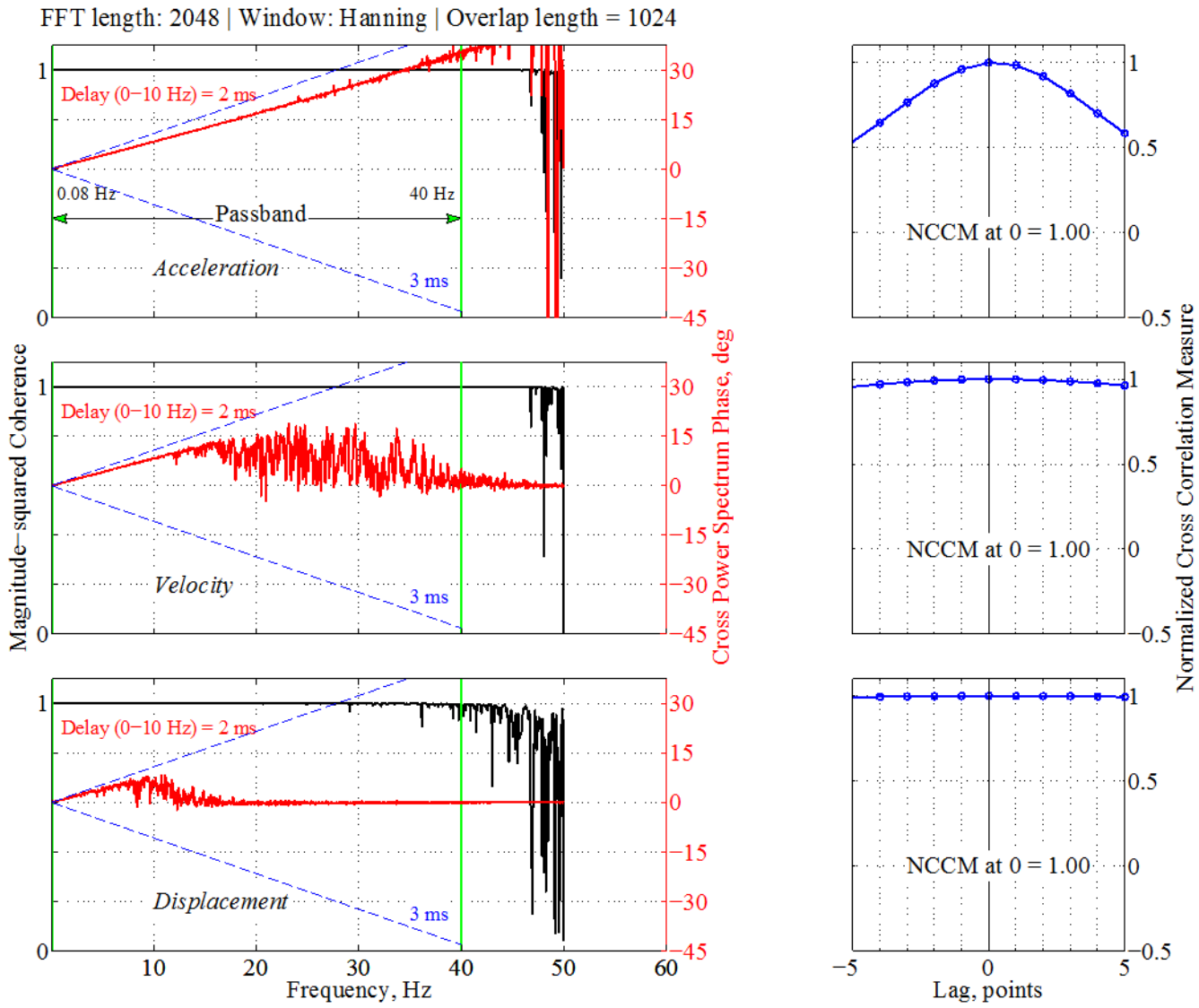


Figure 52. Graphs showing magnitude-squared coherence, cross spectrum phase in degrees, and normalized cross-correlation measure (NCCM) used to measure frequency and time domain similarities between acceleration, velocity, and displacement time series processed by Processing and Review Interface for Strong Motion data (PRISM) and California Strong Motion Instrumentation Program (CSMIP). Vertical green lines show corners of bandpass filter. Time delay in milliseconds (ms) computed based on phase spectrum between 0 and 10 hertz (Hz) is marked; dashed blue lines denote ±3 ms time delay. Data correspond to component HNE of station CE.68150 record from the 2014 *M*6.0 South Napa earthquake in California. FFT, fast Fourier transform.

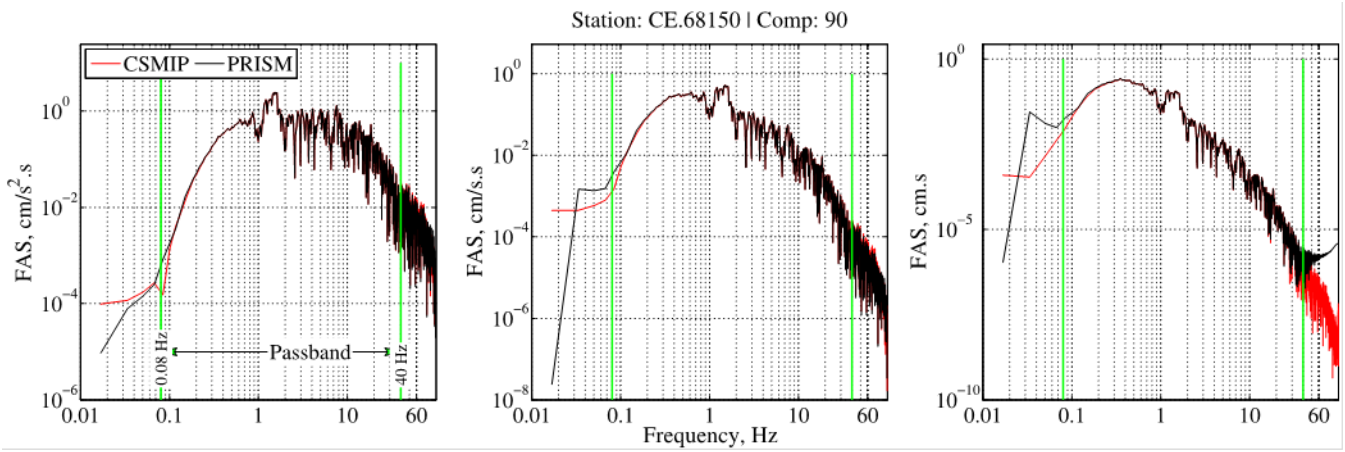


Figure 53. Graphs showing Fourier amplitude spectra (FAS) of acceleration, velocity, and displacement time series obtained by using Processing and Review Interface for Strong Motion data (PRISM) and California Strong Motion Instrumentation Program (CSMIP) to process component (comp) HNE of station CE.68150 record from the 2014 *M*6.0 South Napa earthquake in California. The record processed in PRISM (black lines) overlies the CSMIP version (red lines). Vertical green lines show corners of bandpass filter. cm·s, centimeters second; cm/s·s, centimeters per second second; cm/s$^2$·s, centimeters per second squared second; Hz, hertz.

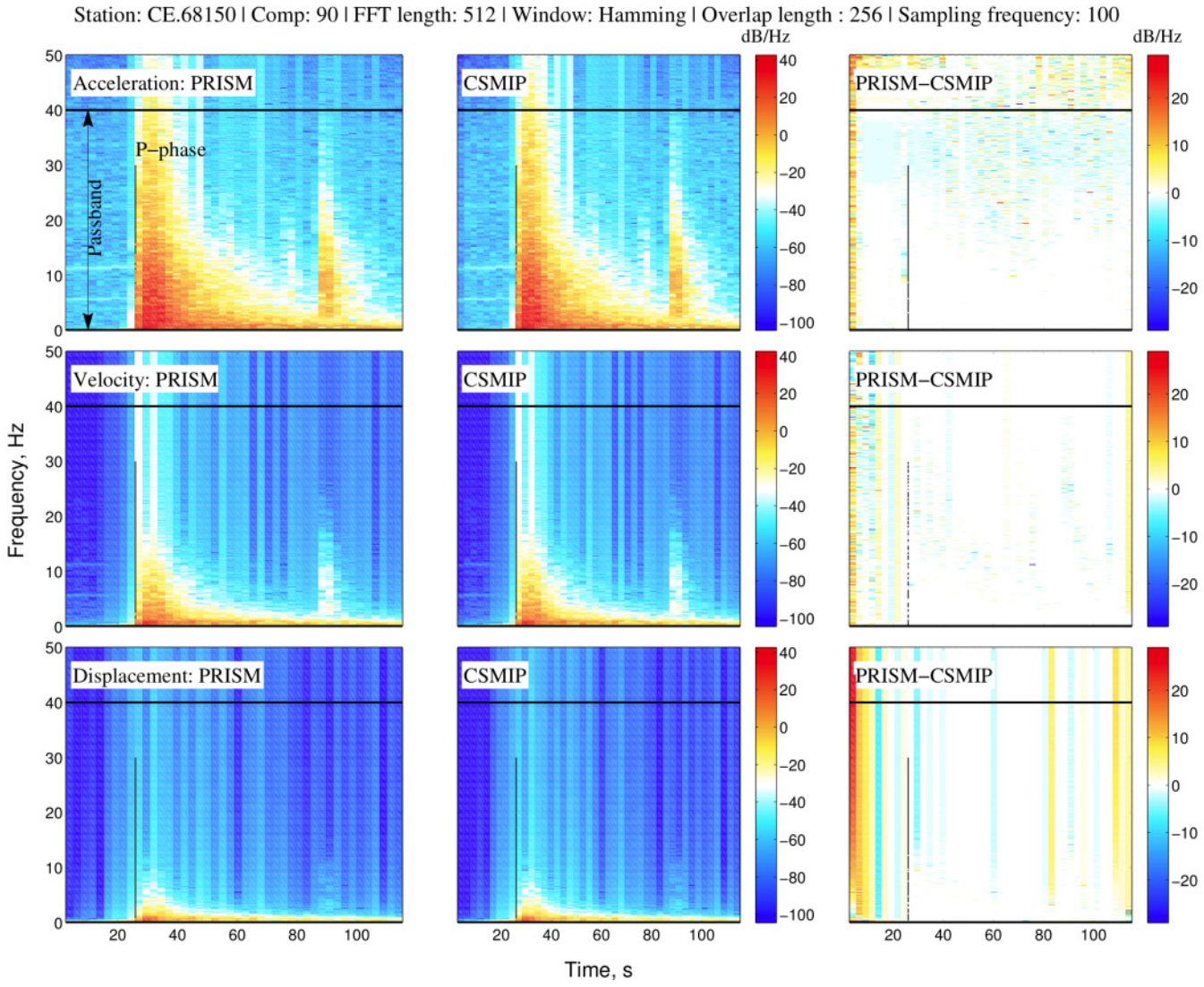


Figure 54. Spectrograms of acceleration, velocity, and displacement time series obtained by using Processing and Review Interface for Strong Motion data (PRISM) and California Strong Motion Instrumentation Program (CSMIP) to process component (comp) HNN of station CE.68150 record from the 2014 *M*6.0 South Napa earthquake in California. Differences in power spectral densities are plotted in right column. Color indicates strength of time series at a range of frequencies over time. Horizontal lines show corners of bandpass filter; vertical black lines denote P-phase arrival time. dB/Hz, decibel per hertz; FFT, fast Fourier transform; Hz, hertz; s, seconds.

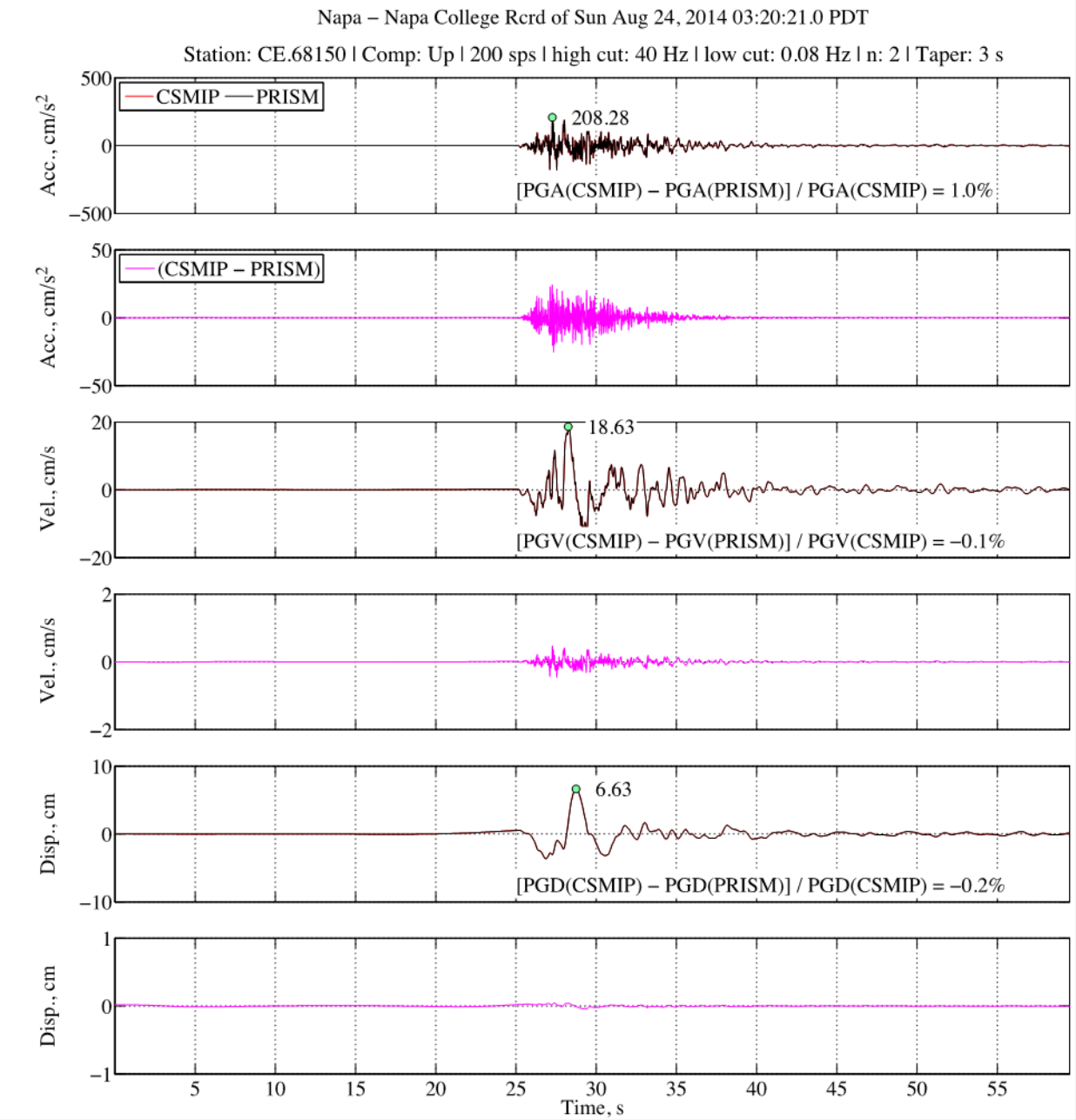


Figure 55. Graphs comparing acceleration (acc.), velocity (vel.), and displacement (disp.) time series obtained by using Processing and Review Interface for Strong Motion data (PRISM) and California Strong Motion Instrumentation Program (CSMIP) to process component (comp) HNZ of station CE.68150 record from the 2014 *M*6.0 South Napa earthquake in California. The record processed in PRISM (black lines) overlies the CSMIP version (red lines). Percent differences in peak ground acceleration (PGA), peak ground velocity (PGV), and peak ground displacement (PGD) are shown. CSMIP processed record is at 100 samples-per-second (sps); whereas PRISM processed record is at 200 sps. Green circles indicate peak values of PRISM processing. cm, centimeters; cm/s, centimeters per second; cm/s$^2$, centimeters per second squared; Hz, hertz; n, Butterworth filter order; PDT, Pacific daylight time; s, seconds; sps, samples-per-second.

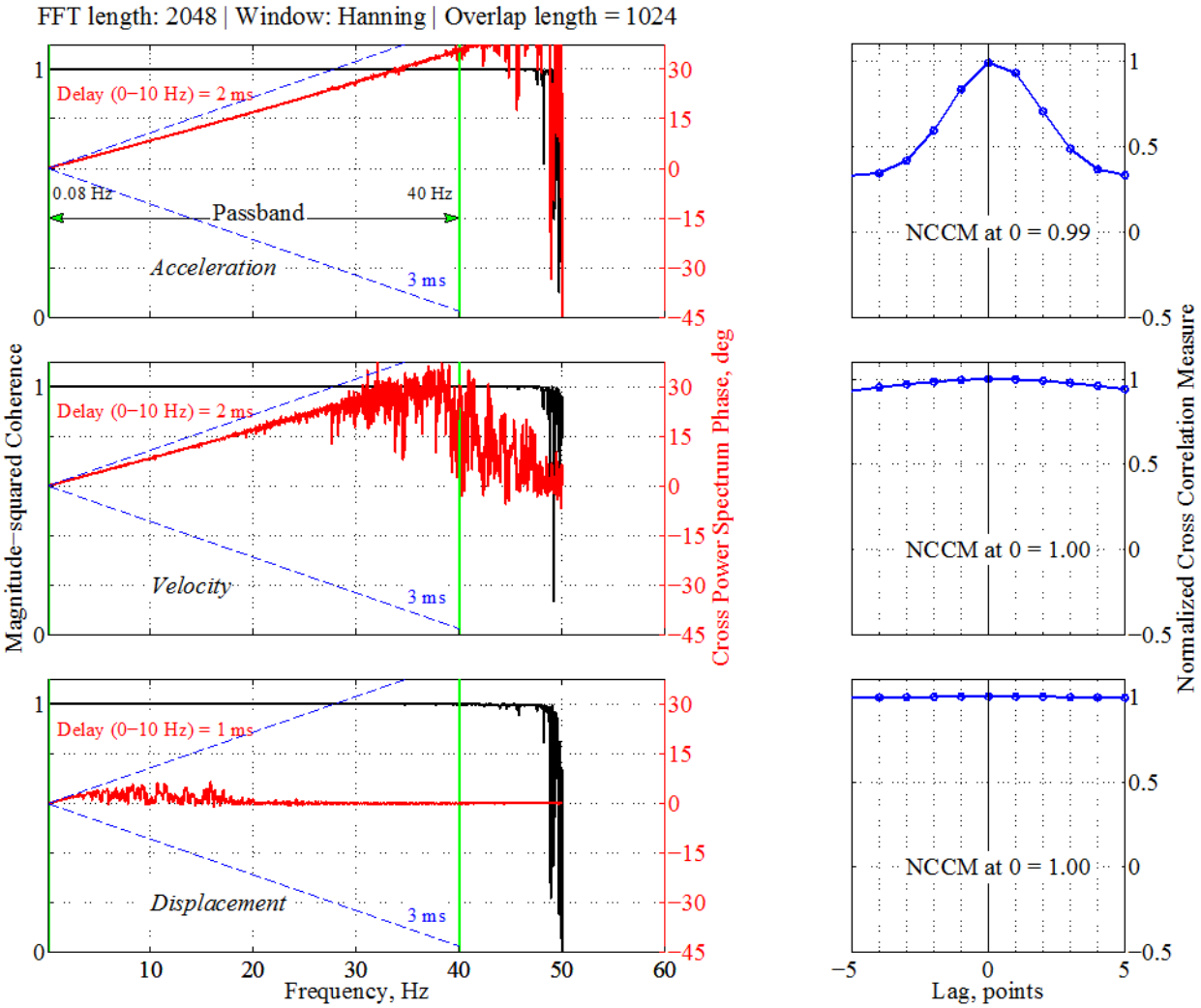


Figure 56. Graphs showing magnitude-squared coherence, cross spectrum phase in degrees, and normalized cross-correlation measure (NCCM) used to measure frequency and time domain similarities between acceleration, velocity, and displacement time series processed by Processing and Review Interface for Strong Motion data (PRISM) and California Strong Motion Instrumentation Program (CSMIP). Vertical green lines show corners of bandpass filter. Time delay in milliseconds (ms) computed based on phase spectrum between 0 and 10 hertz (Hz) is marked; dashed blue lines denote ±3 ms time delay. Data correspond to component HNZ of station CE.68150 record from the 2014 *M*6.0 South Napa earthquake in California. FFT, fast Fourier transform.

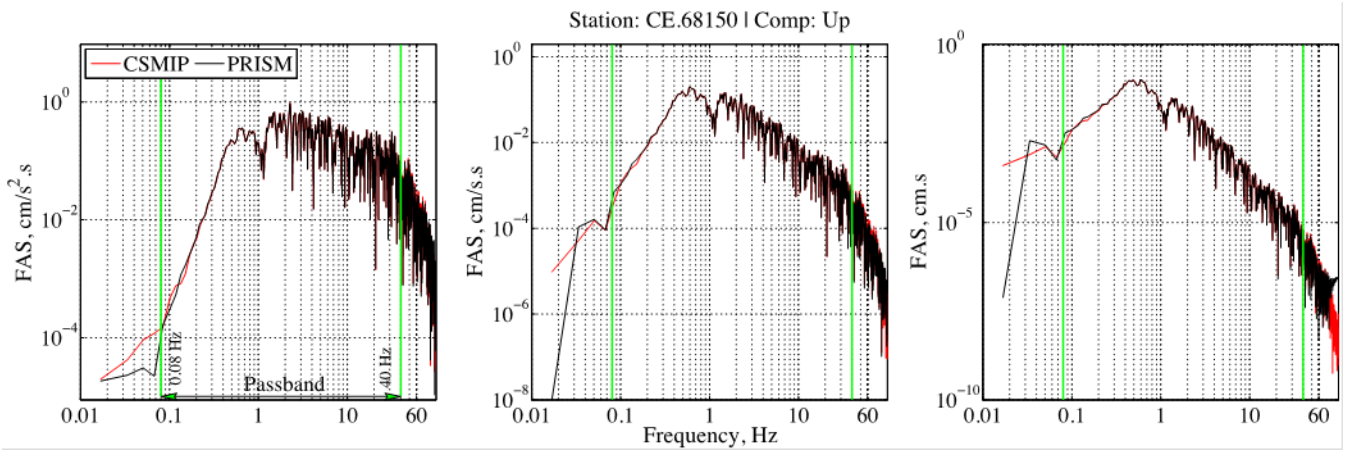


Figure 57. Graphs showing Fourier amplitude spectra (FAS) of acceleration, velocity, and displacement time series obtained by using Processing and Review Interface for Strong Motion data (PRISM) and California Strong Motion Instrumentation Program (CSMIP) to process component (comp) HNZ of station CE.68150 record from the 2014 *M*6.0 South Napa earthquake in California. The record processed in PRISM (black lines) overlies the CSMIP version (red lines). Vertical green lines show corners of bandpass filter. cm·s, centimeters second; cm/s·s, centimeters per second second; cm/s$^2$·s, centimeters per second squared; Hz, hertz.

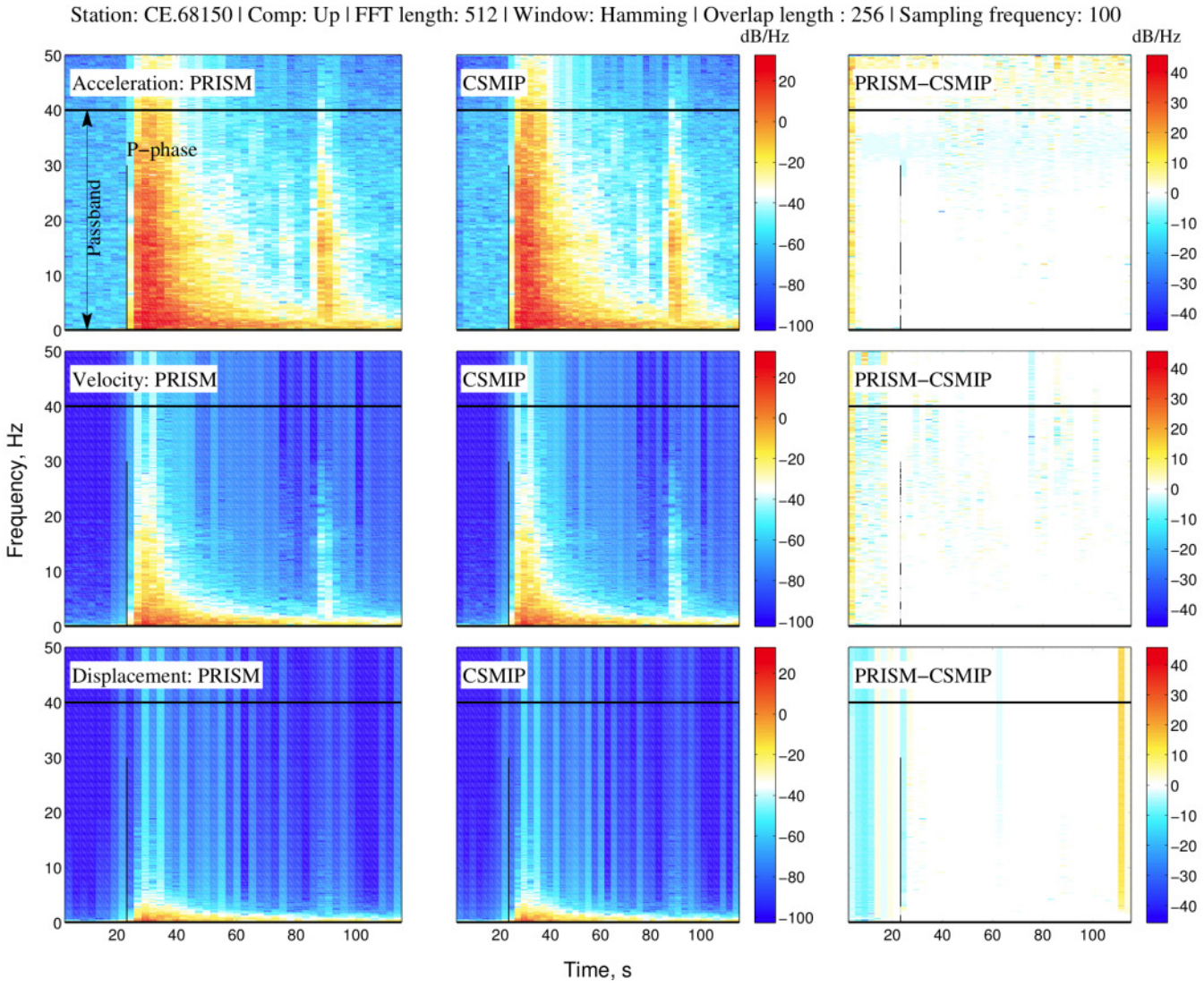


Figure 58. Spectrograms of acceleration, velocity, and displacement time series obtained by using Processing and Review Interface for Strong Motion data (PRISM) and California Strong Motion Instrumentation Program (CSMIP) to process component HNZ of station CE.68150 record from the 2014 *M*6.0 South Napa earthquake in California. Differences in power spectral densities are plotted in right column. Color indicates strength of signal at a range of frequencies over time. Horizontal lines show corners of bandpass filter; vertical black lines denote P-phase arrival time. dB/Hz, decibel per hertz; FFT, fast Fourier transform; Hz, hertz; s, seconds.

## Statistical Evaluation of PRISM and CSMIP Processed Records

To further demonstrate that the products derived by using the PRISM processing agree well with those from the CSMIP processing, 1,822 V1 ground-motion components from eight Californian earthquakes obtained from the CESMD website were processed by using PRISM, and resultant V2 products were compared with those from CSMIP processing. Table 1 lists relevant information about the selected earthquakes, including origin time, magnitude, depth, epicenter distance range of the observations, and number of ground-motion components. Figure 59 displays the magnitude-distance coverage of ground-motions.

Table 1. List of earthquakes in California used for statistical evaluations of Processing and Review Interface for Strong Motion data (PRISM) software and California Strong Motion Instrumentation Program (CSMIP) processing.

[km, kilometers; *M*, moment magnitude; ML, local magnitude; PDT, Pacific daylight time; PST, Pacific standard time]

| No. | Earthquake | Origin Time (dd/mm/yyyy; hh:mm:ss) | Magnitude | Depth (km) | Epicenter distance range, km | Number of ground-motion components |
|---|---|---|---|---|---|---|
| 1 | Yucaipa | 16/6/2005; 13:53:25 PDT | ML4.9 | 12.6 | 2.9–128.9 | 435 |
| 2 | Chino Hills | 29/7/2008; 11:42:15 PDT | *M*5.4 | 13.6 | 4.7–159.3 | 627 |
| 3 | Whittier Narrows | 16/3/2010; 04:04:00 PDT | ML4.4 | 18.0 | 4.0–46.3 | 238 |
| 4 | Ferndale | 9/1/2010; 16:27:38 PST | *M*6.5 | 21.7 | 52.5–159.2 | 27 |
| 5 | Ocotillo | 14/6/2010; 21:26:58 PDT | ML5.7 | 6.9 | 34.7–254.9 | 147 |
| 6 | Morgan Hill | 7/1/2011; 16:10:16 PDT | ML4.1 | 7.1 | 9.0–93.7 | 27 |
| 7 | South Napa | 24/8/2014; 03:20:44 PDT | *M*6.0 | 11.3 | 6.4–114 | 288 |
| 8 | Wasco | 23/2/2016; 16:02:23 PST | *M*4.9 | 22.1 | 16.9–88.6 | 33 |

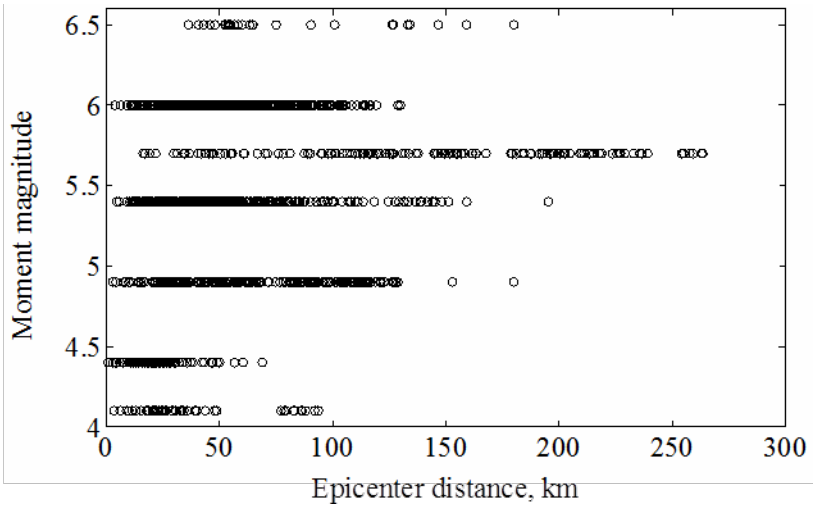


Figure 59. Graph showing magnitude-distance coverage of ground motions used for testing Processing and Review Interface for Strong Motion data (PRISM) and California Strong Motion Instrumentation Program (CSMIP) processing. km, kilometers.

The statistical evaluation of misfit is based on comparing

1. peak amplitudes (PGA, PGV, and PGD) of the processed time series,
2. normalized Euclidian distance ($L^2$ norm) between acceleration, velocity, and displacement time series, and
3. moving window root mean square (RMS) levels of acceleration, velocity, and displacement time series.

Normalized Euclidian distance is used here as a global misfit metric for directly measuring a difference between two waveforms, *x* and *y* as

$$\|x - y\| = \sqrt{\frac{1}{N}\sum_{i=1}^{N}(x_i - y_i)^2} \tag{3}$$

*x* and *y* must have equal duration and number of data points, *N*. For 878 CSMIP processed records the V2 waveforms have lower sampling rates than the corresponding V1 waveforms (for example the V1 record is 200 sps but the CSMIP V2 record is 100 sps). This creates an incompatibility between the number of data samples in the PRISM V2 records and those from CSMIP processing. For such incompatible records, the V2 records from PRISM processing were downsampled prior to computing the Euclidian distance and the RMS level. The resampling procedure used applies an anti-aliasing (low-pass) FIR filter in polyphase implementation to the signal during the resampling process (Parks and Burrus, 1987; Proakis and Manolakis, 2007).

The drawback with the Euclidian distance is that it has no obvious bound value for maximum distance, merely a bound of 0 = absolute identity. Its range of values varies from 0 to some maximum possible discrepancy value which remains unknown until specifically computed. The Euclidean distance varies as a function of the magnitudes of the observations. Basically, it is unknown from the size whether a coefficient indicates a small or large distance. In order to quantify the discrepancy between the two waveforms by using Euclidian distance, we first perform a benchmark study involving a suite of original waveforms and waveforms modified by phase-shifting. Let $s(t)$ be the signal. Its analytical signal can be expressed as $s(t) = A(t)\exp[i\varphi(t)]$, with $A(t)$ being the amplitude and $i\varphi(t)$ being the phase. Then the 1.0 percent phase-shift modified signal $pm01\big(s(t)\big)$ is defined by

$$pm01\big(s(t)\big) = \mathrm{Re}[A(t)\exp(i\varphi(t) + 0.01i\pi)] \tag{4}$$

Following equation 4, acceleration, velocity, and displacement waveforms of twenty CSMIP processed records randomly selected from earthquakes listed in table 1 were used to compute Euclidian distances between the original waveforms and those with 1, 5, 10, 16.6, and 20 percent phase-shift modifications. Misfit results between original and modified waveforms are shown in figure 60 in terms of median and standard deviations of Euclidian distance plotted against phase-shift. Euclidian distance is proportional to the level of pure phase-shift modification. These results may serve as a reference for interpretation of Euclidian distance computed between PRISM and CSMIP processed records.

Another commonly used misfit criterion, RMS level (gain), (for example, Geller and Takeuchi, 1995) is also used as a metric to compare average energy of time series. The RMS level is computed as

$$x_{RMS} = \sqrt{\frac{1}{N}\sum_{i=1}^{N}(x_i)^2} \tag{5}$$

The time histories from PRISM and CSMIP V2 products were divided into four windows of equal duration, and the RMS level of each window was computed in order to differentiate the average energy levels of weak and strong motion segments of the time series. Although the Euclidian distance and RMS level are related, we used them separately to add an extra dimension to the comparisons.

In figure 61, differences in peak amplitudes between products (acceleration, velocity, and displacement time series) derived from PRISM and CSMIP processing are portrayed against PGA, PGV, and PGD amplitudes from PRISM processing for the 2005 ML5.0 Yucaipa earthquake. In this figure, different colors and symbols denote the range of differences from 0 to 4 percent, and horizontal arrows on the top panel signify overestimation or underestimation trends of PRISM processing as compared with CSMIP processing. The median percent difference is depicted by a vertical (brown) thick line for which height indicates the maximum ground-motion value of the dataset (for example, PGA, PGV, or PGD). The horizontal (red) thick line denotes ± one standard deviation of the percent difference about the median, where its height denotes the median ground-motion value of the dataset.

In figure 62, the differences are plotted against the epicenter distances of ground-motion components in order to assess whether there is a distance dependence for differences in PGA, PGV, and PGD values, but there are no obvious distance trends. In this figure, the median percent difference is shown by vertical (brown) thick line with a height indicating the maximum epicenter distance of the dataset. The horizontal (red) thick line denotes ± one standard deviation of the percent difference about the median for which height denotes the median epicenter distance of the dataset.

Figure 63 shows Euclidian distance values computed between acceleration, velocity, and displacement time series from PRISM and CSMIP processing. In this figure Euclidian distance values are plotted against epicenter distances. The lower the Euclidian distance, the smaller the overall difference in time series. Large Euclidian distance values, particularly for acceleration, are because the Euclidian distance is not a normalized parameter, and it is influenced by the overall amplitude and unit of the measure. For instance, small epicenter distances result in higher Euclidian distance values, because acceleration data in general have larger intensities close to a fault. For the same token, large magnitude events yield higher Euclidian distance values as compared with small magnitude events (as will be shown later in fig. 97). Therefore, the results presented in figure 63 and similar plots should be interpreted by considering the benchmark study in figure 60. In figure 63, the horizontal (brown) thick line indicates epicenter distance range, and its height shows the median Euclidian distance. The vertical (red) thick line denotes median epicenter distance, and its height shows ± one standard deviation of Euclidian distance about the median. The low medians as compared with the range of data, and low standard deviations indicate that the majority of the time series from PRISM and CSMIP processing are similar.

Finally, moving window RMS levels of acceleration, velocity, and displacement time series from PRISM and CSMIP processing are compared in figure 64. In this figure, diagonal lines indicate exact match of RMS level between PRISM and CSMIP products. Data are plotted in logarithmic scale to accentuate differences at low amplitudes; RMS levels less than 0.01 are not shown. RMS levels of the second and third windows are generally much higher because those windows cover the S-wave energy of the time series. First and fourth windows cover pre- and post-event segments of the signal, thus they generally have lower RMS levels. The RMS levels of different segments of processed records match well between PRISM and CSMIP. This is evident because the data points fall along the diagonal lines.

Similar results from the statistical evaluation for the remaining seven earthquakes are presented in figure 65 through figure 92. These results collectively demonstrate that the PRISM processed time series are in good agreement with those from CSMIP processing for a range of magnitude and epicenter distance.

To summarize the results for all earthquakes, histograms of absolute differences in peak amplitudes between PRISM and CSMIP are portrayed in figures 93 through 95. The differences are between 1 and 2 percent for the majority of records. For the few outliers, the disparity is as large as 10, 5, and 4 percent for PGA, PGV, and PGD, respectively.

Finally, the median and standard deviation of testing results for absolute differences in peak amplitudes are plotted in figure 96 against earthquake magnitude. Median values in general are close to zero, and there is no obvious dependence on either median or standard deviation values with respect to magnitude. In figure 97, median and standard deviation from eight earthquakes are plotted against Euclidian distance. Although the largest magnitude event (*M*6.5) has a higher median, the medians are in general close to zero for the rest of the earthquakes.

Table 2 consolidates the difference results for PGA, PGV, and PGD in terms of number of records, and figure 98 presents corresponding values as a percentage of all records. For instance, the difference in PGV values between PRISM and CSMIP processed records are within 2 percent for 96 percent of all records. Similarly, for 99 percent of all records, the difference in PGA is equal to or less than 4 percent. For PGD, 10 percent of data show differences on the order of 3 to 4 percent. We attribute this high fraction to different implementation of filtering, differentiation, and integration algorithms between PRISM and CSMIP processing. For example, in CSMIP processing, an initial long-period filter is applied to the instrument-corrected acceleration data, velocity and displacement are subsequently computed by integrating the acceleration and then filtered by using the same long-period filter (Shakal and others, 2003). In contrast, PRISM applies filtering to corrected acceleration only, and velocity and displacement are obtained by integrating the filtered acceleration.

Table 2. Number of ground-motion components within each category of percent differences in the peak amplitude of acceleration, velocity, and displacement time series derived from Processing and Review Interface for Strong Motion data (PRISM) and California Strong Motion Instrumentation Program (CSMIP) processing.

| | Percent difference ([\|CSMIP–PRISM\|×100/CSMIP)] | | | | |
|---|---|---|---|---|---|
| Intensity Measure | 0–1 | 1–2 | 2–3 | 3–4 | >4–10 |
| Peak ground acceleration | 1,451 | 215 | 80 | 63 | 13 |
| Peak ground velocity | 1,709 | 86 | 13 | 1 | 13 |
| Peak ground displacement | 1,298 | 252 | 76 | 196 | 0 |

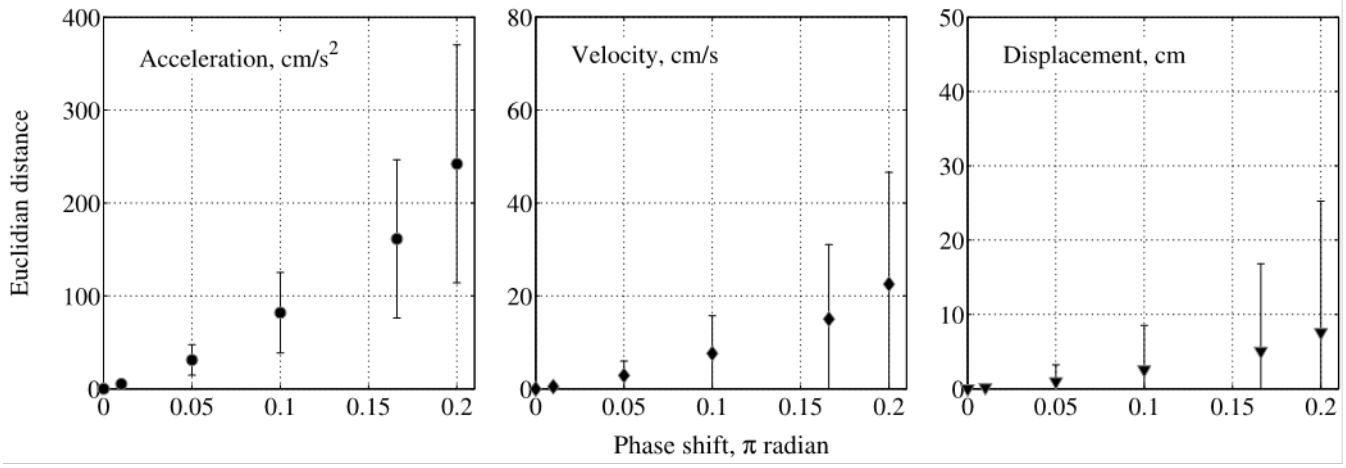


Figure 60. Graphs showing medians and standard deviations of Euclidian distance between identical waveforms with 1, 5, 10, 16.6, and 20 percent phase-shift modifications. Data correspond to randomly selected twenty California Strong Motion Instrumentation Program (CSMIP) processed acceleration, velocity, and displacement time series from eight earthquakes listed in table 1. cm, centimeters; cm/s, centimeters per second; cm/s$^2$, centimeters per second squared.

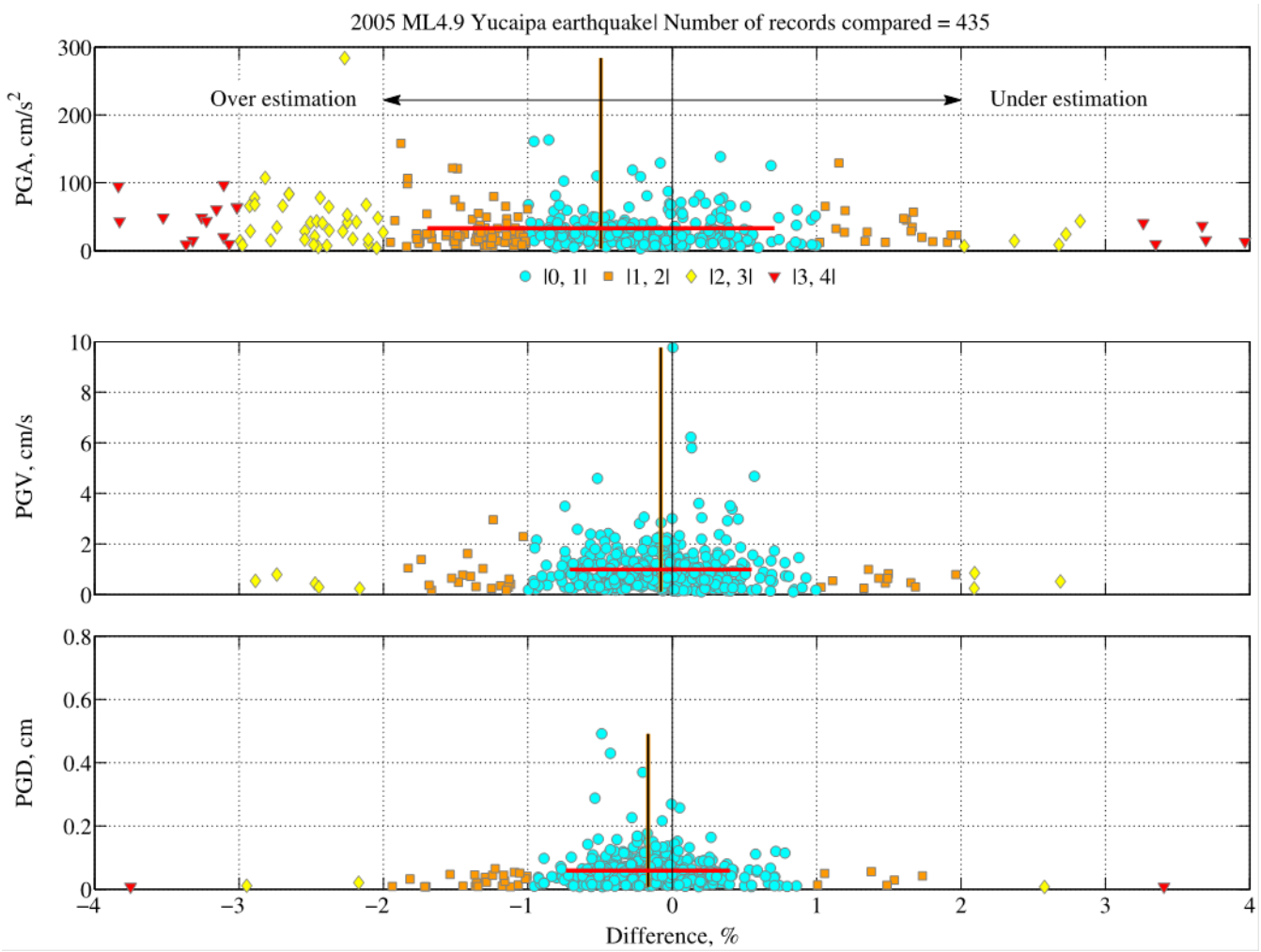


Figure 61. Graphs showing percent differences [(CSMIP - PRISM)*100/CSMIP] in peak ground acceleration (PGA), peak ground velocity (PGV), and peak ground displacement (PGD) of acceleration, velocity, and displacement time series obtained by using Processing and Review Interface for Strong Motion data (PRISM) and California Strong Motion Instrumentation Program (CSMIP) processing. Data include 435 ground-motion components of the 2005 ML4.9 Yucaipa earthquake in California. Color and symbols indicate range of differences within 1 percent bins; for example |0, 1| denotes percent difference between 0 and 1 or between −1 and 0. Horizontal arrows on top panel indicate overestimation or underestimation trends. Median percent difference is shown by vertical (brown) thick line with a height indicating maximum ground-motion value of dataset (for example, PGA, PGV, or PGD). Horizontal (red) thick line denotes ± one standard deviation of percent difference about the median for which height denotes median ground-motion value of dataset. Number of outliers from plot ranges are indicated in table 2. cm, centimeters; cm/s, centimeters per second; cm/s$^2$, centimeters per second squared; ML, local magnitude.

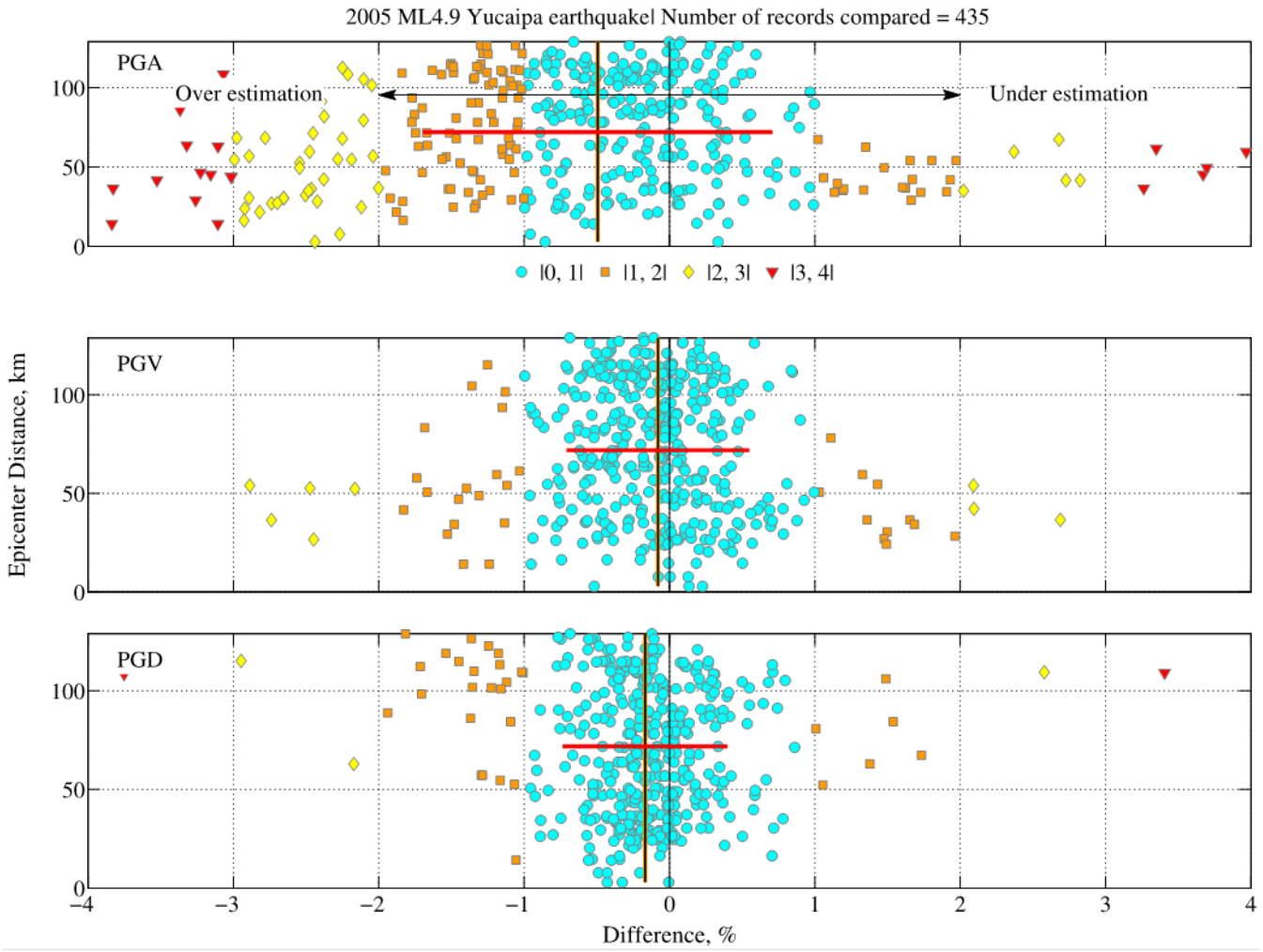


Figure 62. Graphs showing percent differences [(CSMIP−PRISM)×100/CSMIP] in peak ground acceleration (PGA), peak ground velocity (PGV), and peak ground displacement (PGD) of acceleration, velocity, and displacement time series obtained by using Processing and Review Interface for Strong Motion data (PRISM) and California Strong Motion Instrumentation Program (CSMIP) processing against epicenter distances. Data include 435 ground-motion components of the 2005 ML4.9 Yucaipa earthquake in California. Color and symbols indicate range of differences within 1 percent bins; for example |0, 1| denotes percent difference between 0 and 1 or between −1 and 0. Horizontal arrows on top panel indicate overestimation or underestimation trends. Median percent difference is shown by vertical (brown) thick line with a height indicating maximum epicenter distance of dataset. Horizontal (red) thick line denotes ± one standard deviation of percent difference about the median for which height denotes median epicenter distance of dataset. Number of outliers from plot ranges are indicated in table 2. cm, centimeters; cm/s, centimeters per second; $cm/s^2$, centimeters per second squared; ML, local magnitude.

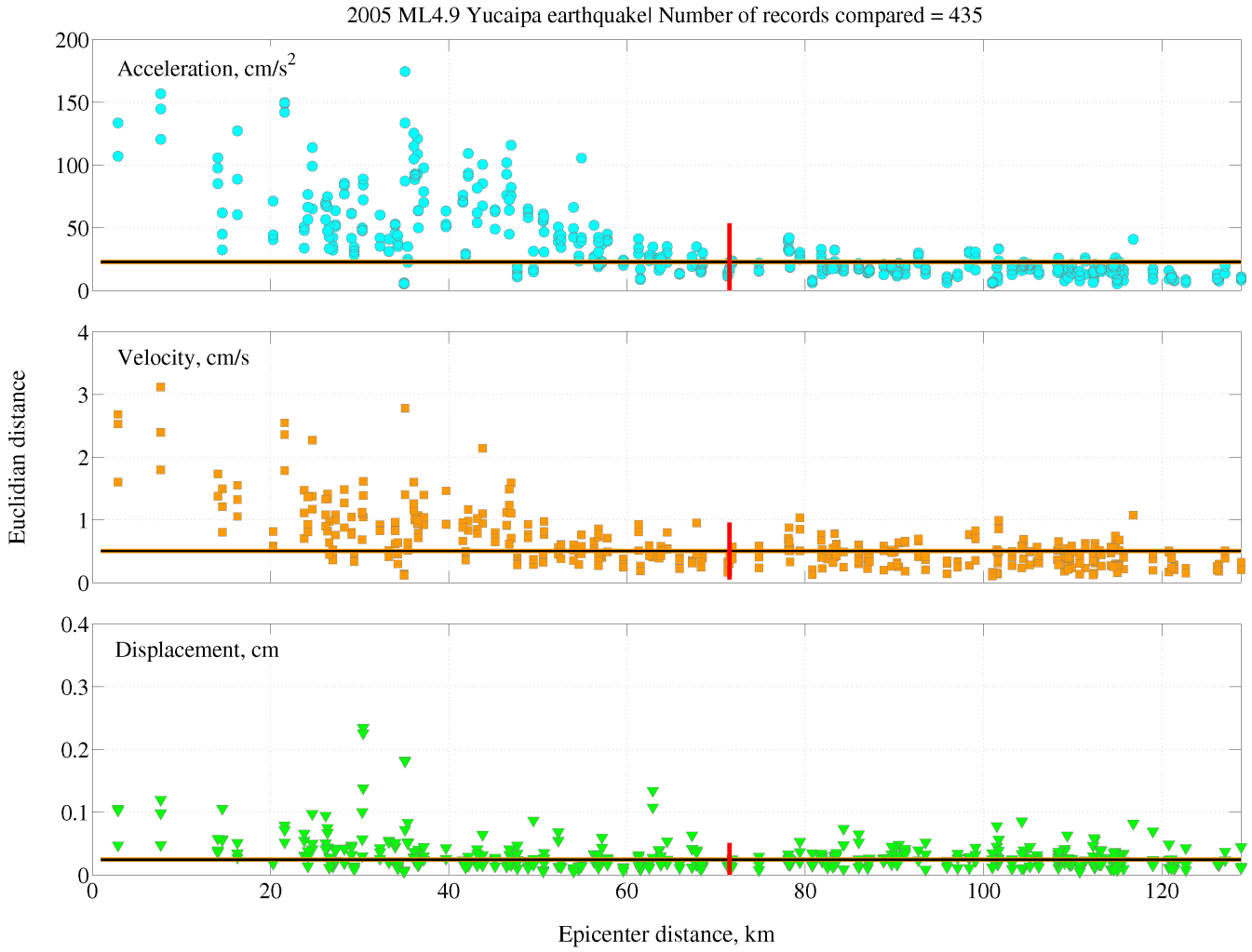


Figure 63. Graphs showing Euclidian distance as a similarity measure between acceleration, velocity, and displacement time series obtained by using Processing and Review Interface for Strong Motion data (PRISM) and California Strong Motion Instrumentation Program (CSMIP) processing against epicenter distances. Data include 435 ground-motion components of the 2005 ML4.9 Yucaipa earthquake in California. Horizontal (brown) thick line indicates epicenter distance range for which height shows median Euclidian distance. Vertical (red) thick line denotes median epicenter distance with a height that shows ± one standard deviation of Euclidian distance about the median. cm, centimeters; cm/s, centimeters per second; cm/s$^2$, centimeters per second squared; km, kilometers; ML, local magnitude.

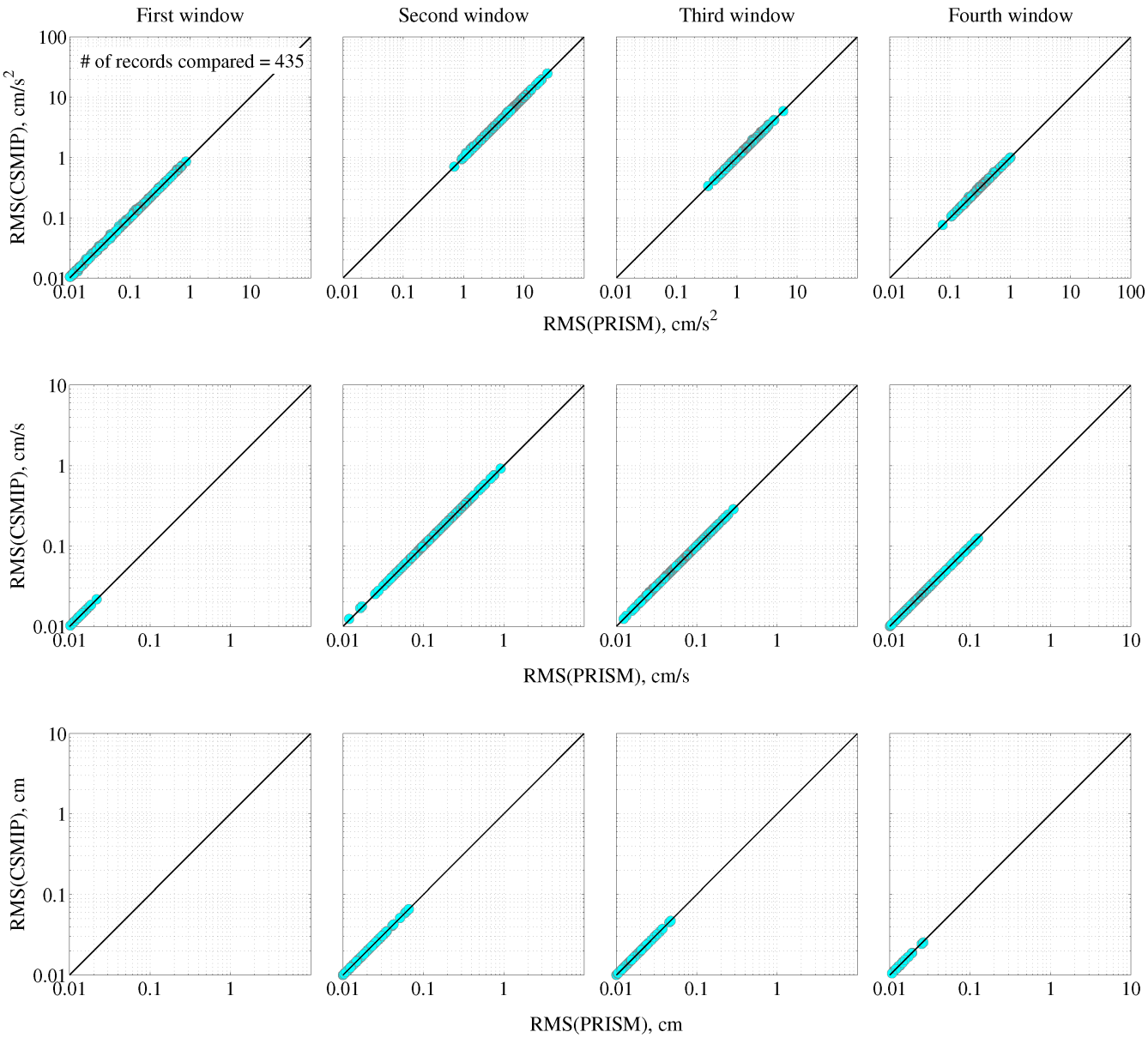


Figure 64. Graphs showing correlation of moving window root mean square (RMS) levels of acceleration (top row), velocity (middle row), and displacement (bottom row) time series obtained by using Processing and Review Interface for Strong Motion data (PRISM) and California Strong Motion Instrumentation Program (CSMIP) processing. Data include 435 ground-motion components of the 2005 *M*L4.9 Yucaipa earthquake in California. Diagonal black line indicates a perfect match in RMS level between products. For RMS computation, ground-motion waveforms were divided into four equal-length windows without overlap (RMS values less than 0.01 are not shown). cm, centimeters; cm/s, centimeters per second; cm/s$^2$, centimeters per second squared.

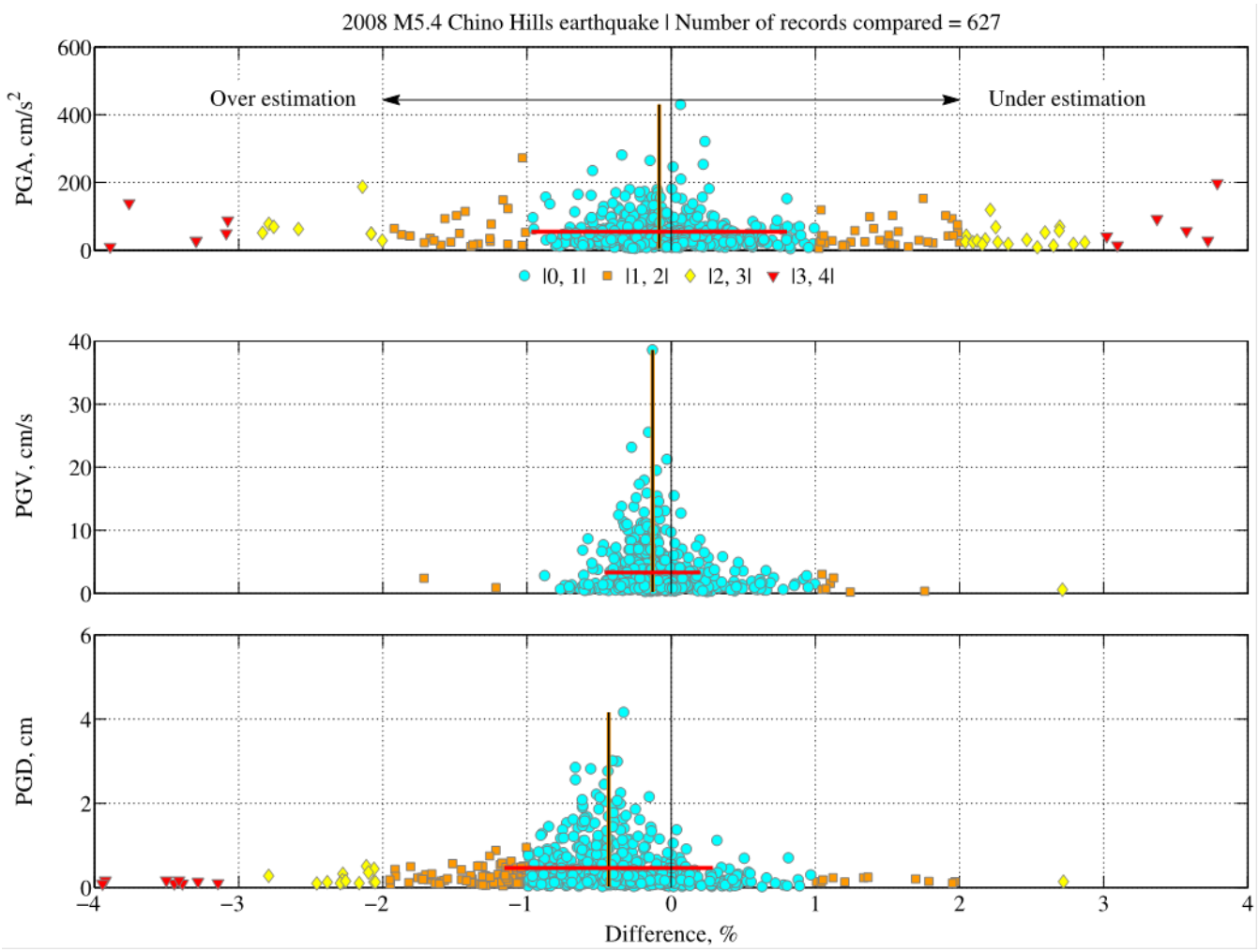


Figure 65. Graphs showing percent differences [(CSMIP−PRISM)×100/CSMIP] in peak ground acceleration (PGA), peak ground velocity (PGV), and peak ground displacement (PGD) of acceleration, velocity, and displacement time series obtained by using Processing and Review Interface for Strong Motion data (PRISM) and California Strong Motion Instrumentation Program (CSMIP) processing. Data include 627 ground-motion components of the 2008 *M*5.4 Chino Hills earthquake in California. Color and symbols indicate range of differences within 1 percent bins; for example |0, 1| denotes percent difference between 0 and 1 or between −1 and 0. Horizontal arrows on top panel indicate overestimation or underestimation trends. Median percent difference is shown by vertical (brown) thick line with a height indicating maximum ground-motion value of dataset (for example, PGA, PGV, or PGD). Horizontal (red) thick line denotes ± one standard deviation of percent difference about the median for which height denotes median ground-motion value of dataset. Number of outliers from plot ranges are indicated in table 2. cm, centimeters; cm/s, centimeters per second; cm/s$^2$, centimeters per second squared; *M*, moment magnitude.

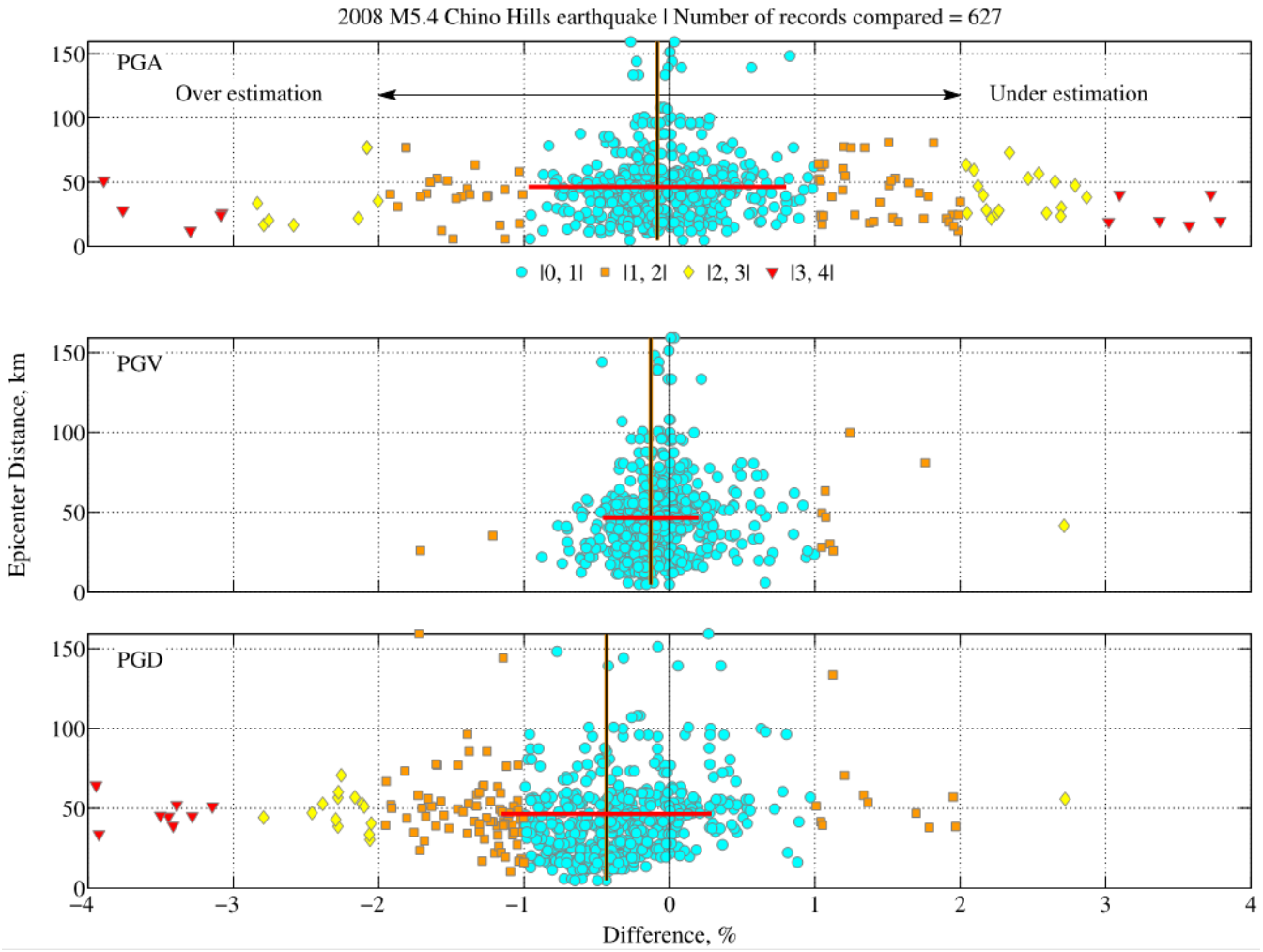


Figure 66. Graphs showing percent differences [(CSMIP−PRISM)×100/CSMIP] in peak ground acceleration (PGA), peak ground velocity (PGV), and peak ground displacement (PGD) of acceleration, velocity, and displacement time series obtained by using Processing and Review Interface for Strong Motion data (PRISM) and California Strong Motion Instrumentation Program (CSMIP) processing against epicenter distances. Data include 627 ground-motion components of the 2008 *M*5.4 Chino Hills earthquake in California. Color and symbols indicate range of differences within 1 percent bins; for example |0, 1| denotes percent difference between 0 and 1 or between −1 and 0. Horizontal arrows on top panel indicate overestimation or underestimation trends. Median percent difference is shown by vertical (brown) thick line with a height indicating maximum epicenter distance of dataset. Horizontal (red) thick line denotes ± one standard deviation of percent difference about the median for which height denotes median epicenter distance of dataset. Number of outliers from plot ranges are indicated in table 2. km, kilometers; *M*, moment magnitude.

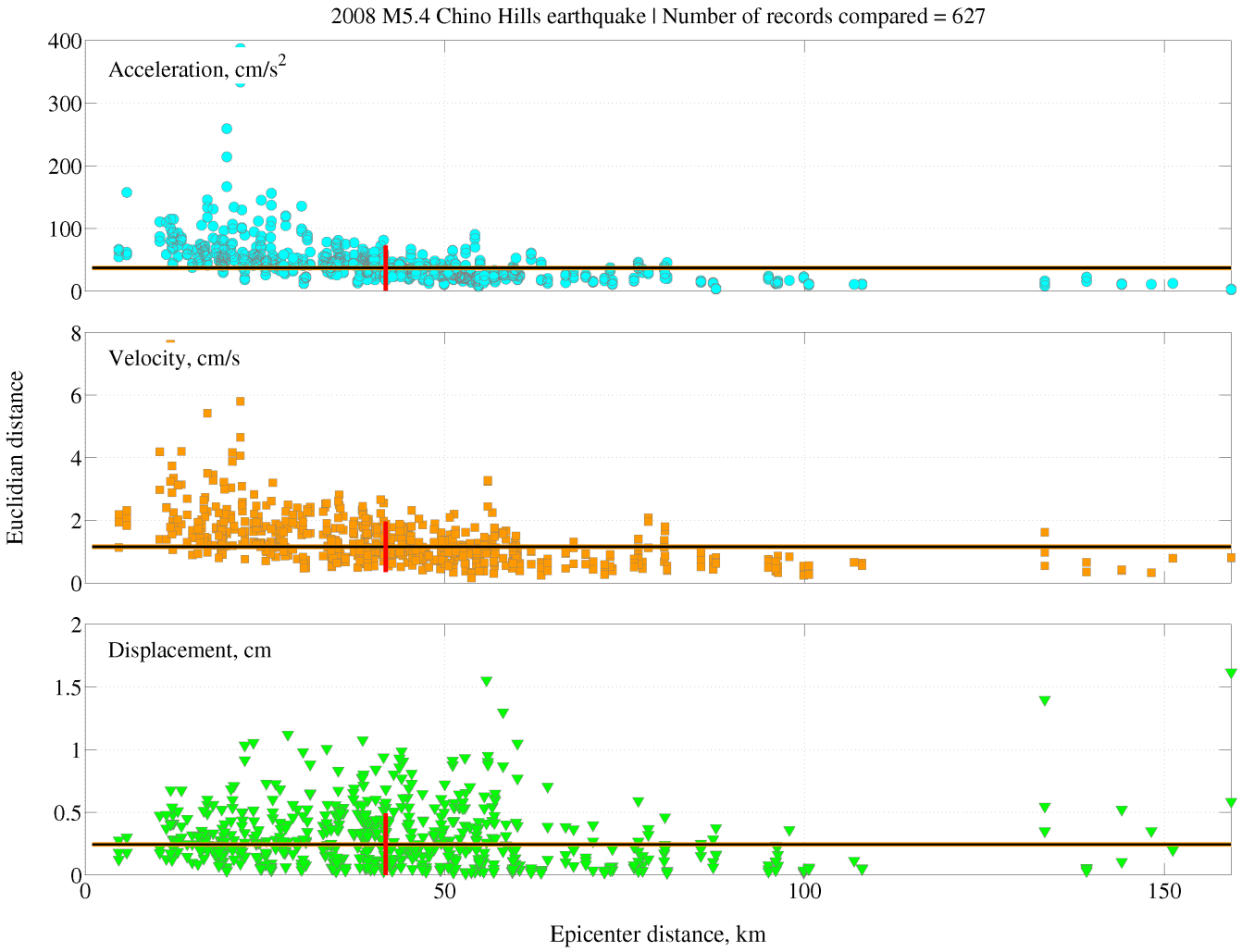


Figure 67. Graphs showing Euclidian distance as a similarity measure between acceleration, velocity, and displacement time series obtained by using Processing and Review Interface for Strong Motion data (PRISM) and California Strong Motion Instrumentation Program (CSMIP) processing against epicenter distances. Data include 627 ground-motion components of the 2008 *M*5.4 Chino Hills earthquake in California. Horizontal (brown) thick line indicates epicenter distance range for which height shows median Euclidian distance. Vertical (red) thick line denotes median epicenter distance with a height that shows ± one standard deviation of Euclidian distance about the median. cm, centimeters; cm/s, centimeters per second; cm/s$^2$, centimeters per second squared; *M*, moment magnitude.

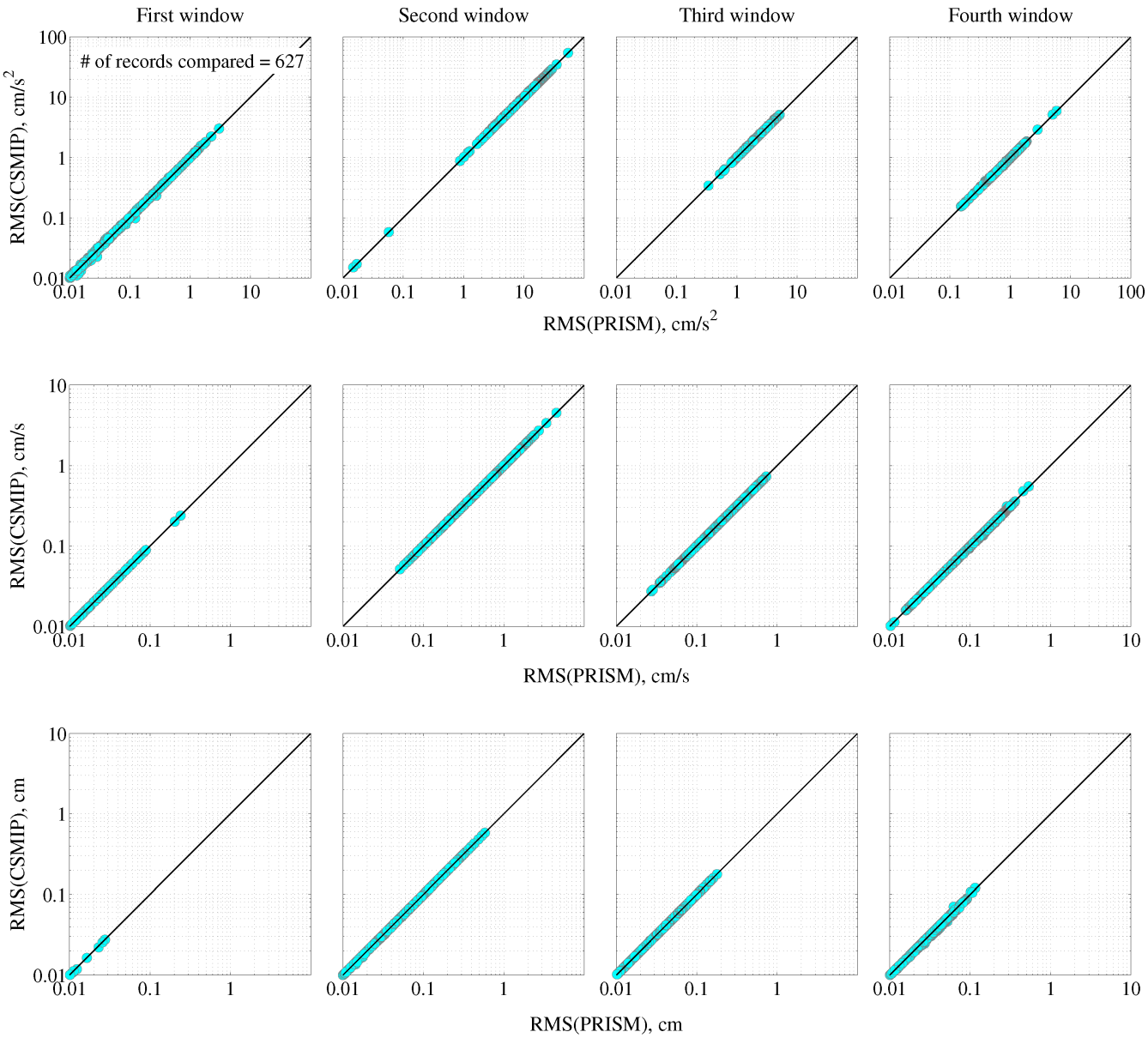


Figure 68. Graphs showing correlation of moving window root mean square (RMS) levels of acceleration (top row), velocity (middle row), and displacement (bottom row) time series obtained by using Processing and Review Interface for Strong Motion data (PRISM) and California Strong Motion Instrumentation Program (CSMIP) processing. Data include 627 ground-motion components of the 2008 *M*5.4 Chino Hills earthquake in California. Diagonal black line indicates a perfect match in RMS level between products. For RMS computation, ground-motion waveforms were divided into four equal-length windows without overlap (RMS values less than 0.01 are not shown). cm, centimeters; cm/s, centimeters per second; cm/s$^2$, centimeters per second squared.

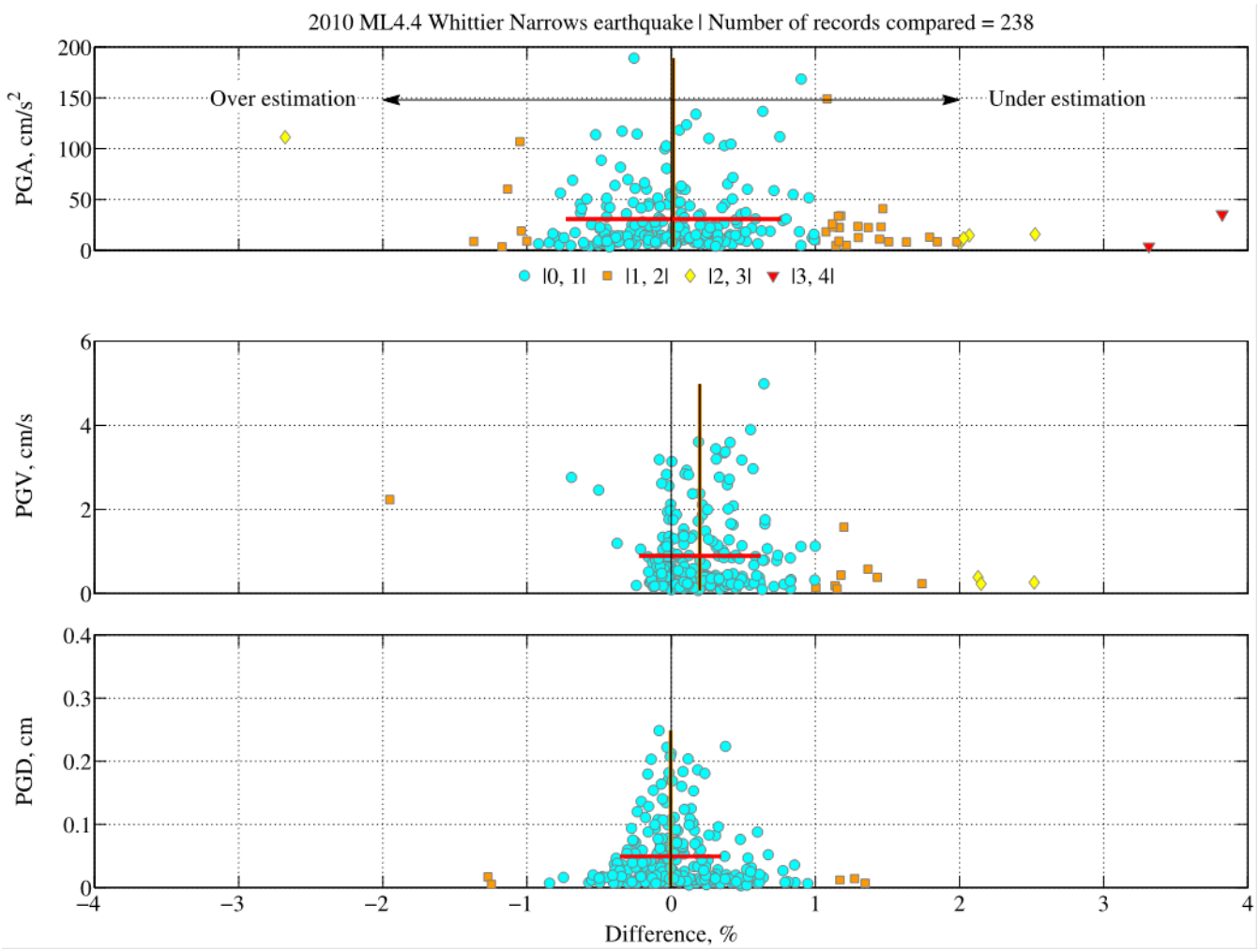


Figure 69. Graphs showing percent differences [(CSMIP−PRISM)×100/CSMIP] in peak ground acceleration (PGA), peak ground velocity (PGV), and peak ground displacement (PGD) of acceleration, velocity, and displacement time series obtained by using Processing and Review Interface for Strong Motion data (PRISM) and California Strong Motion Instrumentation Program (CSMIP) processing. Data include 238 ground-motion components of the 2010 ML4.4 Whittier Narrows earthquake in California. Color and symbols indicate range of differences within 1 percent bins; for example |0, 1| denotes percent difference between 0 and 1 or between −1 and 0. Horizontal arrows on top panel indicate overestimation or underestimation trends. Median percent difference is shown by vertical (brown) thick line with a height indicating maximum ground-motion value of dataset (for example, PGA, PGV, or PGD). Horizontal (red) thick line denotes ± one standard deviation of percent difference about the median for which height denotes median ground-motion value of dataset. Number of outliers from plot ranges are indicated in table 2. cm, centimeters; cm/s, centimeters per second; cm/s$^2$, centimeters per second squared; ML, local magnitude.

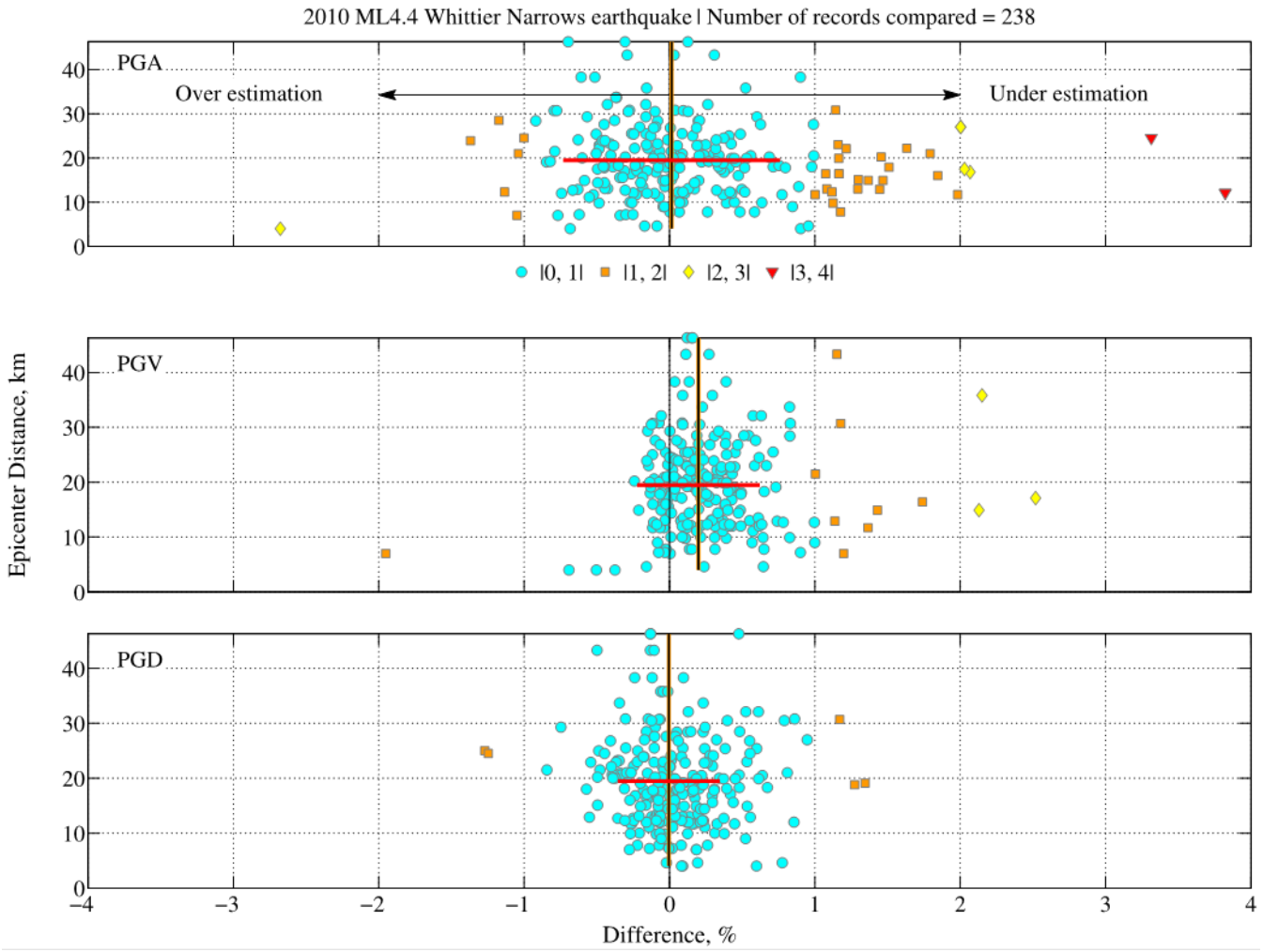


Figure 70. Graphs showing percent differences [(CSMIP−PRISM)×100/CSMIP] in peak ground acceleration (PGA), peak ground velocity (PGV), and peak ground displacement (PGD) of acceleration, velocity, and displacement time series obtained by using Processing and Review Interface for Strong Motion data (PRISM) and California Strong Motion Instrumentation Program (CSMIP) processing against epicenter distances. Data include 238 ground-motion components of the 2010 ML4.4 Whittier Narrows earthquake in California. Color and symbols indicate range of differences within 1 percent bins; for example |0, 1| denotes percent difference between 0 and 1 or between −1 and 0. Horizontal arrows on top panel indicate overestimation or underestimation trends. Median percent difference is shown by vertical (brown) thick line with a height indicating maximum epicenter distance of dataset. Horizontal (red) thick line denotes ± one standard deviation of percent difference about the median for which height denotes median epicenter distance of dataset. Number of outliers from plot ranges are indicated in table 2. km, kilometers; ML, local magnitude.

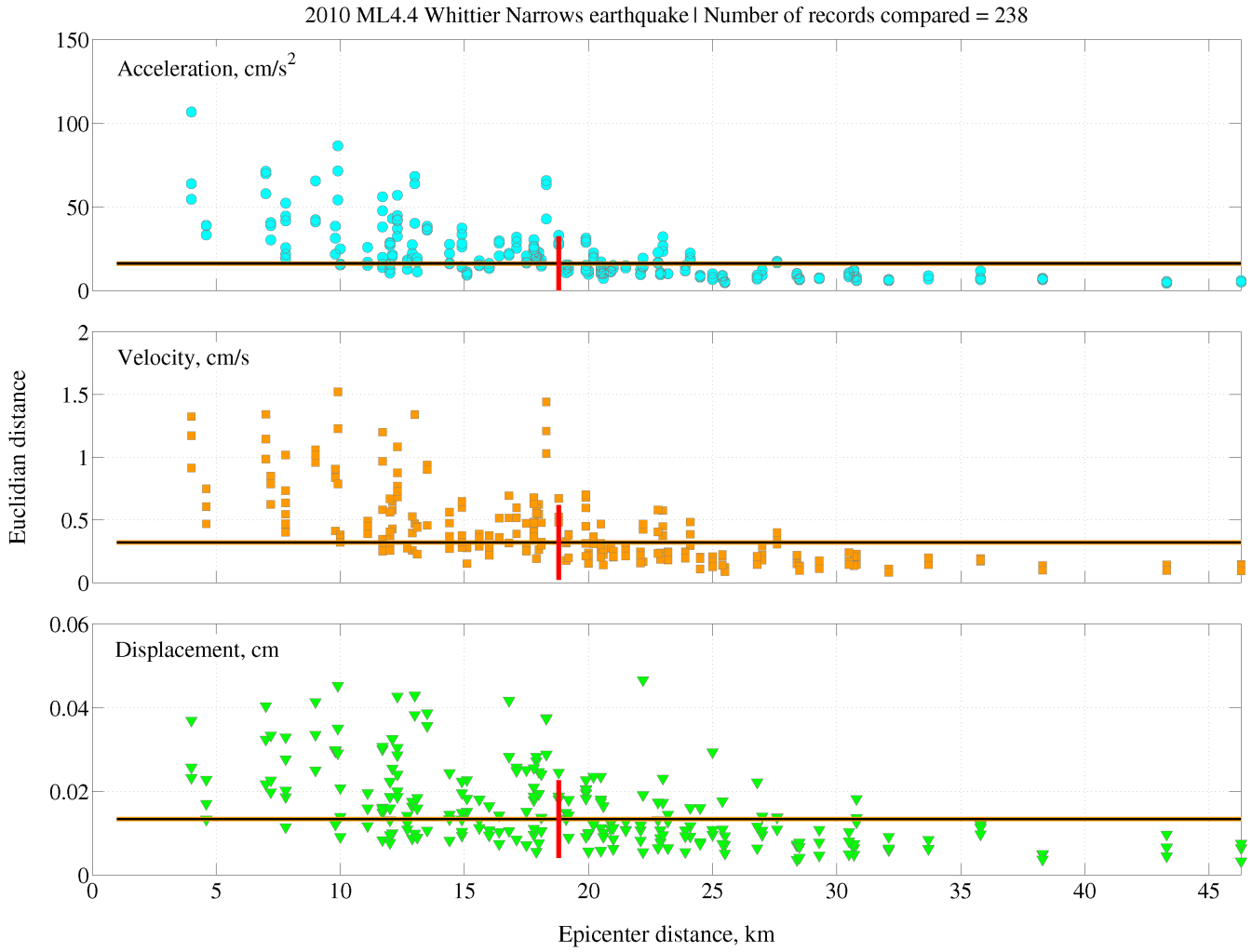


Figure 71. Graphs showing Euclidian distance as a similarity measure between acceleration, velocity, and displacement time series obtained by using Processing and Review Interface for Strong Motion data (PRISM) and California Strong Motion Instrumentation Program (CSMIP) processing against epicenter distances. Data include 238 ground-motion components of the 2010 ML4.4 Whittier Narrows earthquake in California. Horizontal (brown) thick line indicates epicenter distance range for which height shows median Euclidian distance. Vertical (red) thick line denotes median epicenter distance with a height that shows ± one standard deviation of Euclidian distance about the median. cm, centimeters; cm/s, centimeters per second; cm/s$^2$, centimeters per second squared; km, kilometers; ML, local magnitude.

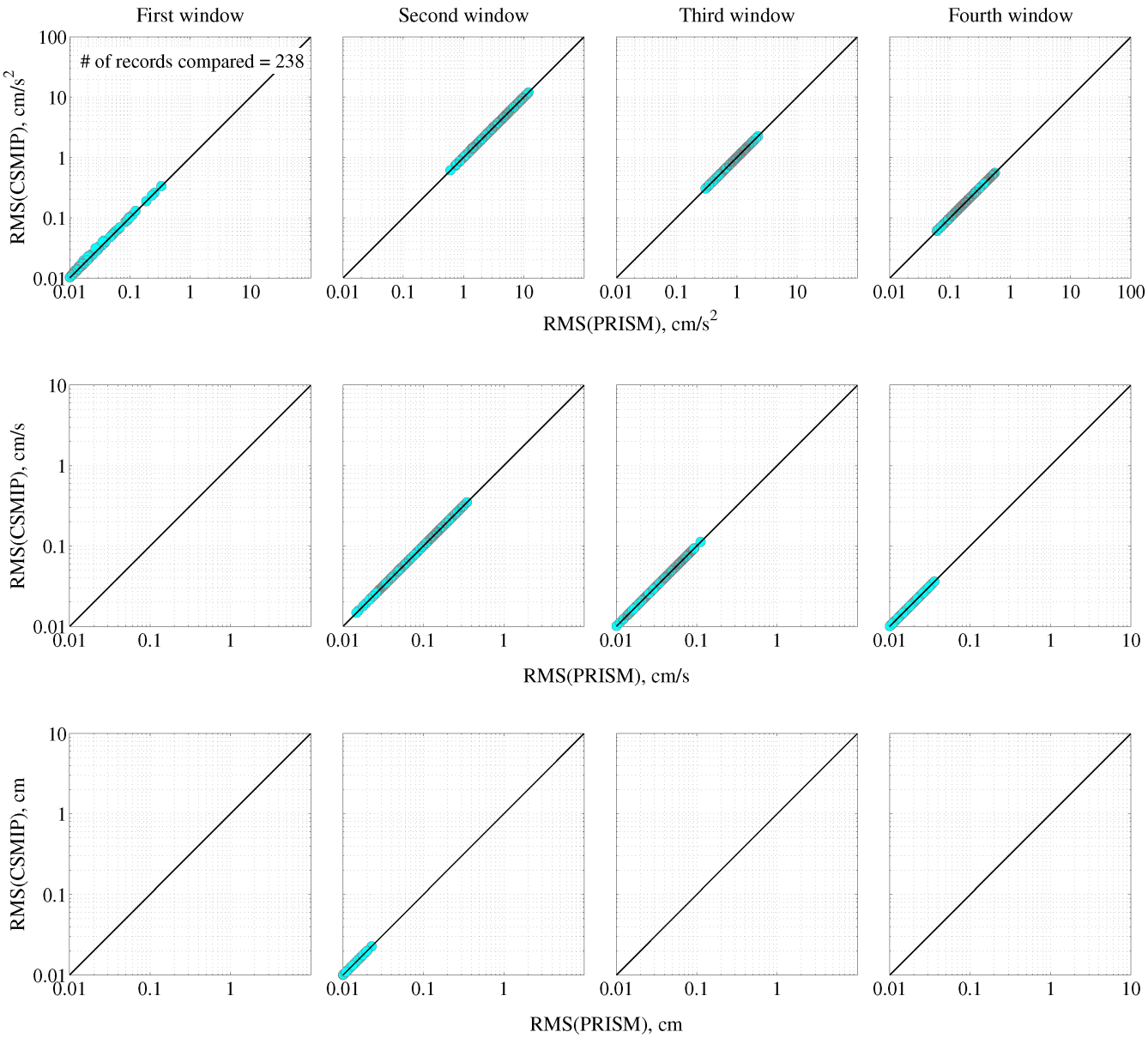


Figure 72. Graphs showing correlation of moving window root mean square (RMS) levels of acceleration (top row), velocity (middle row), and displacement (bottom row) time series obtained by using Processing and Review Interface for Strong Motion data (PRISM) and California Strong Motion Instrumentation Program (CSMIP) processing. Data include 238 ground-motion components of the 2010 ML4.4 Whittier Narrows earthquake in California. Diagonal black line indicates a perfect match in RMS level between products. For RMS computation, ground-motion waveforms were divided into four equal-length windows without overlap (RMS values less than 0.01 are not shown). cm, centimeters; cm/s, centimeters per second; $cm/s^2$, centimeters per second squared.

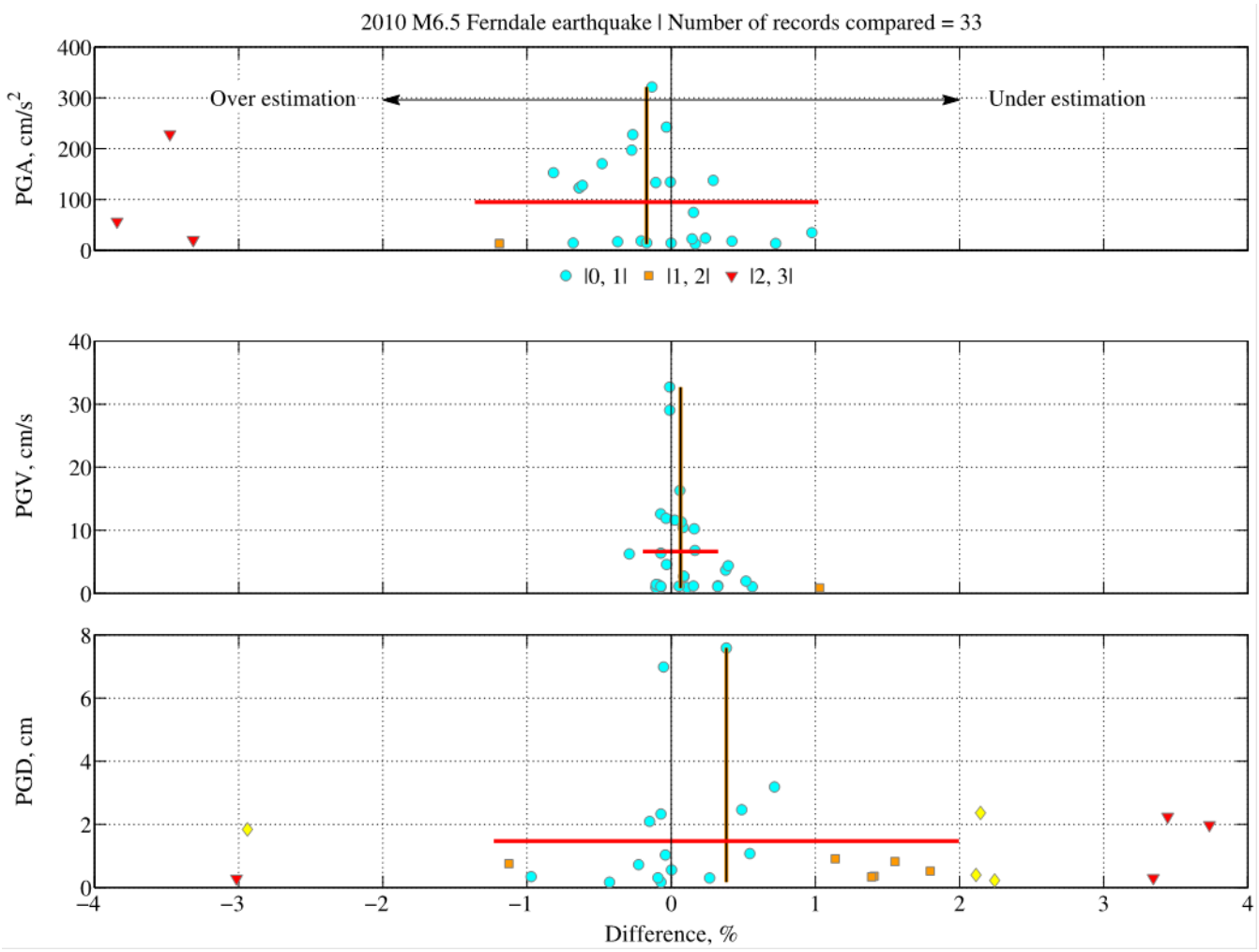


Figure 73. Graphs showing percent differences [(CSMIP−PRISM)×100/CSMIP] in peak ground acceleration (PGA), peak ground velocity (PGV), and peak ground displacement (PGD) of acceleration, velocity, and displacement time series obtained by using Processing and Review Interface for Strong Motion data (PRISM) and California Strong Motion Instrumentation Program (CSMIP) processing. Data include 33 ground-motion components of the 2010 *M*6.5 Ferndale earthquake in California. Color and symbols indicate range of differences within 1 percent bins; for example |0, 1| denotes percent difference between 0 and 1 or between −1 and 0. Horizontal arrows on top panel indicate overestimation or underestimation trends. Median percent difference is shown by vertical (brown) thick line with a height indicating maximum ground-motion value of dataset (for example, PGA, PGV, or PGD). Horizontal (red) thick line denotes ± one standard deviation of percent difference about the median for which height denotes median ground-motion value of dataset. Number of outliers from plot ranges are indicated in table 2. cm, centimeters; cm/s, centimeters per second; cm/s$^2$, centimeters per second squared; *M*, moment magnitude.

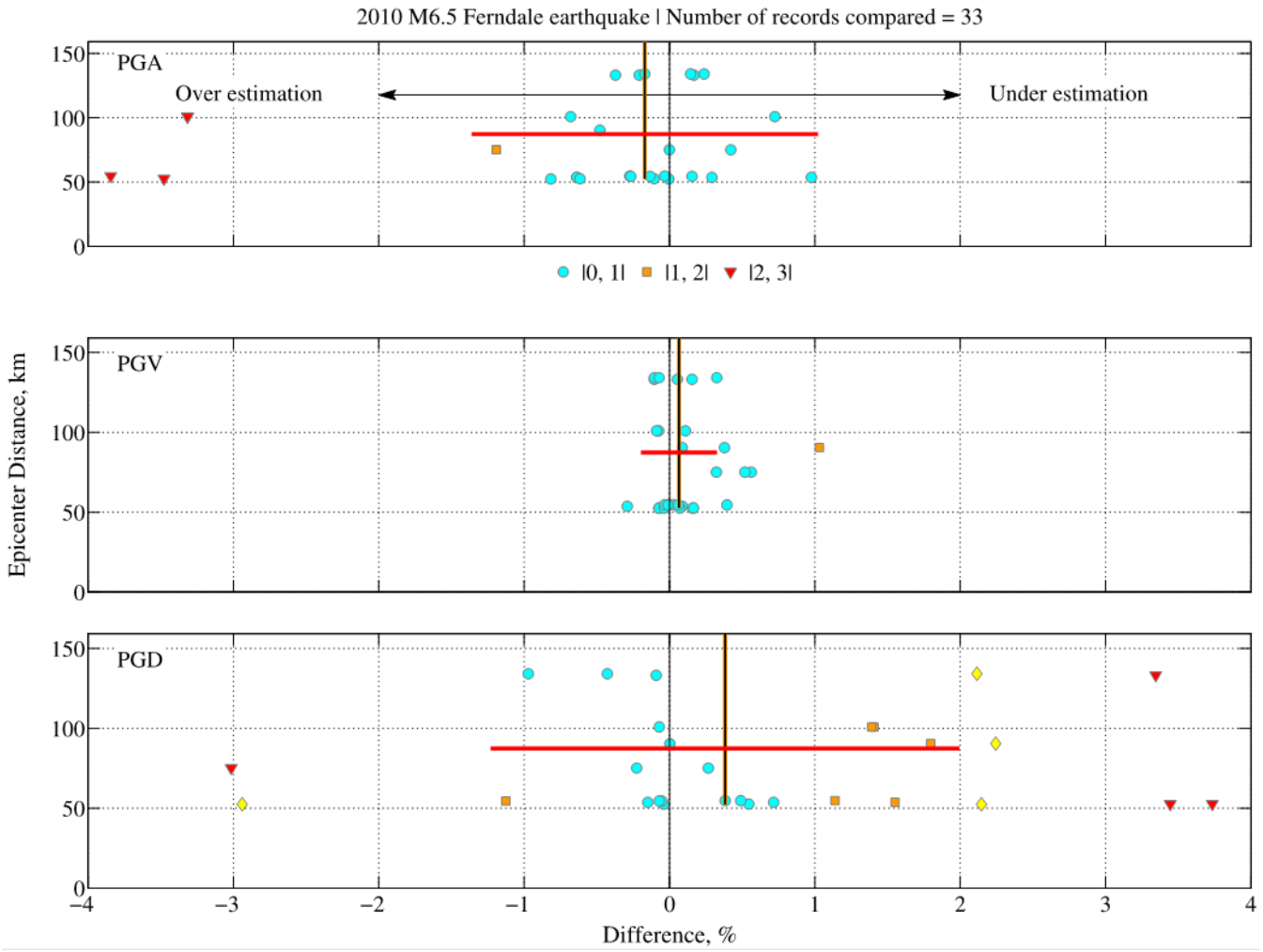


Figure 74. Graphs showing percent differences [(CSMIP−PRISM)×100/CSMIP] in peak ground acceleration (PGA), peak ground velocity (PGV), and peak ground displacement (PGD) of acceleration, velocity, and displacement time series obtained by using Processing and Review Interface for Strong Motion data (PRISM) and California Strong Motion Instrumentation Program (CSMIP) processing against epicenter distances. Data include 33 ground-motion components of the 2010 *M*6.5 Ferndale earthquake in California. Color and symbols indicate range of differences within 1 percent bins; for example |0, 1| denotes percent difference between 0 and 1 or between −1 and 0. Horizontal arrows on top panel indicate overestimation or underestimation trends. Median percent difference is shown by vertical (brown) thick line with a height indicating maximum epicenter distance of dataset. Horizontal (red) thick line denotes ± one standard deviation of percent difference about the median for which height denotes median epicenter distance of dataset. Number of outliers from plot ranges are indicated in table 2. km, kilometers; *M*, moment magnitude.

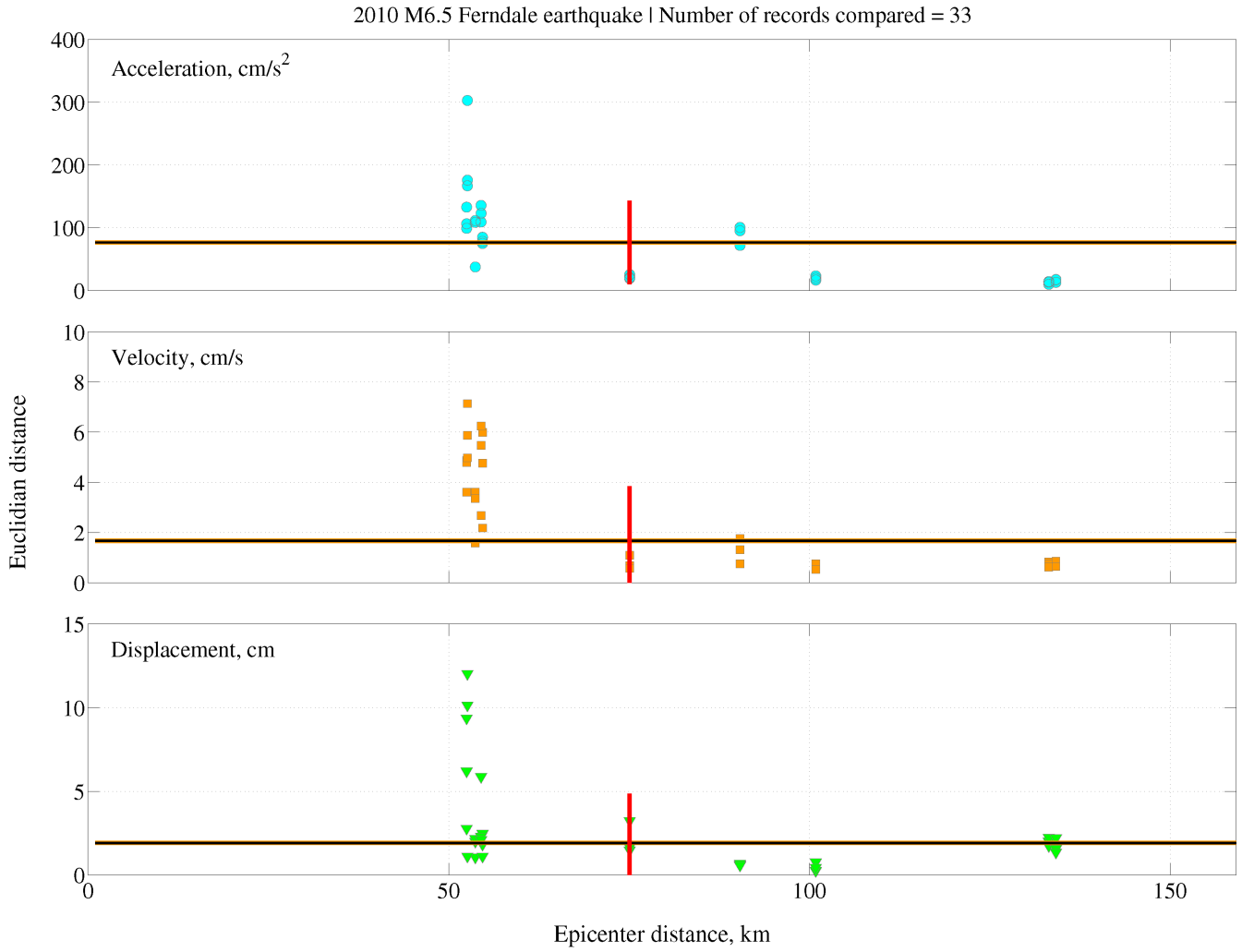


Figure 75. Graphs showing Euclidian distance as a similarity measure between acceleration, velocity, and displacement time series obtained by using Processing and Review Interface for Strong Motion data (PRISM) and California Strong Motion Instrumentation Program (CSMIP) processing against epicenter distances. Data include 33 ground-motion components of the 2010 *M*6.5 Ferndale earthquake in California. Horizontal (brown) thick line indicates epicenter distance range for which height shows median Euclidian distance. Vertical (red) thick line denotes median epicenter distance with a height that shows ± one standard deviation of Euclidian distance about the median. cm, centimeters; cm/s, centimeters per second; cm/s$^2$, centimeters per second squared; km, kilometers; *M*, moment magnitude.

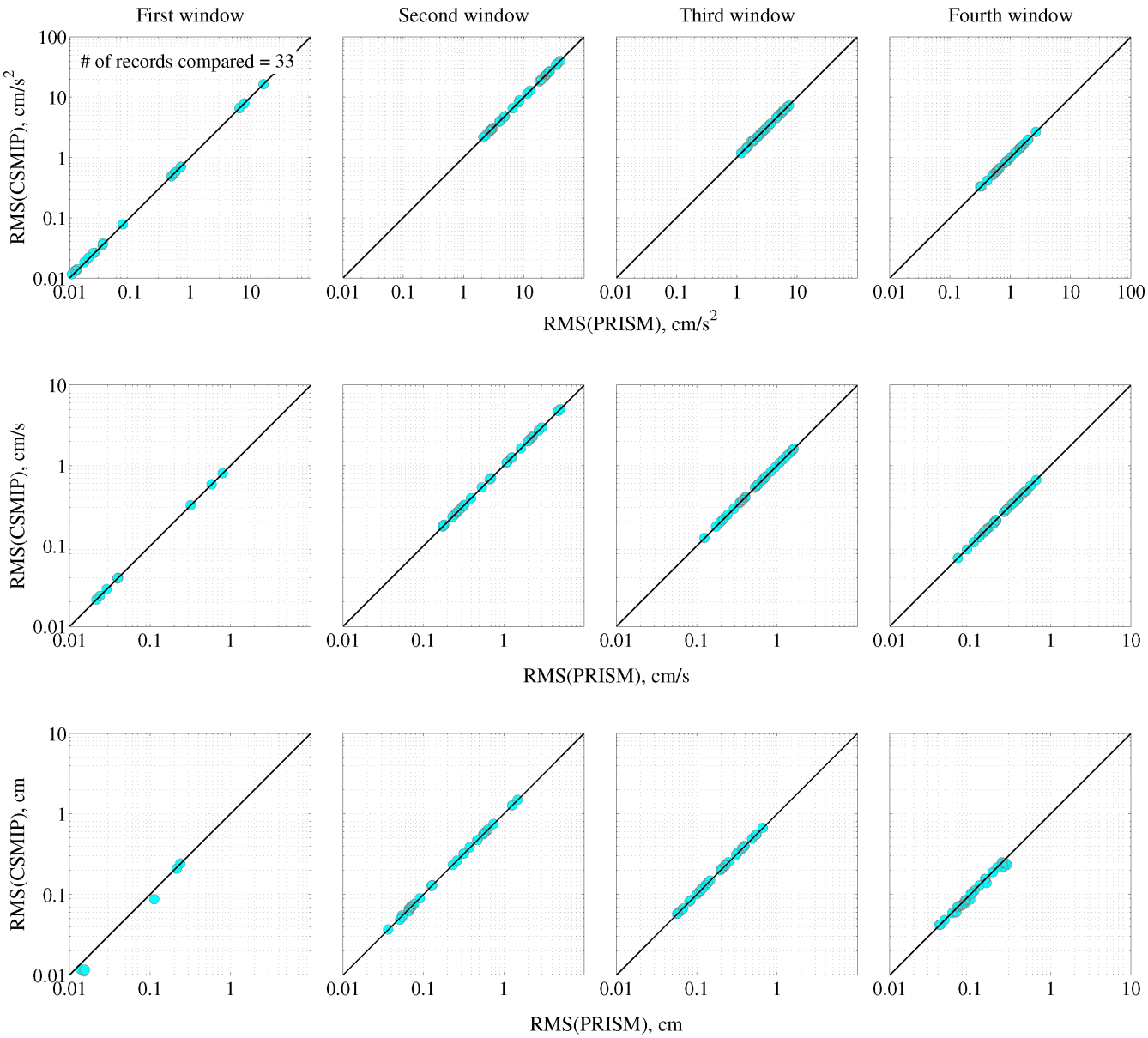


Figure 76. Graphs showing correlation of moving window root mean square (RMS) levels of acceleration (top row), velocity (middle row), and displacement (bottom row) time series obtained by using Processing and Review Interface for Strong Motion data (PRISM) and California Strong Motion Instrumentation Program (CSMIP) processing. Data include 33 ground-motion components of the 2010 *M*6.5 Ferndale earthquake in California. Diagonal black line indicates a perfect match in RMS level between products. For RMS computation, ground-motion waveforms were divided into four equal-length windows without overlap (RMS values less than 0.01 are not shown). cm, centimeters; cm/s, centimeters per second; cm/s$^2$, centimeters per second squared.

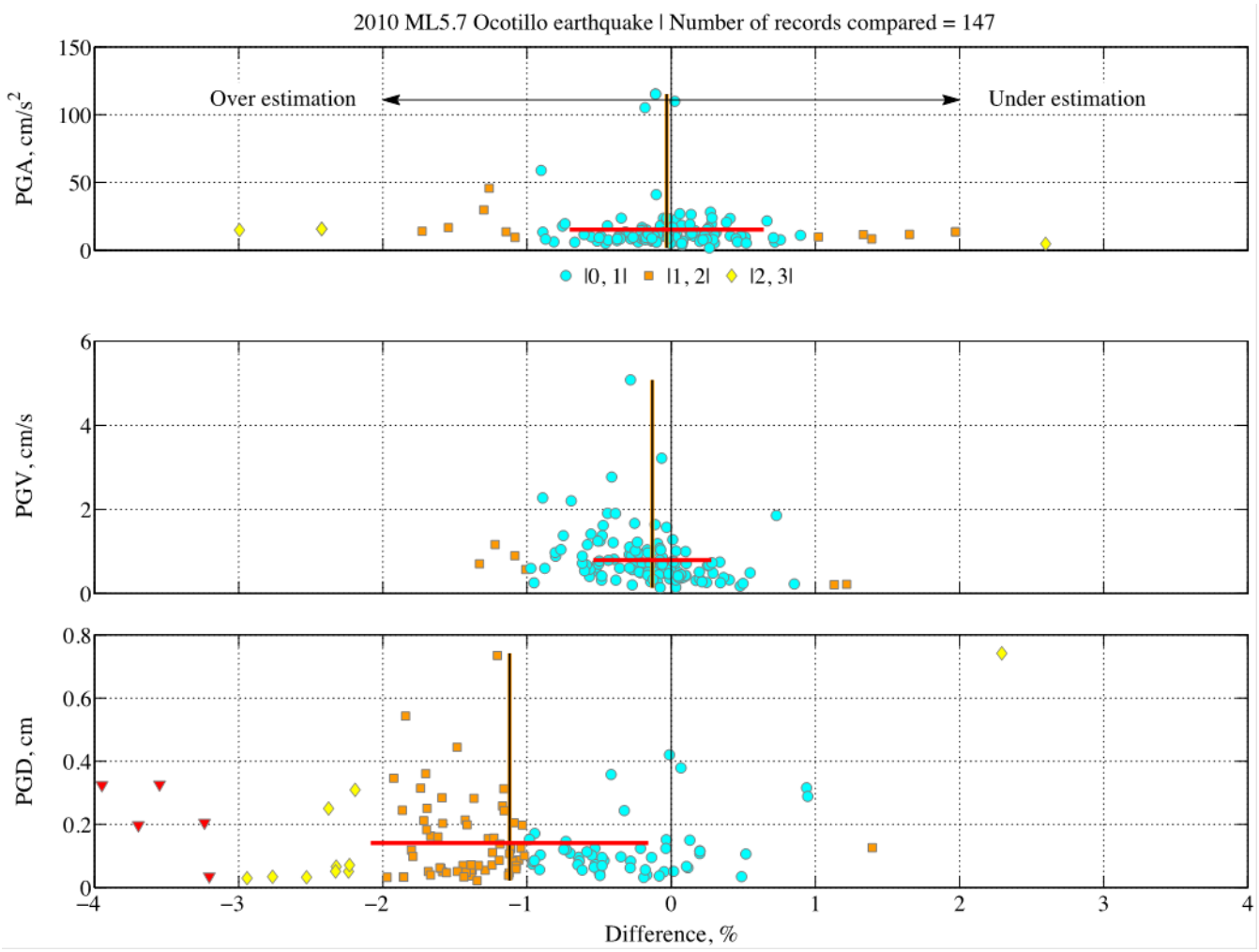


Figure 77. Graphs showing percent differences [(CSMIP−PRISM)×100/CSMIP] in peak ground acceleration (PGA), peak ground velocity (PGV), and peak ground displacement (PGD) of acceleration, velocity, and displacement time series obtained by using Processing and Review Interface for Strong Motion data (PRISM) and California Strong Motion Instrumentation Program (CSMIP) processing. Data include 147 ground-motion components of the 2010 ML5.7 Ocotillo earthquake in California. Color and symbols indicate range of differences within 1 percent bins; for example |0, 1| denotes percent difference between 0 and 1 or between −1 and 0. Horizontal arrows on top panel indicate overestimation or underestimation trends. Median percent difference is shown by vertical (brown) thick line with a height indicating maximum ground-motion value of dataset (for example, PGA, PGV, or PGD). Horizontal (red) thick line denotes ± one standard deviation of percent difference about the median for which height denotes median ground-motion value of dataset. Number of outliers from plot ranges are indicated in table 2. cm, centimeters; cm/s, centimeters per second; cm/s$^2$, centimeters per second squared; ML, local magnitude.

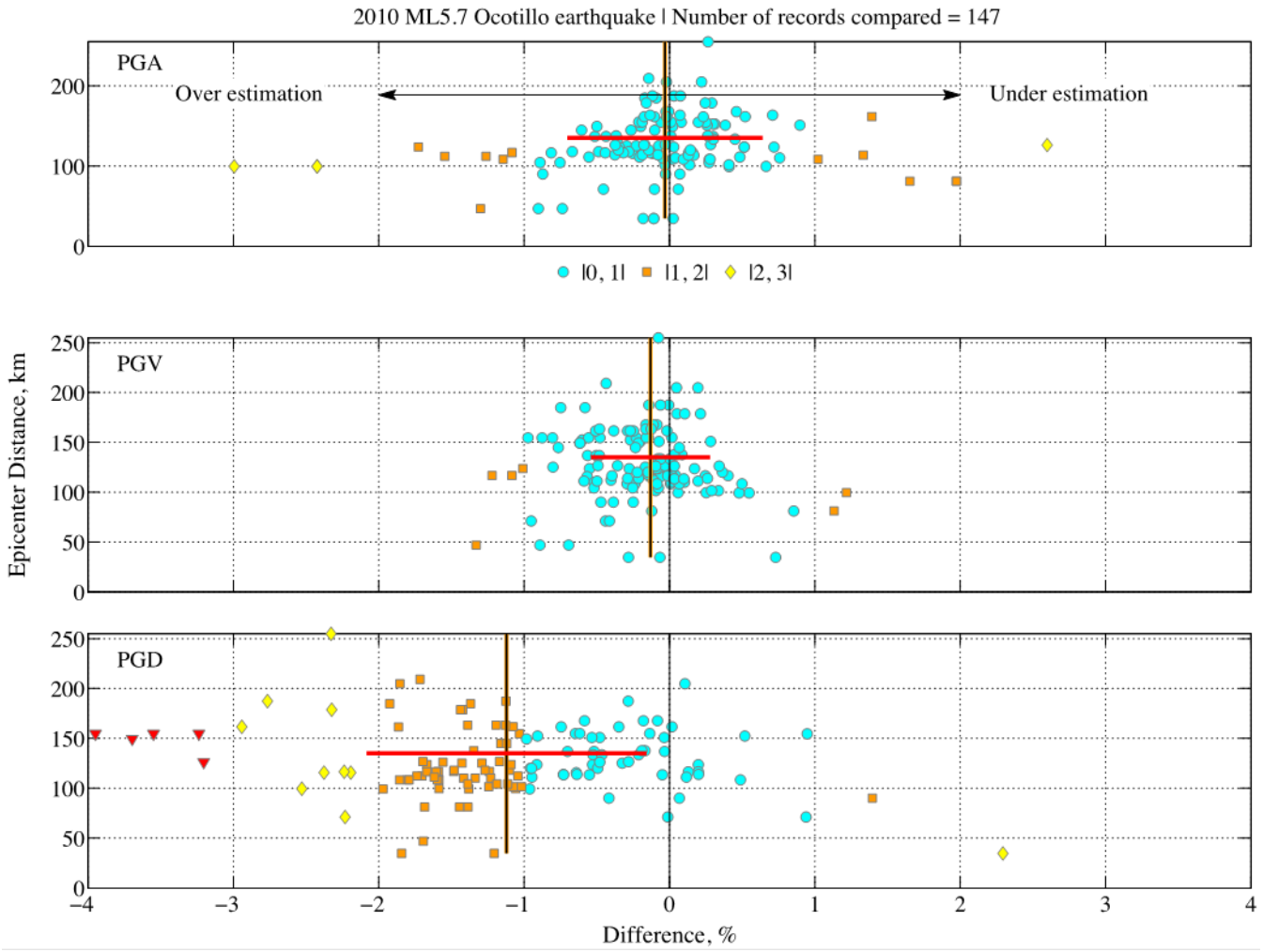


Figure 78. Graphs showing percent differences [(CSMIP−PRISM)×100/CSMIP] in peak ground acceleration (PGA), peak ground velocity (PGV), and peak ground displacement (PGD) of acceleration, velocity, and displacement time series obtained by using Processing and Review Interface for Strong Motion data (PRISM) and California Strong Motion Instrumentation Program (CSMIP) processing against epicenter distances. Data include 147 ground-motion components of the 2010 ML5.7 Ocotillo earthquake in California. Color and symbols indicate range of differences within 1 percent bins; for example |0, 1| denotes percent difference between 0 and 1 or between −1 and 0. Horizontal arrows on top panel indicate overestimation or underestimation trends. Median percent difference is shown by vertical (brown) thick line with a height indicating maximum epicenter distance of dataset. Horizontal (red) thick line denotes ± one standard deviation of percent difference about the median for which height denotes median epicenter distance of dataset. Number of outliers from plot ranges are indicated in table 2. km, kilometers; ML, local magnitude.

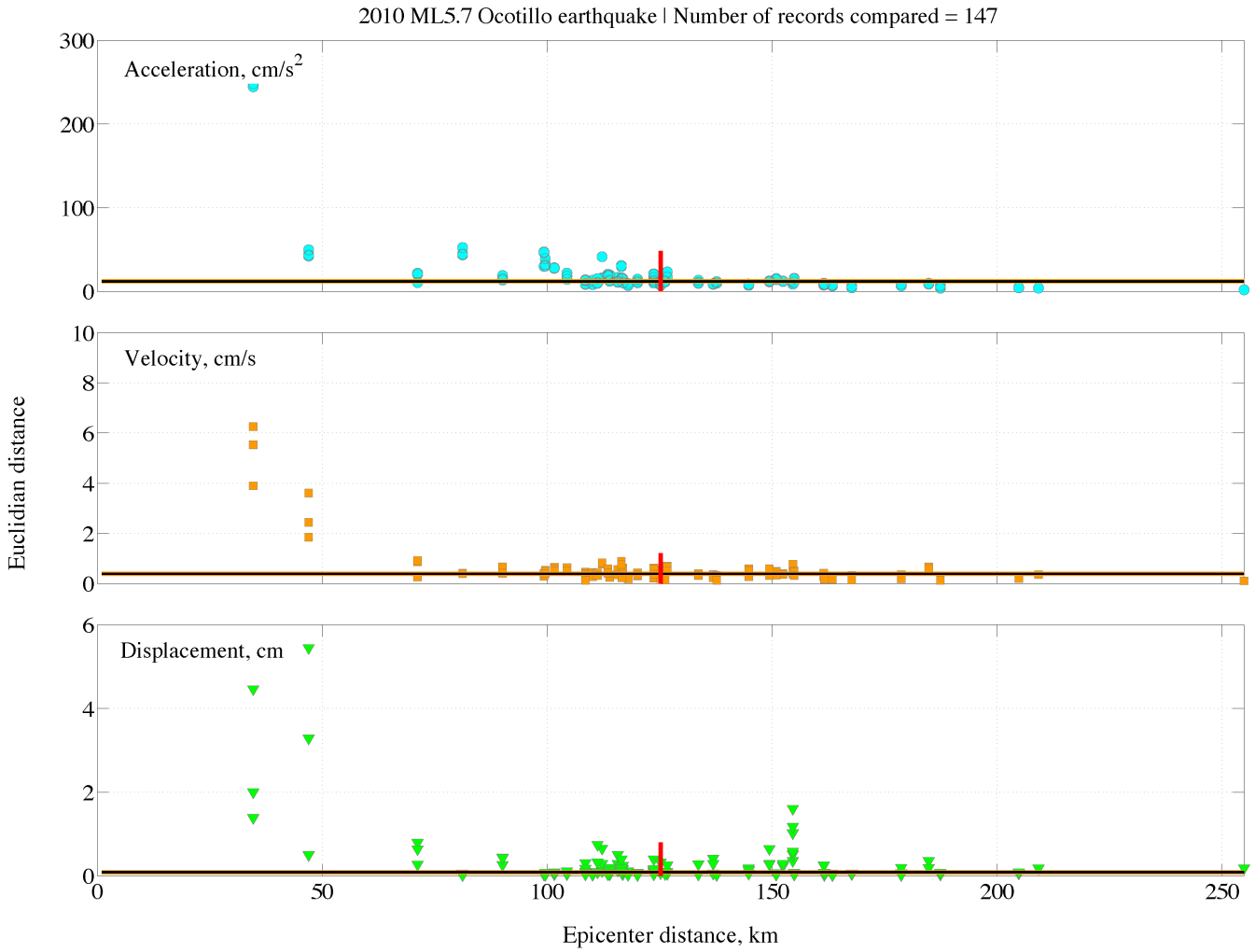


Figure 79. Graphs showing Euclidian distance as a similarity measure between acceleration, velocity, and displacement time series obtained by using Processing and Review Interface for Strong Motion data (PRISM) and California Strong Motion Instrumentation Program (CSMIP) processing against epicenter distances. Data include 147 ground-motion components of the 2010 ML5.7 Ocotillo earthquake in California. Horizontal (brown) thick line indicates epicenter distance range for which height shows median Euclidian distance. Vertical (red) thick line denotes median epicenter distance with a height that shows ± one standard deviation of Euclidian distance about the median. cm, centimeters; cm/s, centimeters per second; cm/s$^2$, centimeters per second squared; km, kilometers; ML, local magnitude.

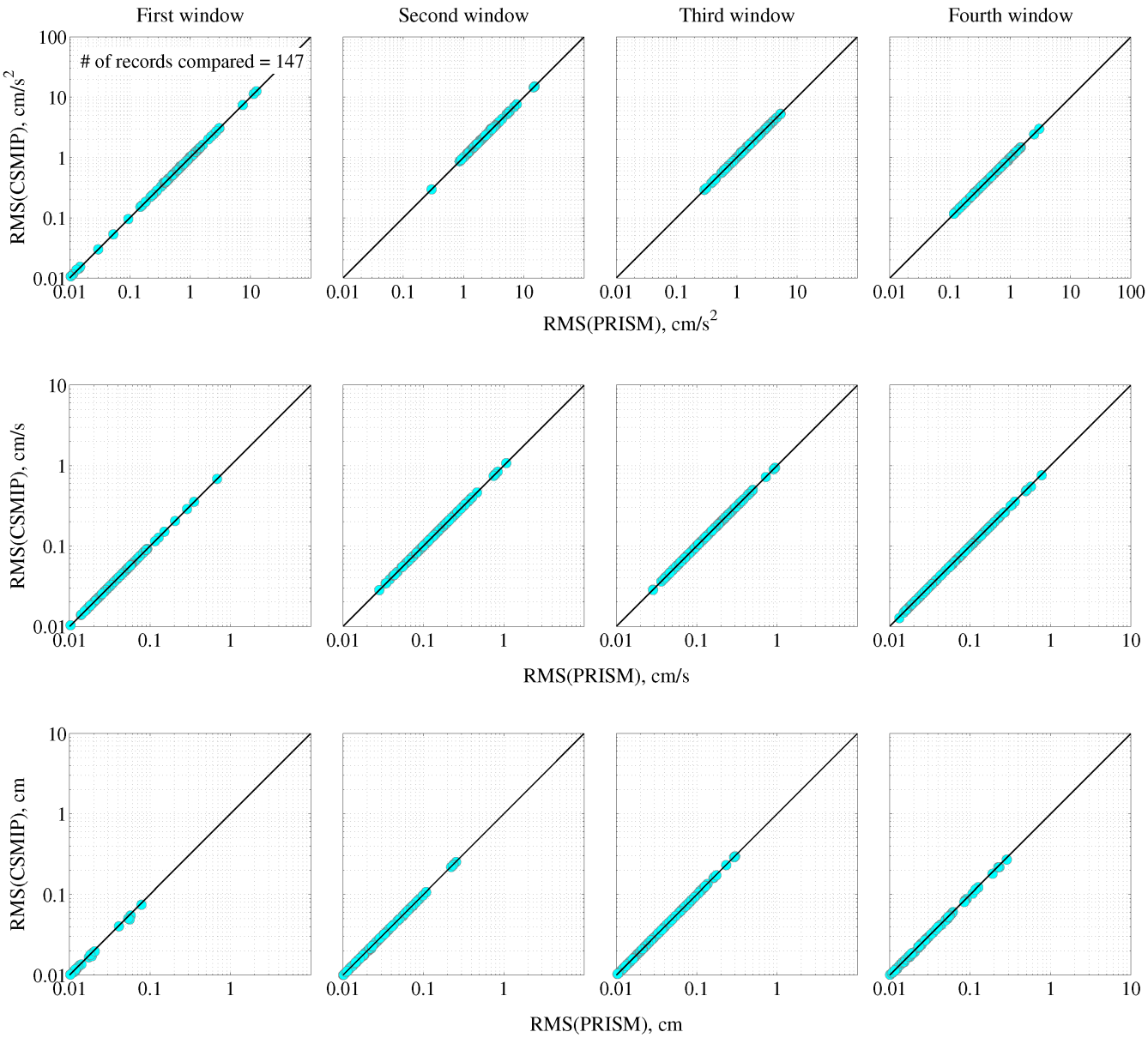


Figure 80. Graphs showing correlation of moving window root mean square (RMS) levels of acceleration (top row), velocity (middle row), and displacement (bottom row) time series obtained by using Processing and Review Interface for Strong Motion data (PRISM) and California Strong Motion Instrumentation Program (CSMIP) processing. Data include 147 ground-motion components of the 2010 *M*4.5 Ocotillo earthquake in California. Diagonal black line indicates a perfect match in RMS level between products. For RMS computation, ground-motion waveforms were divided into four equal-length windows without overlap (RMS values less than 0.01 are not shown). cm, centimeters; cm/s, centimeters per second; $cm/s^2$, centimeters per second squared.

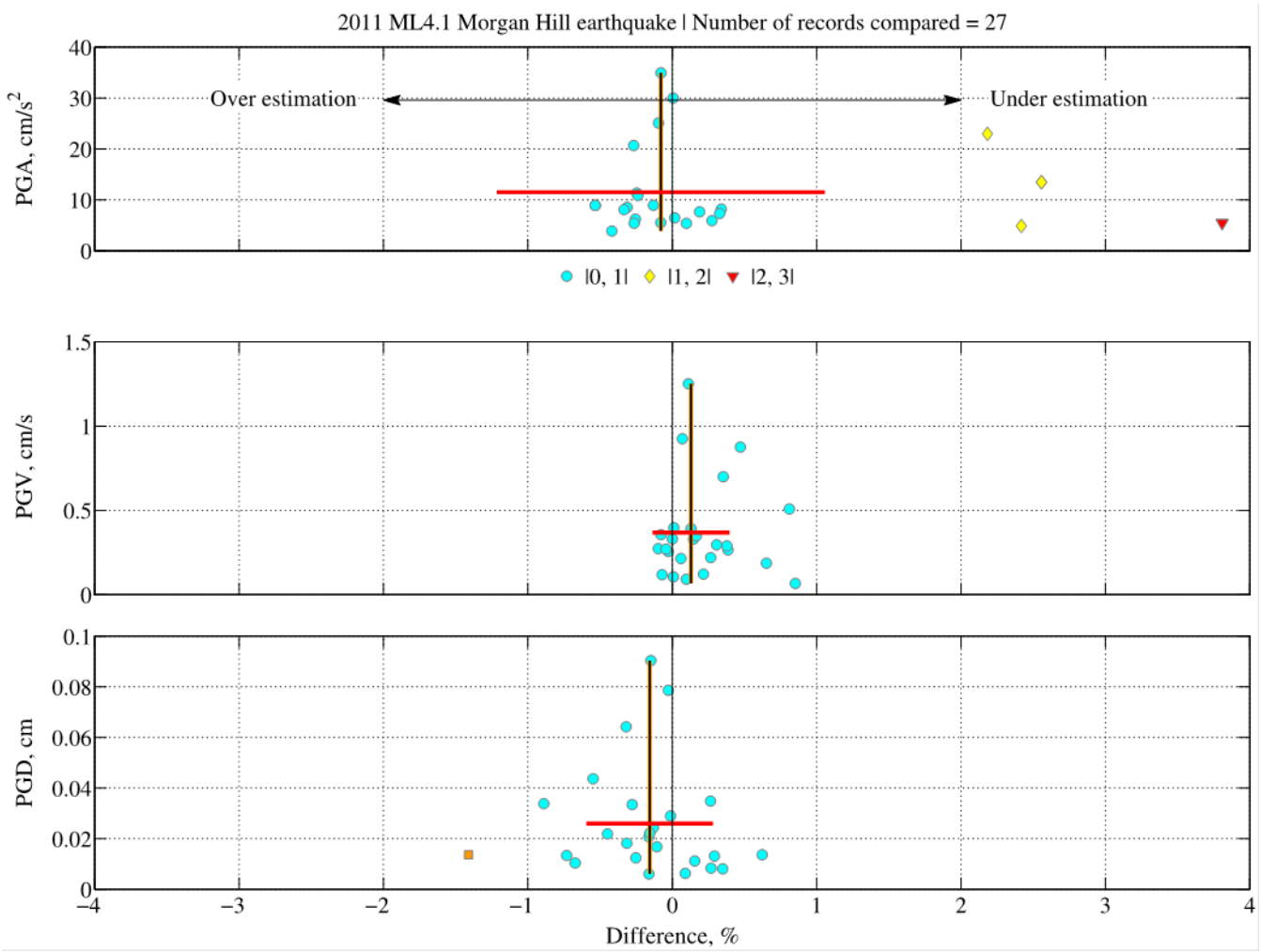


Figure 81. Graphs showing percent differences [(CSMIP−PRISM)×100/CSMIP] in peak ground acceleration (PGA), peak ground velocity (PGV), and peak ground displacement (PGD) of acceleration, velocity, and displacement time series obtained by using Processing and Review Interface for Strong Motion data (PRISM) and California Strong Motion Instrumentation Program (CSMIP) processing. Data include 27 ground-motion components of the 2011 ML4.1 Morgan Hill earthquake in California. Color and symbols indicate range of differences within 1 percent bins; for example |0, 1| denotes percent difference between 0 and 1 or between −1 and 0. Horizontal arrows on top panel indicate overestimation or underestimation trends. Median percent difference is shown by vertical (brown) thick line with a height indicating maximum ground-motion value of dataset (for example, PGA, PGV, or PGD). Horizontal (red) thick line denotes ± one standard deviation of percent difference about the median for which height denotes median ground-motion value of dataset. Number of outliers from plot ranges are indicated in table 2. cm, centimeters; cm/s, centimeters per second; cm/s$^2$, centimeters per second squared; ML, local magnitude.

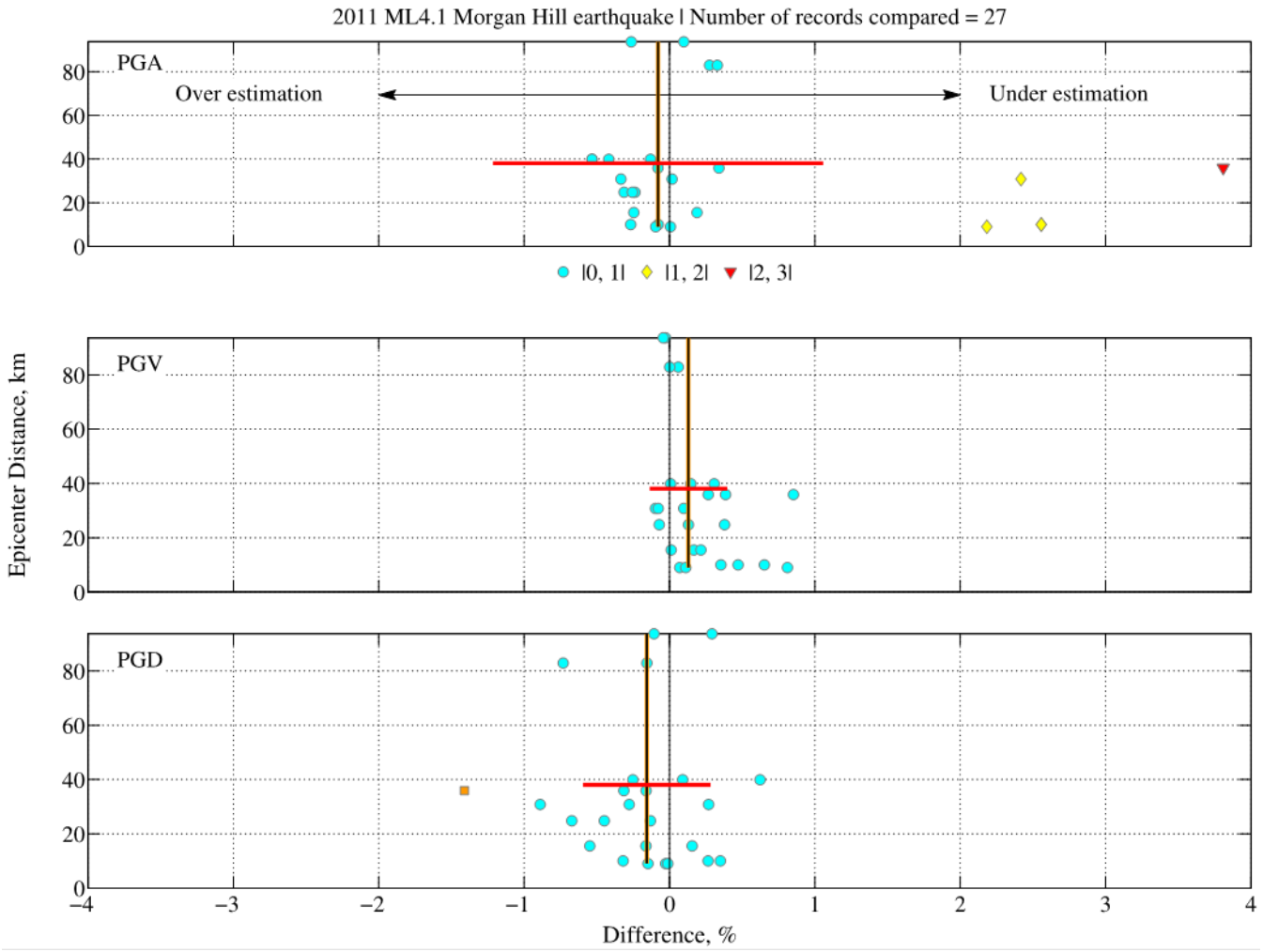


Figure 82. Graphs showing percent differences [(CSMIP−PRISM)×100/CSMIP] in peak ground acceleration (PGA), peak ground velocity (PGV), and peak ground displacement (PGD) of acceleration, velocity, and displacement time series obtained by using Processing and Review Interface for Strong Motion data (PRISM) and California Strong Motion Instrumentation Program (CSMIP) processing against epicenter distances. Data include 27 ground-motion components of the 2011 ML4.1 Morgan Hill earthquake in California. Color and symbols indicate range of differences within 1 percent bins; for example |0, 1| denotes percent difference between 0 and 1 or between −1 and 0. Horizontal arrows on top panel indicate overestimation or underestimation trends. Median percent difference is shown by vertical (brown) thick line with a height indicating maximum epicenter distance of dataset. Horizontal (red) thick line denotes ± one standard deviation of percent difference about the median for which height denotes median epicenter distance of dataset. Number of outliers from plot ranges are indicated in table 2. km, kilometers; ML, local magnitude.

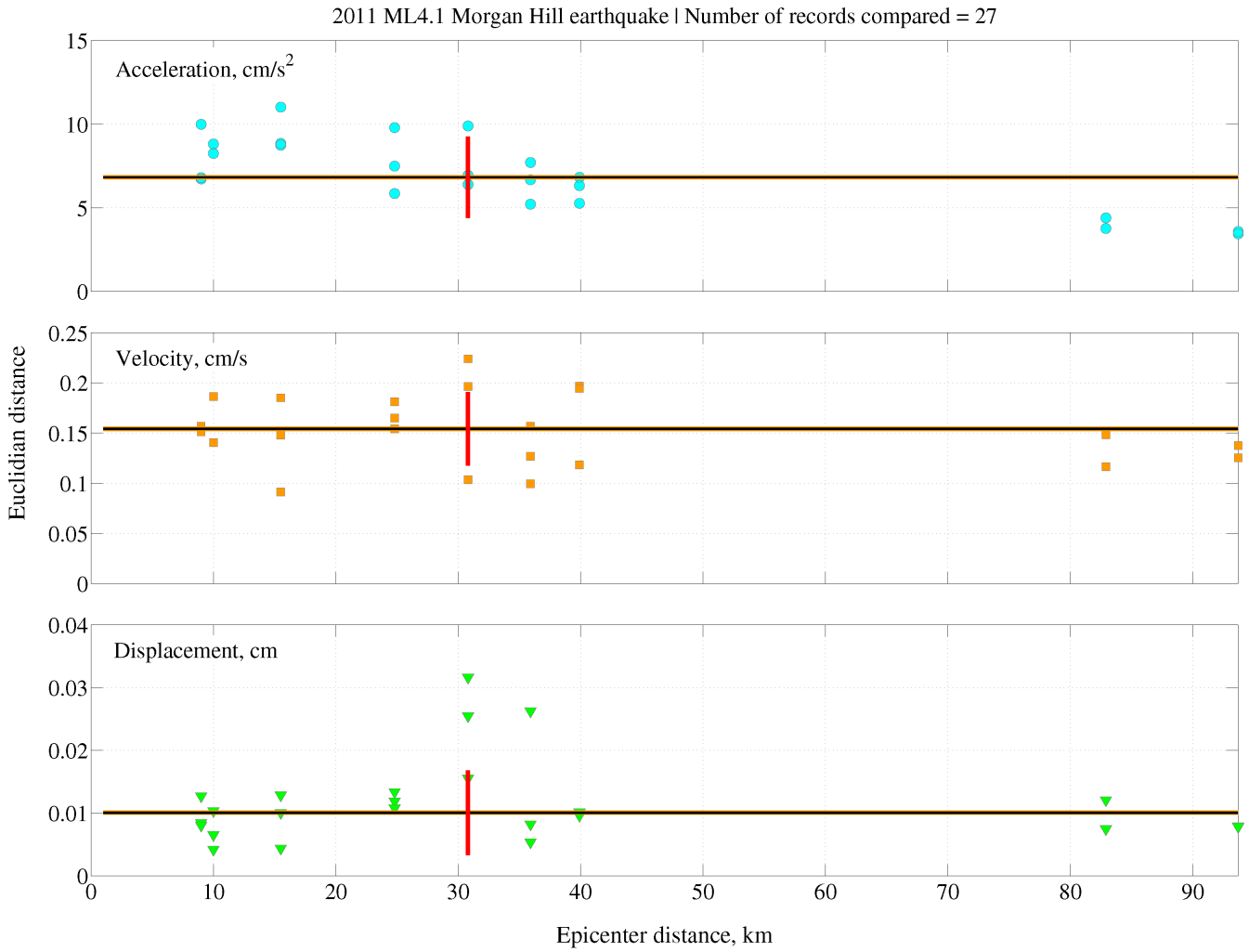


Figure 83. Graphs showing Euclidian distance as a similarity measure between acceleration, velocity, and displacement time series obtained by using Processing and Review Interface for Strong Motion data (PRISM) and California Strong Motion Instrumentation Program (CSMIP) processing against epicenter distances. Data include 27 ground-motion components of the 2011 ML4.1 Morgan Hill earthquake in California. Horizontal (brown) thick line indicates epicenter distance range for which height shows median Euclidian distance. Vertical (red) thick line denotes median epicenter distance with a height that shows ± one standard deviation of Euclidian distance about the median. cm, centimeters; cm/s, centimeters per second; cm/s$^2$, centimeters per second squared; km, kilometers; ML, local magnitude.

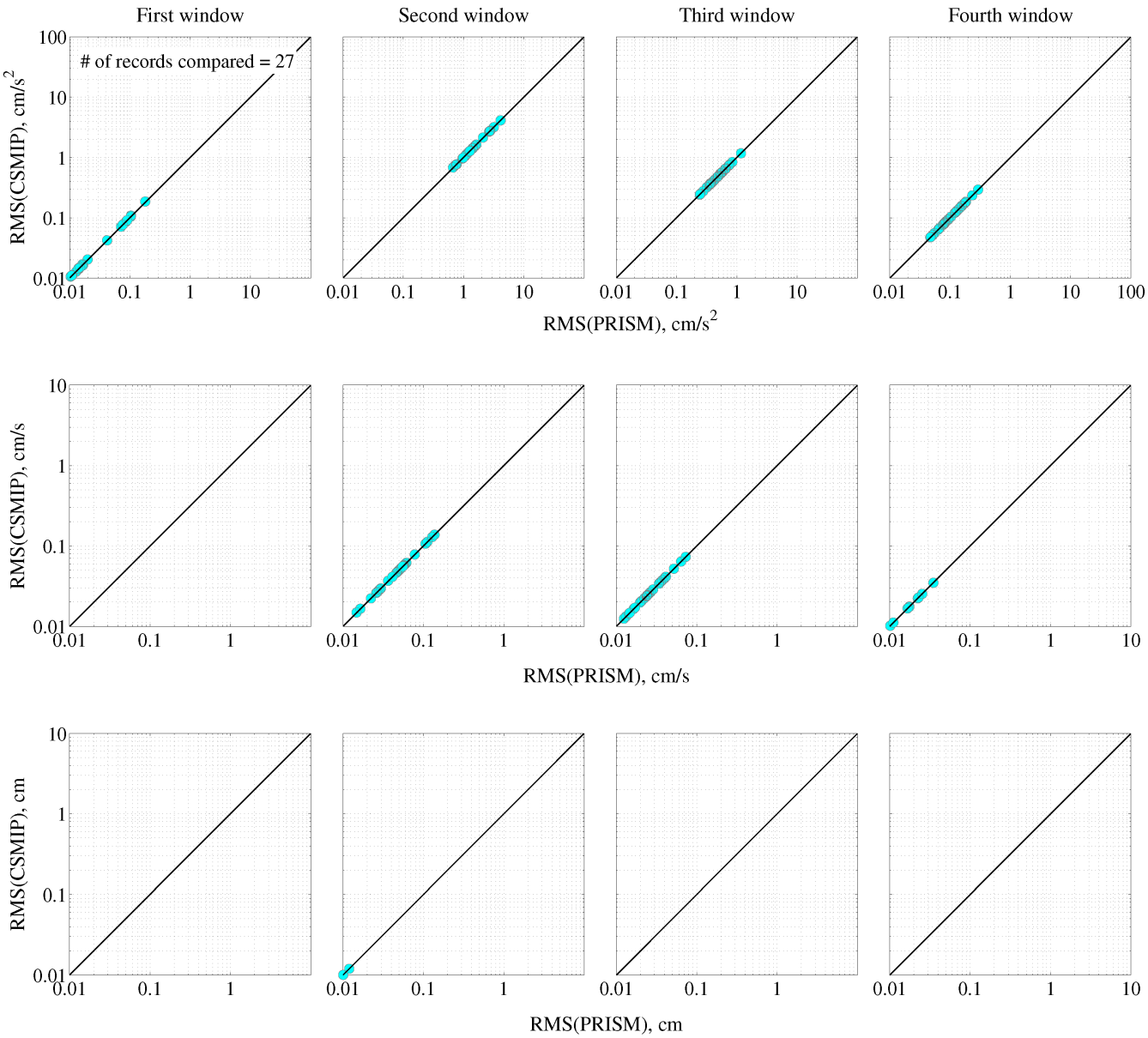


Figure 84. Graphs showing correlation of moving window root mean square (RMS) levels of acceleration (top row), velocity (middle row), and displacement (bottom row) time series obtained by using Processing and Review Interface for Strong Motion data (PRISM) and California Strong Motion Instrumentation Program (CSMIP) processing. Data include 27 ground-motion components of the 2011 ML4.1 Morgan Hill earthquake in California. Diagonal black line indicates a perfect match in RMS level between products. For RMS computation, ground-motion waveforms were divided into four equal-length windows without overlap (RMS values less than 0.01 are not shown). cm, centimeters; cm/s, centimeters per second; cm/s$^2$, centimeters per second squared.

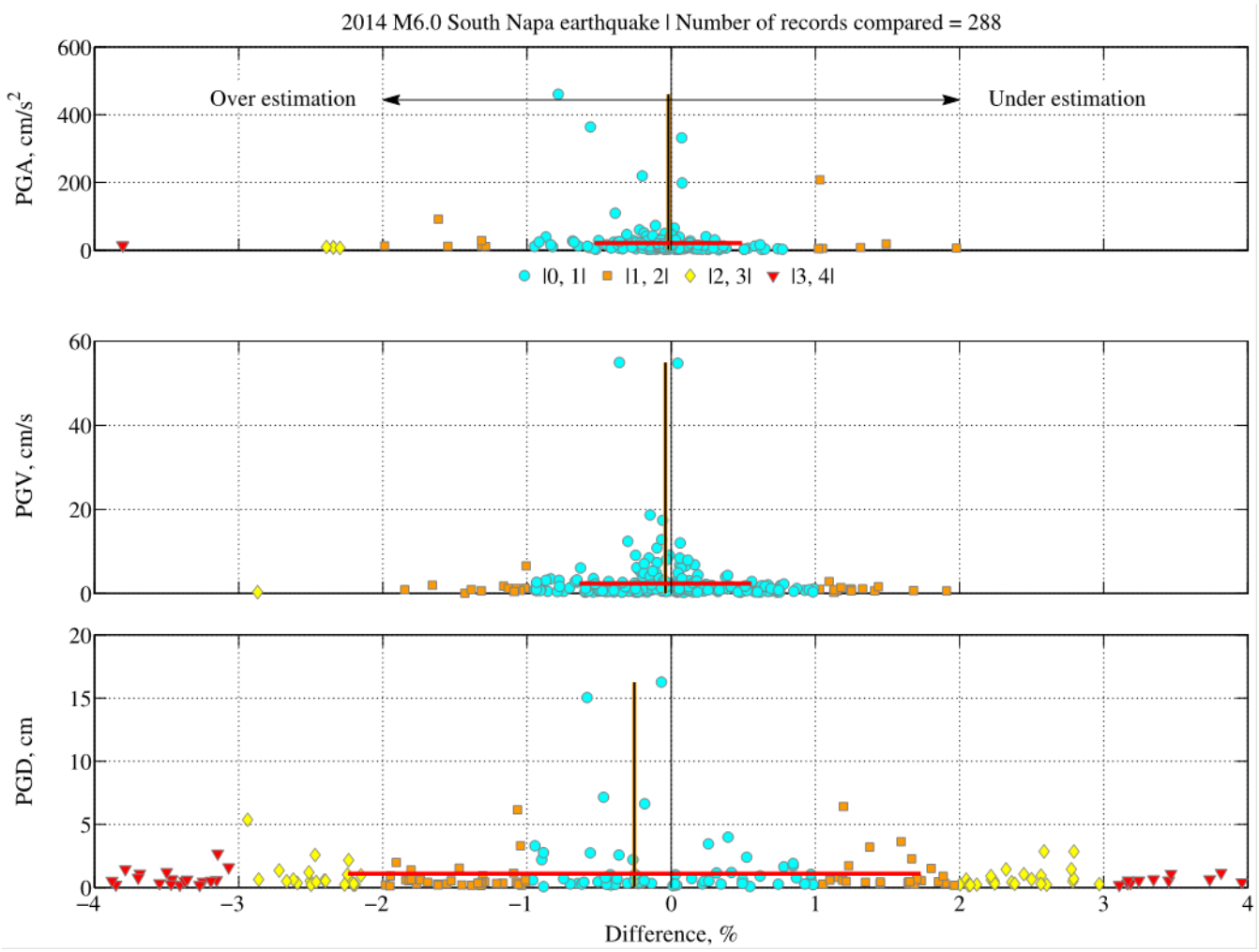


Figure 85. Graphs showing percent differences [(CSMIP−PRISM)×100/CSMIP] in peak ground acceleration (PGA), peak ground velocity (PGV), and peak ground displacement (PGD) of acceleration, velocity, and displacement time series obtained by using Processing and Review Interface for Strong Motion data (PRISM) and California Strong Motion Instrumentation Program (CSMIP) processing. Data include 288 ground-motion components of the 2014 *M*6.0 South Napa earthquake in California. Color and symbols indicate range of differences within 1 percent bins; for example |0, 1| denotes percent difference between 0 and 1 or between −1 and 0. Horizontal arrows on top panel indicate overestimation or underestimation trends. Median percent difference is shown by vertical (brown) thick line with a height indicating maximum ground-motion value of dataset (for example, PGA, PGV, or PGD). Horizontal (red) thick line denotes ± one standard deviation of percent difference about the median for which height denotes median ground-motion value of dataset. Number of outliers from plot ranges are indicated in table 2. cm, centimeters; cm/s, centimeters per second; cm/s$^2$, centimeters per second squared; *M*, moment magnitude.

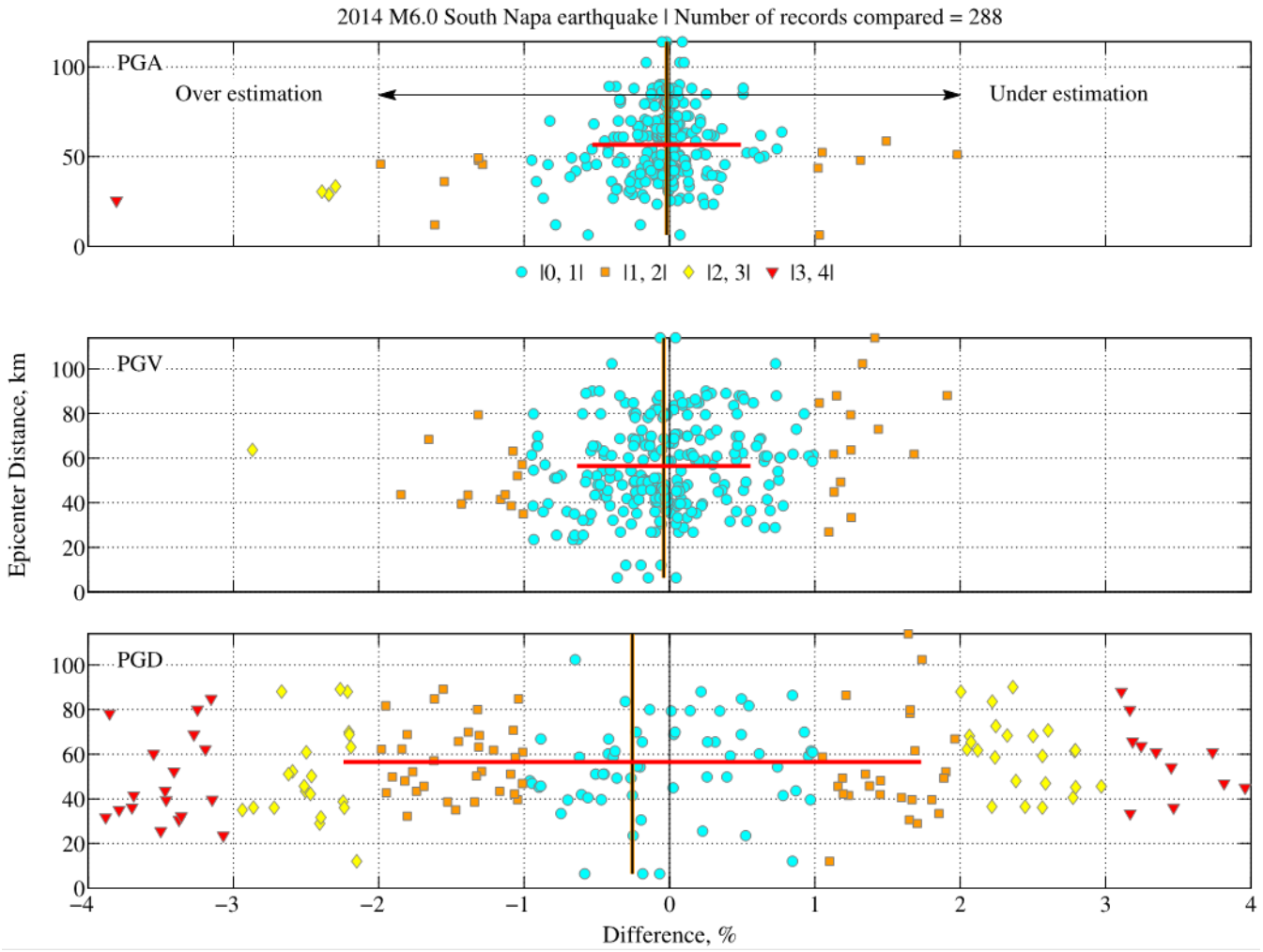


Figure 86. Graphs showing percent differences [(CSMIP−PRISM)×100/CSMIP] in peak ground acceleration (PGA), peak ground velocity (PGV), and peak ground displacement (PGD) of acceleration, velocity, and displacement time series obtained by using Processing and Review Interface for Strong Motion data (PRISM) and California Strong Motion Instrumentation Program (CSMIP) processing against epicenter distances. Data include 288 ground-motion components of the 2014 *M*6.0 South Napa earthquake in California. Color and symbols indicate range of differences within 1 percent bins; for example |0, 1| denotes percent difference between 0 and 1 or between −1 and 0. Horizontal arrows on top panel indicate overestimation or underestimation trends. Median percent difference is shown by vertical (brown) thick line with a height indicating maximum epicenter distance of dataset. Horizontal (red) thick line denotes ± one standard deviation of percent difference about the median for which height denotes median epicenter distance of dataset. Number of outliers from plot ranges are indicated in table 2. km, kilometers; *M*, moment magnitude.

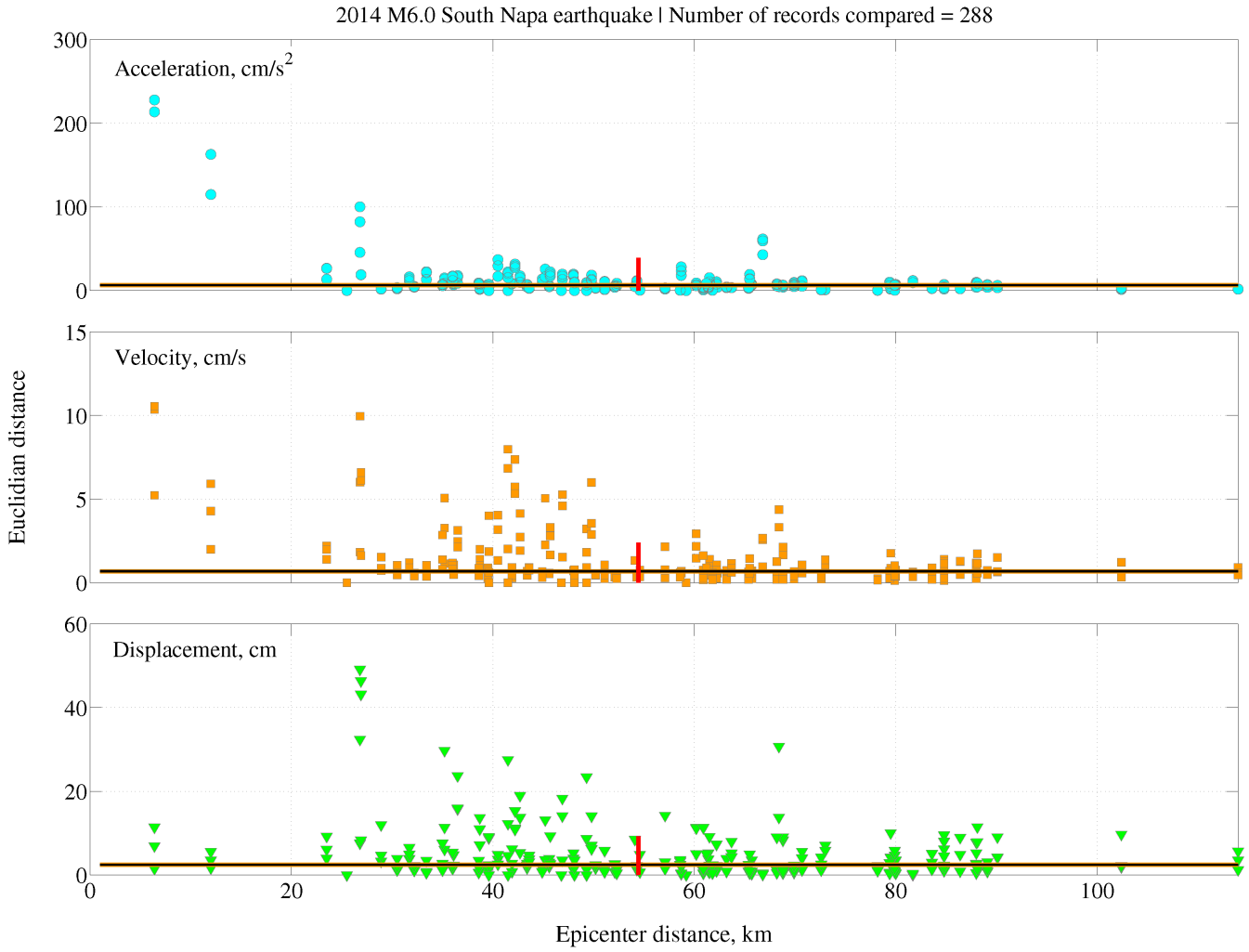


Figure 87. Graphs showing Euclidian distance as a similarity measure between acceleration, velocity, and displacement time series obtained by using Processing and Review Interface for Strong Motion data (PRISM) and California Strong Motion Instrumentation Program (CSMIP) processing against epicenter distances. Data include 288 ground-motion components of the 2014 *M*6.0 South Napa earthquake in California. Horizontal (brown) thick line indicates epicenter distance range for which height shows median Euclidian distance. Vertical (red) thick line denotes median epicenter distance with a height that shows ± one standard deviation of Euclidian distance about the median. cm, centimeters; cm/s, centimeters per second; cm/s$^2$, centimeters per second squared; km, kilometers; *M*, moment magnitude.

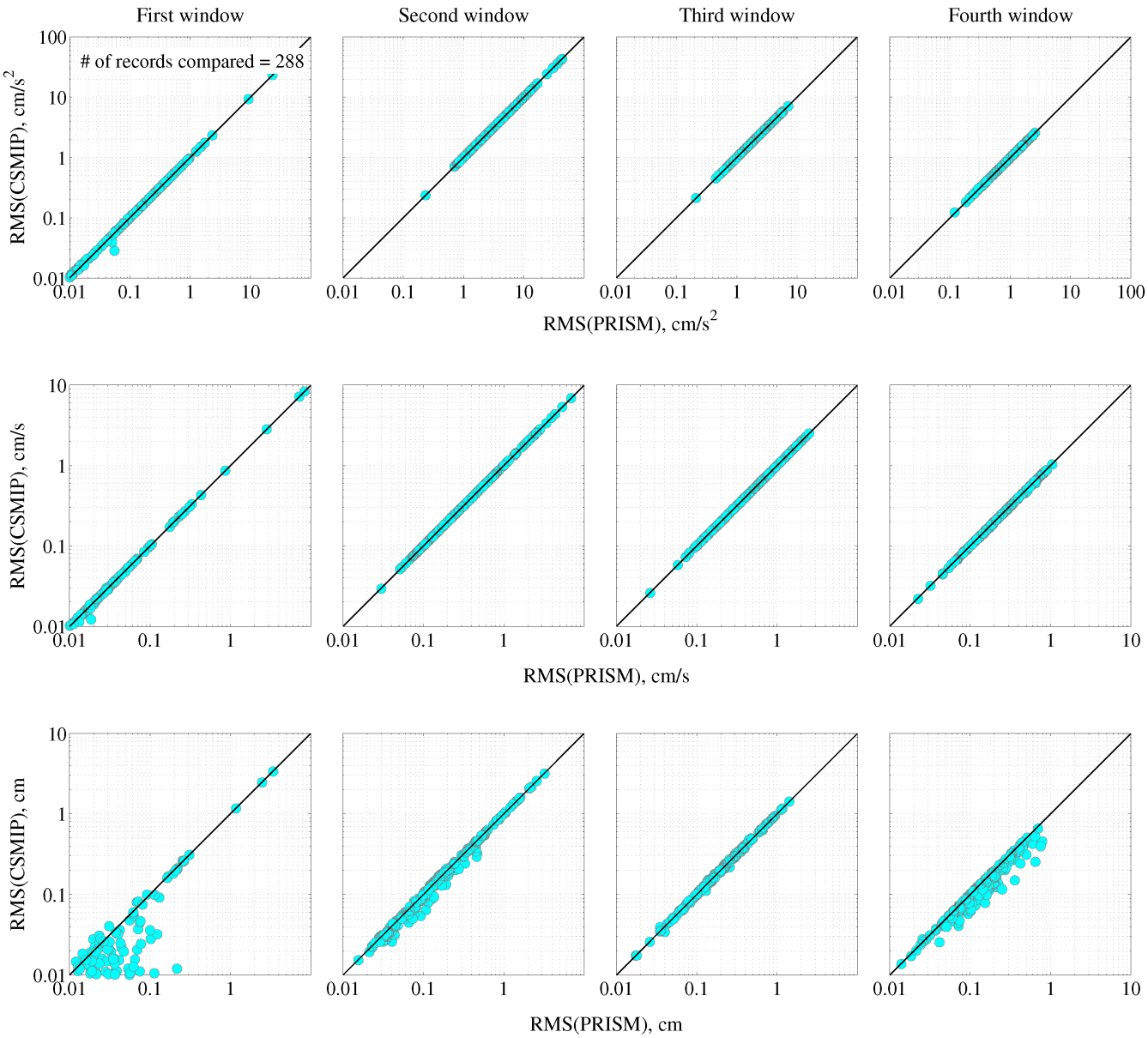


Figure 88. Graphs showing correlation of moving window root mean square (RMS) levels of acceleration (top row), velocity (middle row), and displacement (bottom row) time series obtained by using Processing and Review Interface for Strong Motion data (PRISM) and California Strong Motion Instrumentation Program (CSMIP) processing. Data include 288 ground-motion components of the 2014 *M*6.0 South Napa earthquake in California. Diagonal black line indicates a perfect match in RMS level between products. For RMS computation, ground-motion waveforms were divided into four equal-length windows without overlap (RMS values less than 0.01 are not shown). cm, centimeters; cm/s, centimeters per second; cm/s$^2$, centimeters per second squared.

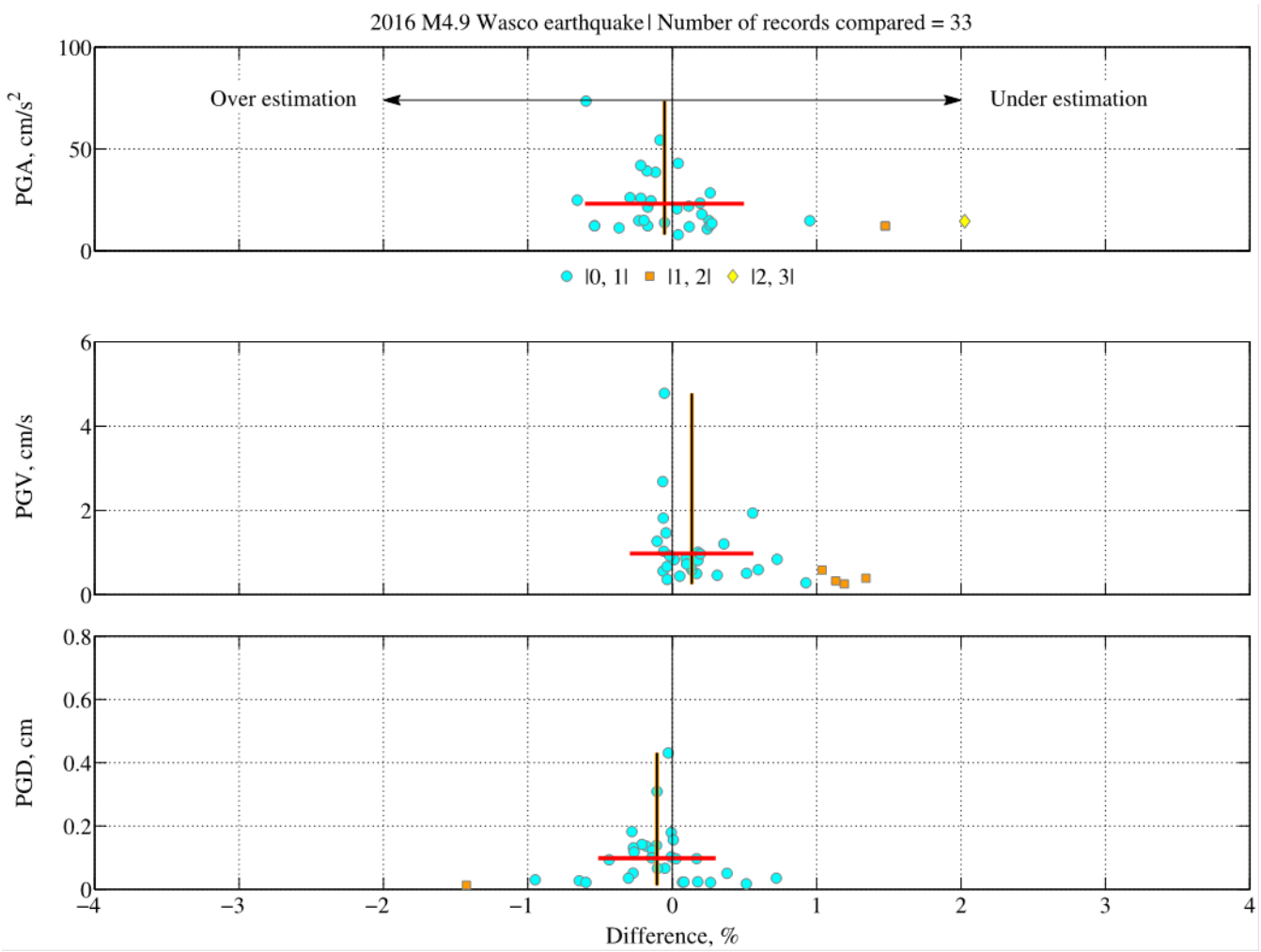


Figure 89. Graphs showing percent differences [(CSMIP−PRISM)×100/CSMIP] in peak ground acceleration (PGA), peak ground velocity (PGV), and peak ground displacement (PGD) of acceleration, velocity, and displacement time series obtained by using Processing and Review Interface for Strong Motion data (PRISM) and California Strong Motion Instrumentation Program (CSMIP) processing. Data include 33 ground-motion components of the 2016 *M*4.9 Wasco earthquake in California. Color and symbols indicate range of differences within 1 percent bins; for example |0, 1| denotes percent difference between 0 and 1 or between −1 and 0. Horizontal arrows on top panel indicate overestimation or underestimation trends. Median percent difference is shown by vertical (brown) thick line with a height indicating maximum ground-motion value of dataset (for example, PGA, PGV, or PGD). Horizontal (red) thick line denotes ± one standard deviation of percent difference about the median for which height denotes median ground-motion value of dataset. Number of outliers from plot ranges are indicated in table 2. cm, centimeters; cm/s, centimeters per second; cm/s$^2$, centimeters per second squared; *M*, moment magnitude.

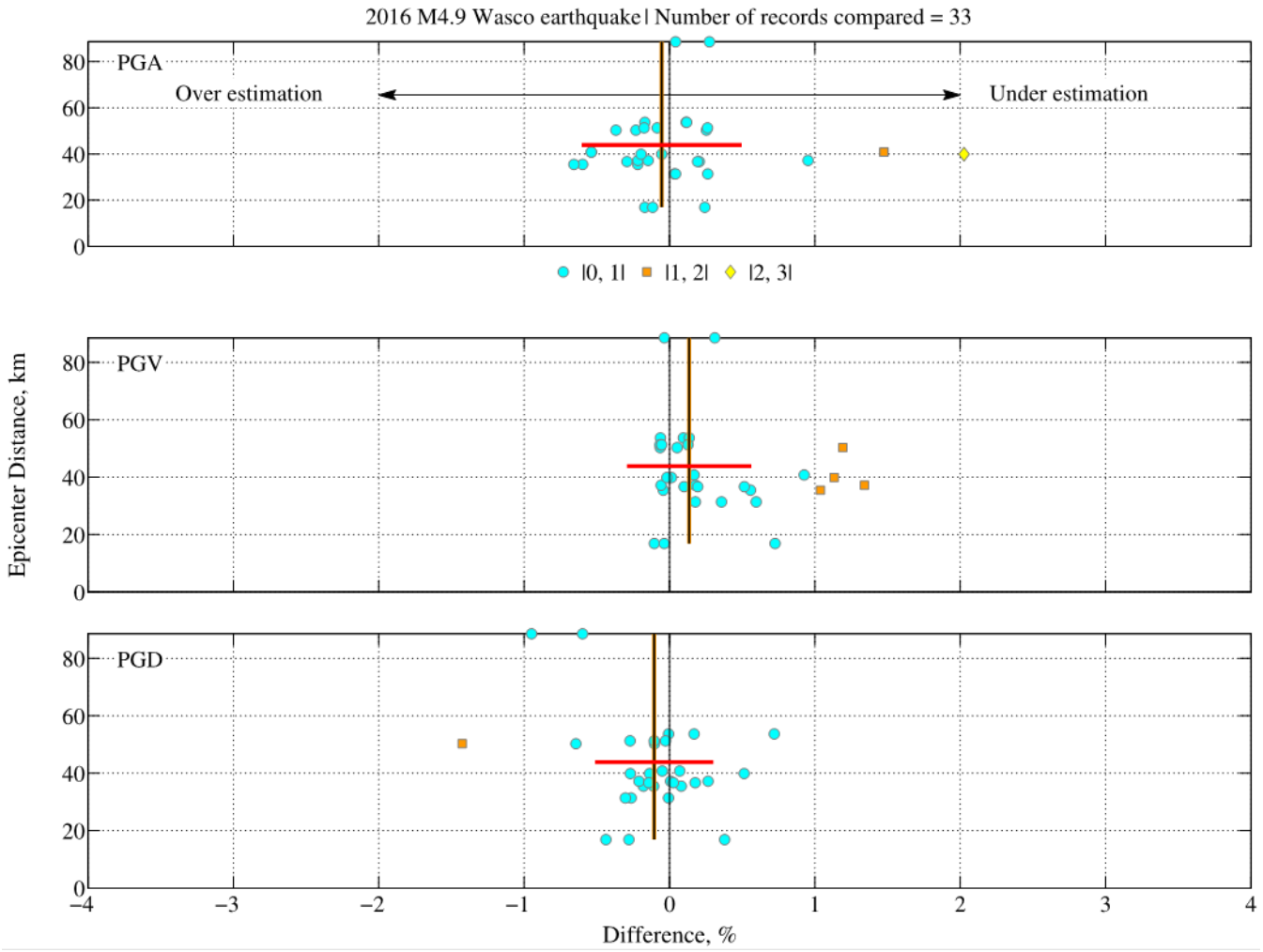


Figure 90. Graphs showing percent differences [(CSMIP−PRISM)×100/CSMIP] in peak ground acceleration (PGA), peak ground velocity (PGV), and peak ground displacement (PGD) of acceleration, velocity, and displacement time series obtained by using Processing and Review Interface for Strong Motion data (PRISM) and California Strong Motion Instrumentation Program (CSMIP) processing against epicenter distances. Data include 33 ground-motion components of the 2016 *M*4.9 Wasco earthquake in California. Color and symbols indicate range of differences within 1 percent bins; for example |0, 1| denotes percent difference between 0 and 1 or between −1 and 0. Horizontal arrows on top panel indicate overestimation or underestimation trends. Median percent difference is shown by vertical (brown) thick line with a height indicating maximum epicenter distance of dataset. Horizontal (red) thick line denotes ± one standard deviation of percent difference about the median for which height denotes median epicenter distance of dataset. Number of outliers from plot ranges are indicated in table 2. km, kilometers; *M*, moment magnitude.

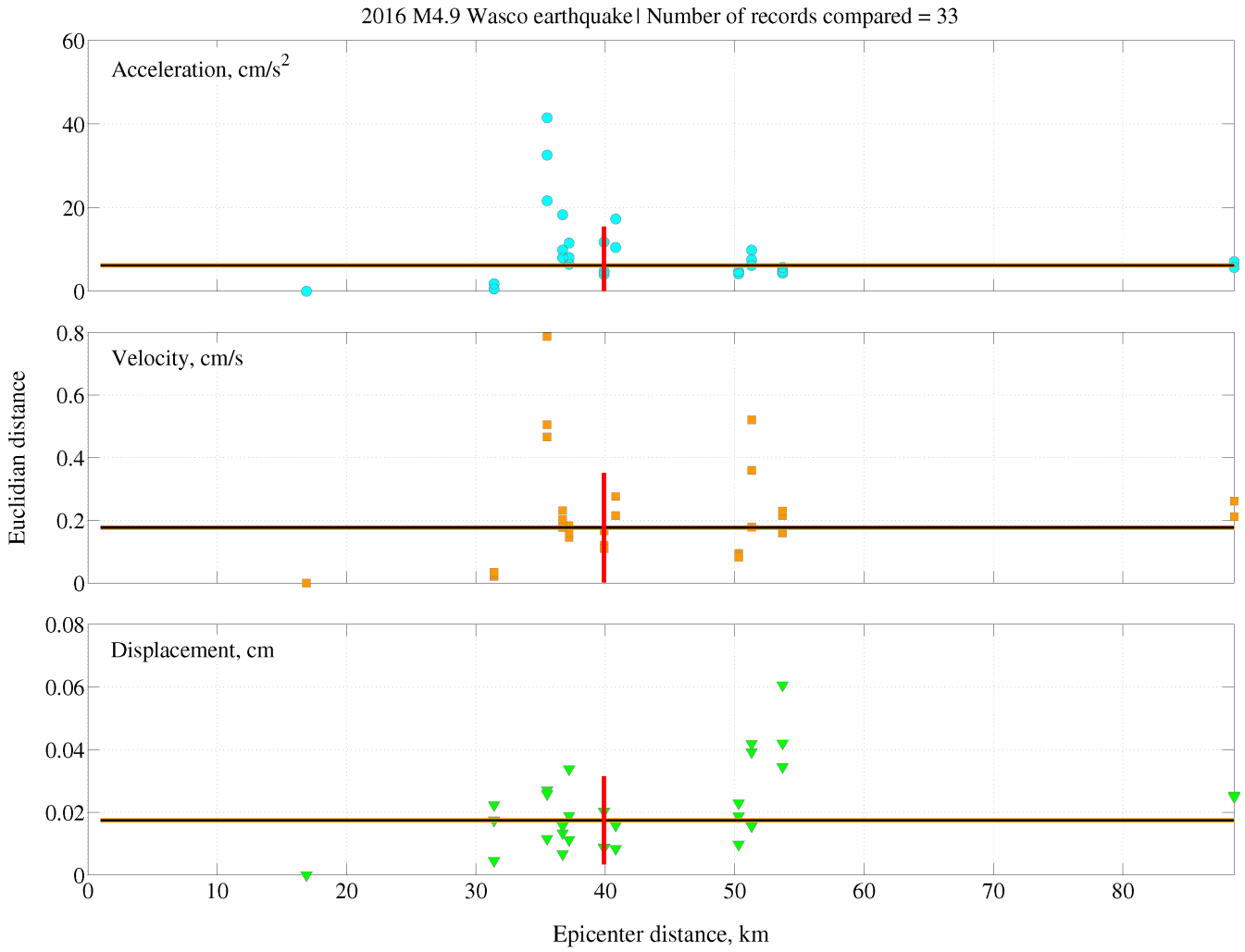


Figure 91. Graphs showing Euclidian distance as a similarity measure between acceleration, velocity, and displacement time series obtained by using Processing and Review Interface for Strong Motion data (PRISM) and California Strong Motion Instrumentation Program (CSMIP) processing against epicenter distances. Data include 33 ground-motion components of the 2016 *M*4.9 Wasco earthquake in California. Horizontal (brown) thick line indicates epicenter distance range for which height shows median Euclidian distance. Vertical (red) thick line denotes median epicenter distance with a height that shows ± one standard deviation of Euclidian distance about the median. cm, centimeters; cm/s, centimeters per second; cm/s$^2$, centimeters per second squared; km, kilometers; *M*, moment magnitude.

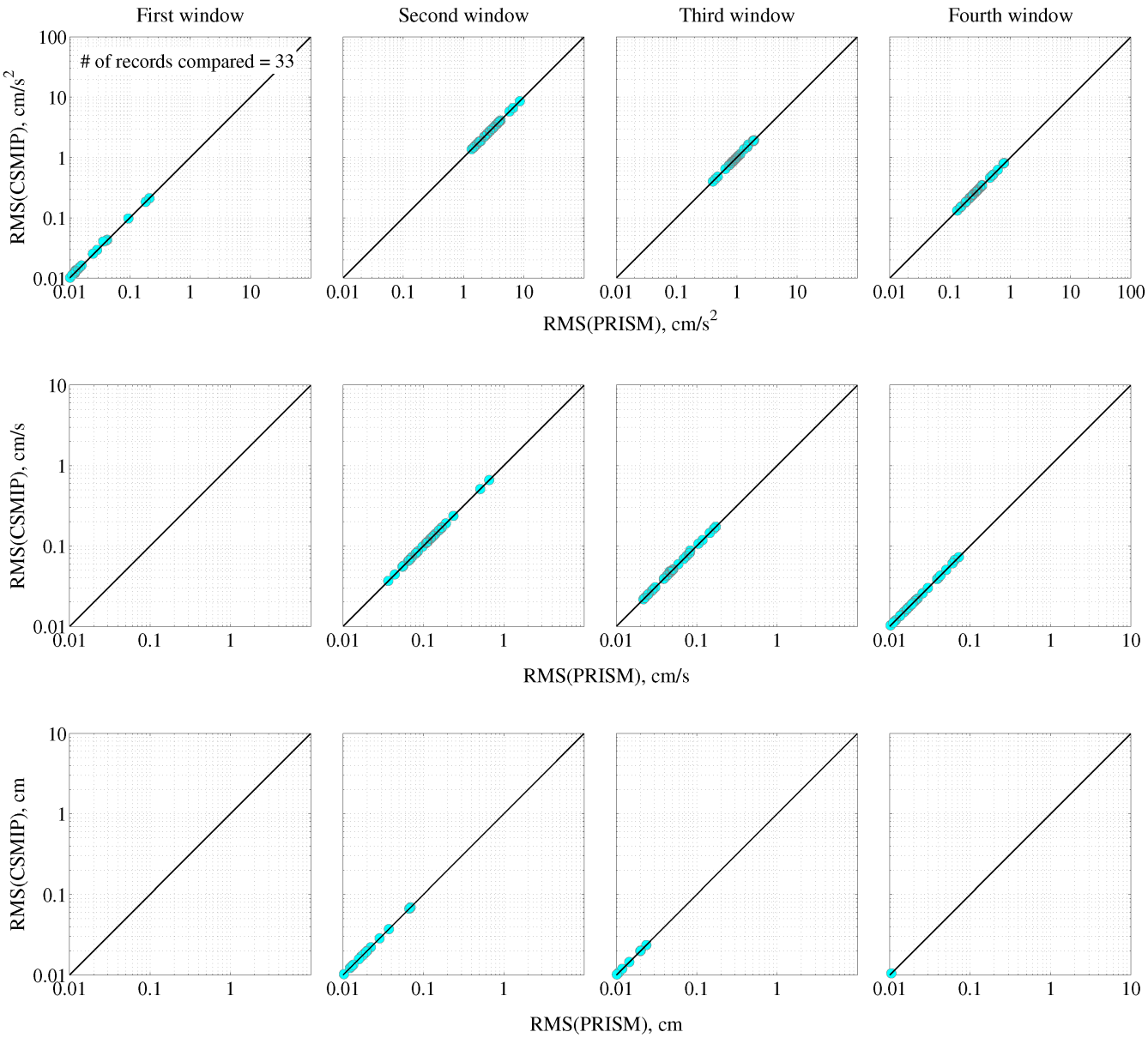


Figure 92. Graphs showing correlation of moving window root mean square (RMS) levels of acceleration (top row), velocity (middle row), and displacement (bottom row) time series obtained by using Processing and Review Interface for Strong Motion data (PRISM) and California Strong Motion Instrumentation Program (CSMIP) processing. Data include 33 ground-motion components of the 2016 *M*4.9 Wasco earthquake in California. Diagonal black line indicates a perfect match in RMS level between products. For RMS computation, ground-motion waveforms were divided into four equal-length windows without overlap (RMS values less than 0.01 are not shown). cm, centimeters; cm/s, centimeters per second; cm/s$^2$, centimeters per second squared.

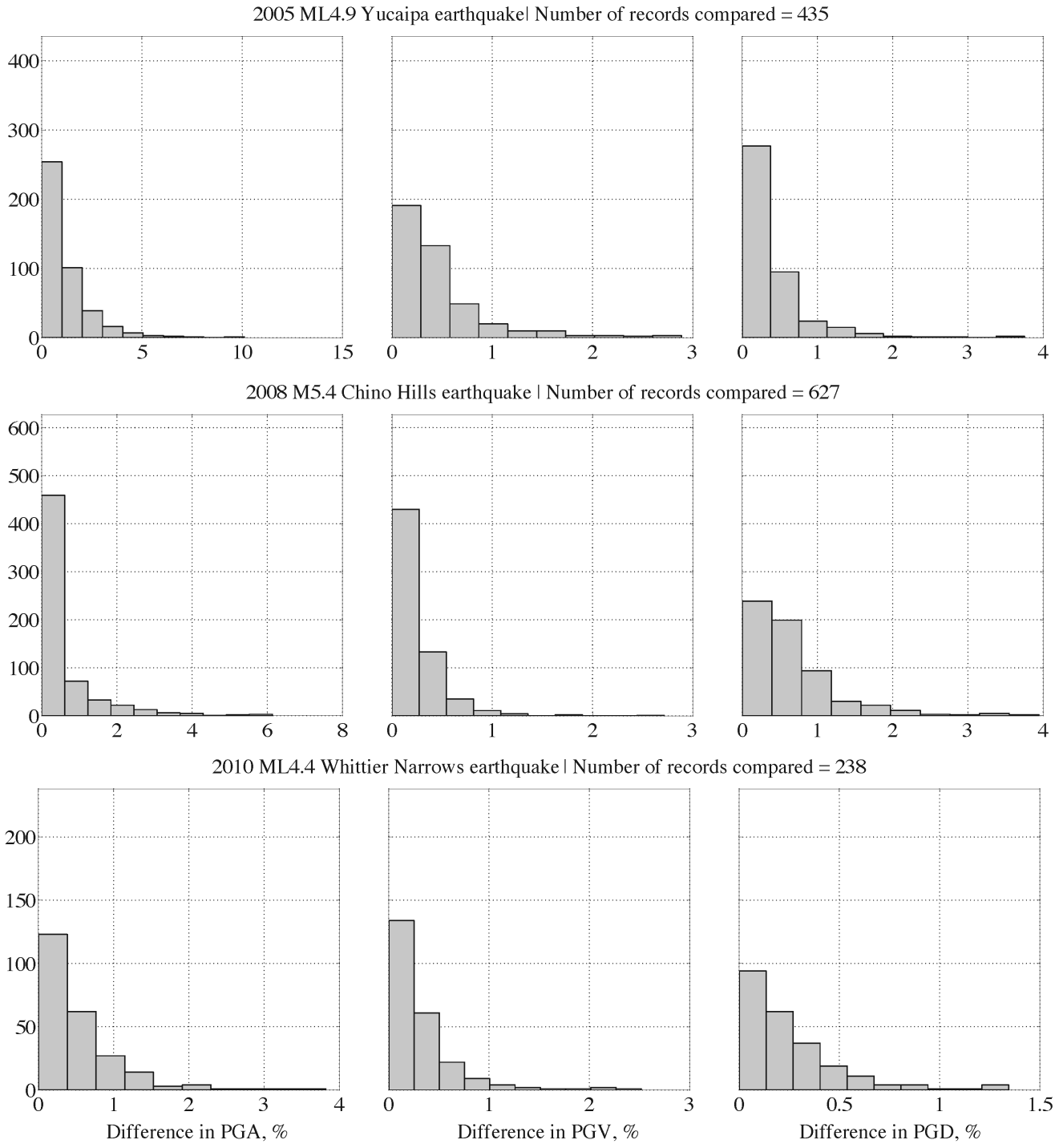


Figure 93. Histograms showing absolute differences [|CSMIP−PRISM|×100/CSMIP] in peak ground acceleration (PGA), peak ground velocity (PGV), and peak ground displacement (PGD) between Processing and Review Interface for Strong Motion data (PRISM) and California Strong Motion Instrumentation Program (CSMIP) for various earthquakes; y-axis shows number of records. *M*, moment magnitude; ML, local magnitude.

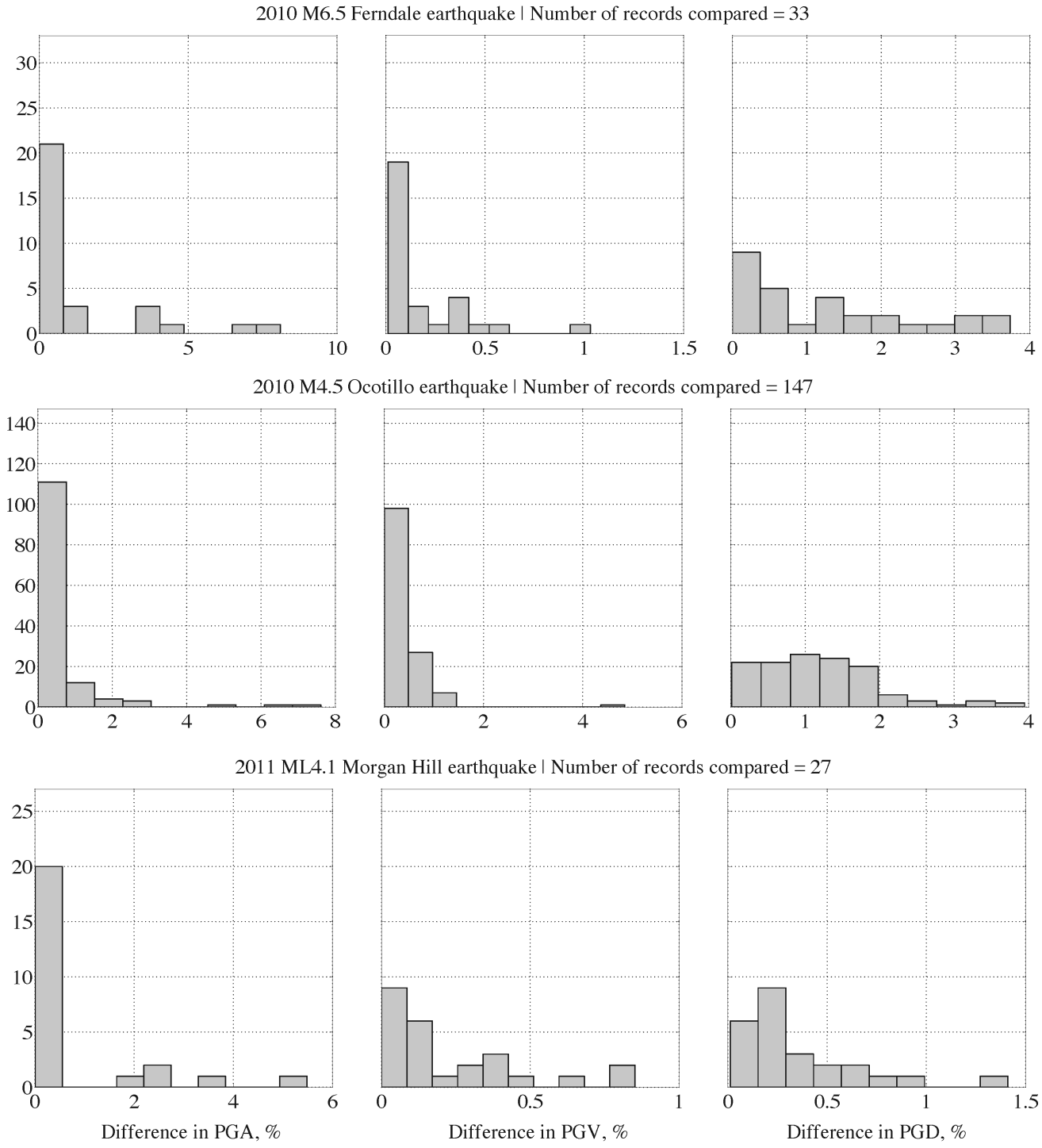


Figure 94. Histograms showing absolute differences [|CSMIP−PRISM|×100/CSMIP] in peak ground acceleration (PGA), peak ground velocity (PGV), and peak ground displacement (PGD) between Processing and Review Interface for Strong Motion data (PRISM) and California Strong Motion Instrumentation Program (CSMIP) for various earthquakes; y-axis shows number of records. *M*, moment magnitude; ML, local magnitude.

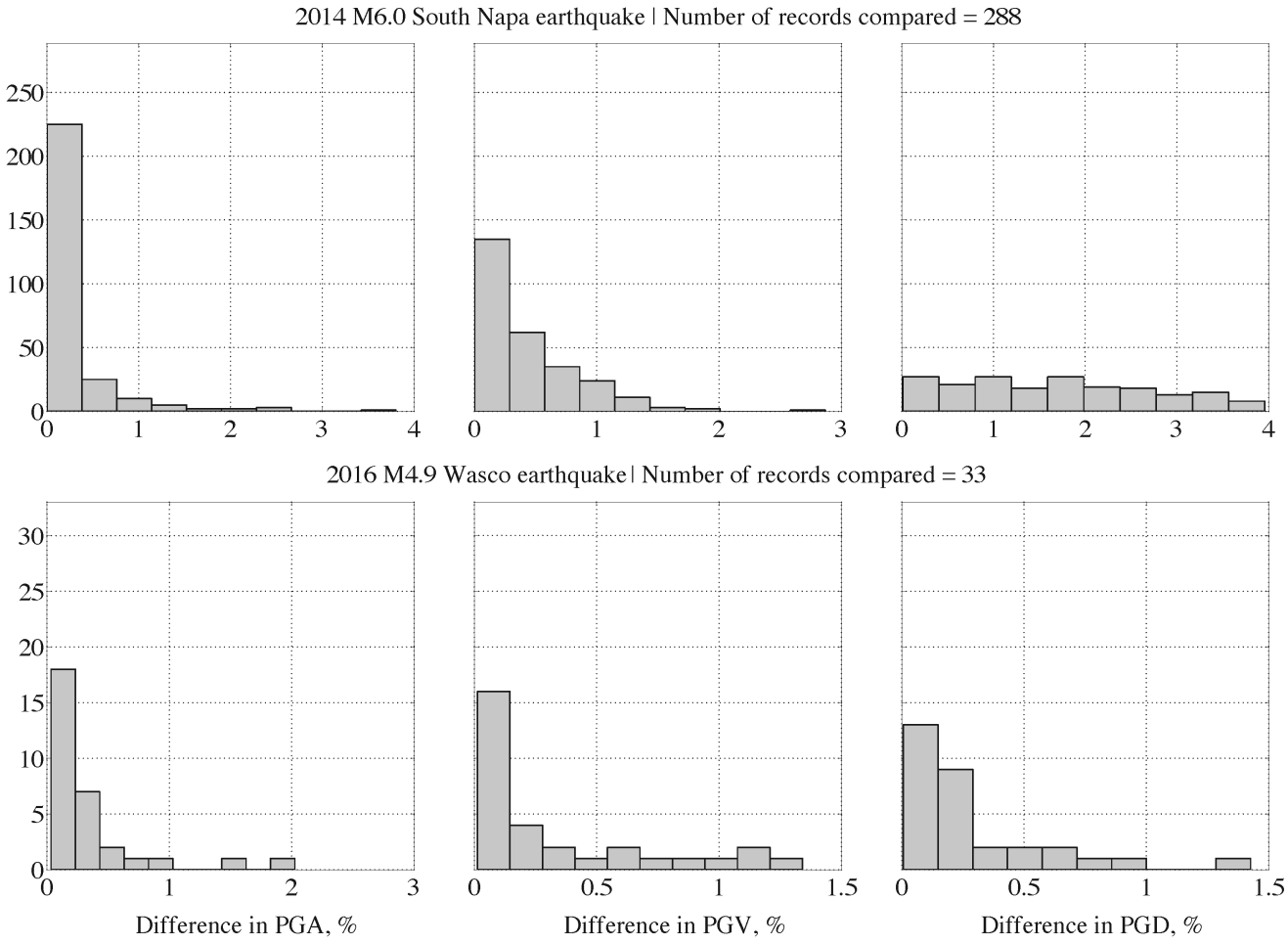


Figure 95. Histograms showing absolute differences [|CSMIP−PRISM|×100/CSMIP] in peak ground acceleration (PGA), peak ground velocity (PGV), and peak ground displacement (PGD) between Processing and Review Interface for Strong Motion data (PRISM) and California Strong Motion Instrumentation Program (CSMIP) for various earthquakes; y-axis shows number of records. *M*, moment magnitude.

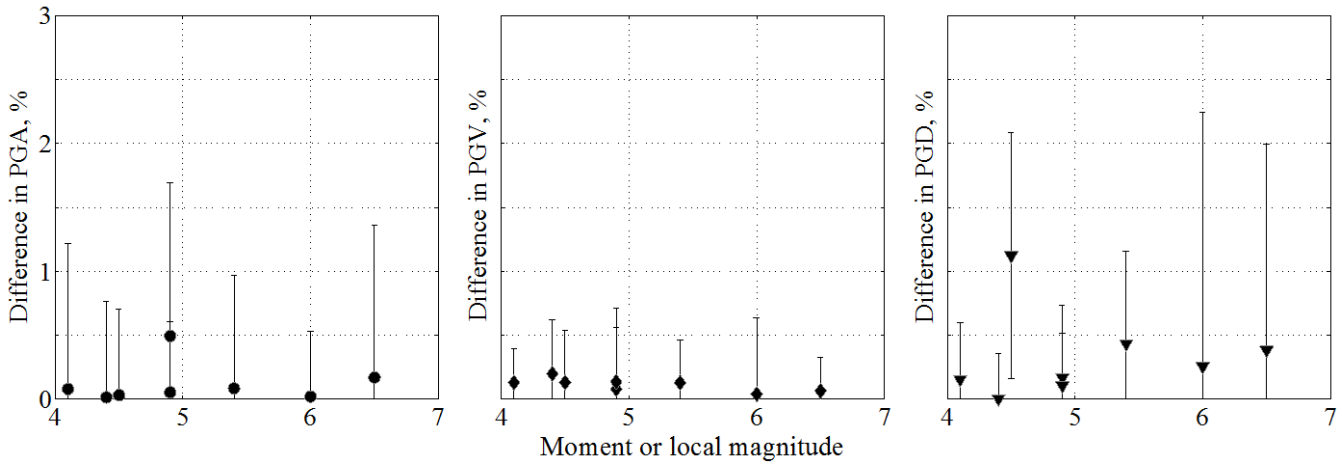


Figure 96. Graphs showing median and standard deviation of absolute differences computed as [|CSMIP−PRISM|×100/CSMIP] in peak ground acceleration (PGA), peak ground velocity (PGV), and peak ground displacement (PGD) between Processing and Review Interface for Strong Motion data (PRISM) and California Strong Motion Instrumentation Program (CSMIP) processing against magnitude of eight earthquakes; data include 1,822 ground-motion components.

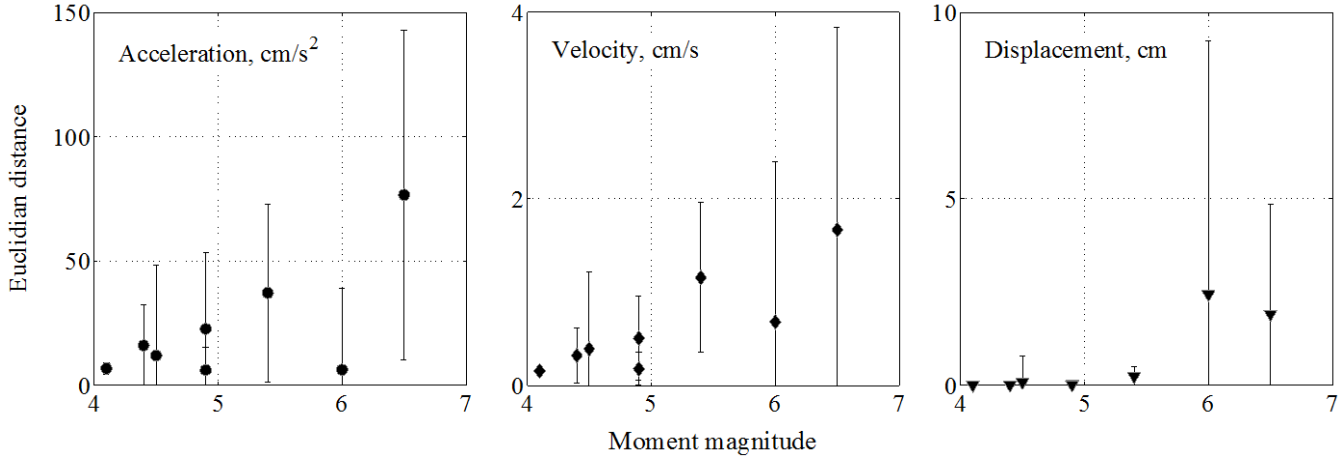


Figure 97. Graphs showing median and standard deviation of Euclidian distance between Processing and Review Interface for Strong Motion data (PRISM) and California Strong Motion Instrumentation Program (CSMIP) products against magnitude of eight earthquakes; data include 1,822 ground-motion components. cm, centimeters; cm/s, centimeters per second; cm/s$^2$, centimeters per second squared.

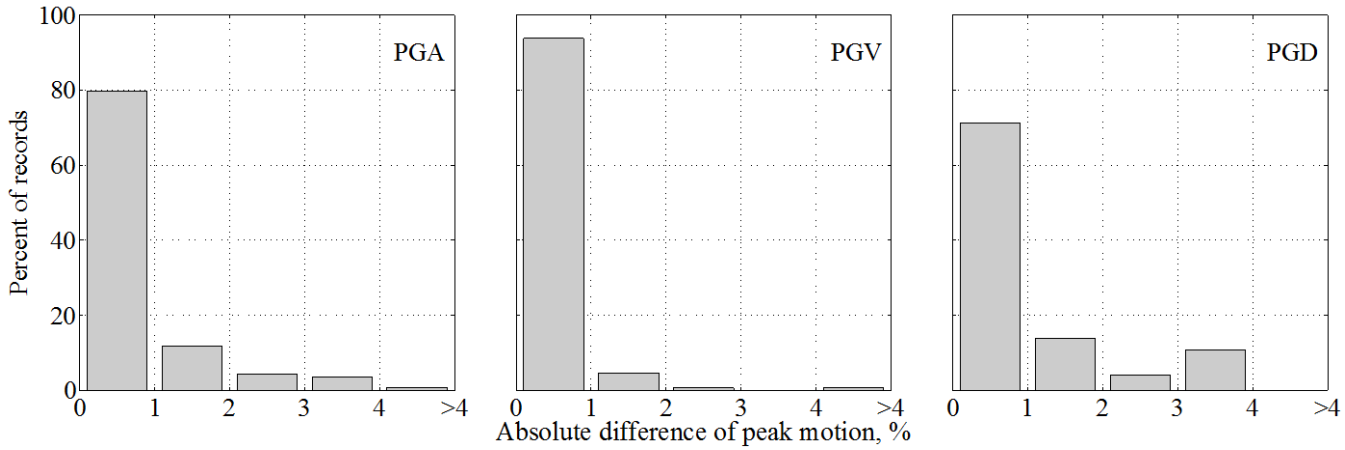


Figure 98. Bar graphs showing ratio of absolute differences computed as (|CSMIP−PRISM|×100/CSMIP) in peak ground acceleration (PGA), peak ground velocity (PGV), and peak ground displacement (PGD) in terms of percentage between Processing and Review Interface for Strong Motion data (PRISM) and California Strong Motion Instrumentation Program (CSMIP) processing as percentage of all (1,822) ground-motion components. For instance, for 80 percent of ground-motion components, PRISM provides PGA values that are within 1 percent of CSMIP PGA values.

## Concluding Remarks

We have measured signal similarities among products derived by using the updated version of PRISM, BAP, and CSMIP processing by (1) comparing peak amplitude values (PGA, PGV, and PGD) of processed time series; (2) computing coherence, cross spectrum phase, and cross correlation of the time series; (3) comparing Fourier amplitude spectrum (FAS) of acceleration, velocity, and displacement time series; and (4) comparing spectrograms of power spectra.

We have also run a statistical evaluation of PRISM and CSMIP processing by using 1,822 ground-motion components from eight Californian earthquakes that occurred between 2005 and 2016. The statistical evaluation of misfit is based on comparing (1) PGA, PGV, and PGD of processed time series; (2) Euclidian distance (L2 norm) between acceleration, velocity, and displacement time series; and (3) moving window root mean square (RMS) levels of acceleration, velocity, and displacement time series.

Based on these quantitative comparisons, the following conclusions are drawn:

- The application of acausal bandpass filters in acceleration rather than in velocity avoids frequency-dependent effects that result from trapezoid integration observed in development stage of PRISM.
- The use of a 5-point central difference operator in PRISM is shown to have a superior performance in reducing numerical error as compared with a 3-point central difference operator.
- Re-sampling low time-resolution (100 sps and less) records to at least 200 sps prior to differentiation, and then downsampling to the original sampling rate for generating final products significantly reduces numerical noise. PRISM employs this technique.
- Acceleration, velocity, and displacement time series generated by using the revised processing methods in PRISM closely match those computed by using BAP and those generated by CSMIP. The largest discrepancy in PGA is 3.8 percent for a weak-motion record with high-frequency content, and 1 percent for a strong-motion record with long-period content.

- Apparent discrepancies in spectral comparisons between PRISM and CSMIP processing mostly result from relative time delays on the order of few milliseconds, generally less than the sampling interval.
- Statistical evaluations considering more than 1,800 ground-motion components indicate that PRISM and CSMIP processed records are in good agreement overall. Differences in PGA obtained from PRISM and CSMIP processing are equal to or less than 4 percent for 99 percent of data, and within 2 percent for 91 percent of data. For PGV, the difference is less than 4 percent for 99 percent of data, and within 2 percent for 98.5 percent of data. For PGD, the difference is less than 4 percent for 100 percent of data, and within 2 percent for 85.1 percent of data. Other statistical measures, including Euclidian distance (L2 norm) and root mean square levels of processed time series, also indicate that both processing schemes produce comparable products.

## References Cited


Bendat, J.S., and Piersol, A.G., 2010, Random data: Analysis and measurement procedures, 4th edition, ISBN: 978-0-470-24877-5, 640 p.

Buck, J.R., Daniel, M.M., and Singer, A.C., 2002, Computer explorations in signals and systems using MATLAB®, 2nd Edition: Upper Saddle River, New Jersey, Prentice Hall, 207 p.

Converse, A.M., and Brady, A.G., 1992, BAP—Basic strong-motion accelerogram processing software, version 1.0: U.S. Geological Survey Open-File Report 92–296A, 174 p.

Consortium of Organizations for Strong-Motion Observation Systems, 2001, Guidelines for installation of advanced national seismic system strong-motion reference stations: Richmond, Calif., Pacific Earthquake Engineering Research Center, accessed November 2016 at http://www.cosmos-eq.org/publications/reports/Guidelines_ANSS.pdf.

Geller, R.J., and Takeuchi, N., 1995, A new method for computing highly accurate DSM synthetic seismograms: Geophysical Journal International, v. 123, p. 449–470.

Hamming, R.W., 1989, Digital filters, third edition: Dover Publications, Inc., Mineola, New York, 284 p., ISBN 0-486-65088-X (pbk.)

Jones, J., Kalkan, E., and Stephens, C., 2017, Processing and review interface for strong motion data (PRISM) software, version 1.0.0—Methodology and automated processing: U.S. Geological Survey Open-File Report 2017–1008, 81 p., https://doi.org/10.3133/ofr20171008.

Oppenheim, A.V., Schafer, R.W., and Buck, J.R., 1999, Discrete-time signal processing: Upper Saddle River, New Jersey, Prentice Hall, 870 p.

Parks, T.W., and Burrus, C.S., 1987, Digital filter design: John Wiley & Sons Inc., p. 54–83.

Proakis, J.G., and Manolakis, D.G., 2007, Digital signal processing—Principles, algorithms, and applications, fourth edition: Upper Saddle River, New Jersey, Prentice Hall.

Shakal, A.F., Huang, M.J., and Graizer, V., 2003, Strong-motion data processing, Lee, W.H.K., Kanamori, H., Jennings, P.C., and Kisslinger, C., eds., *in* International handbook of earthquake and engineering seismology, B: Amsterdam, Academic Press, p. 967–981.

Shakal, A., Huang, M.J., and Graizer, V., 2004, California Strong-Motion Instrumentation Program processing methods and procedures: Proceedings of the COSMOS Invited Workshop on Strong-Motion Processing: COSMOS Pub. CP-2004/02, p. 111–122.

Stoica, P., and Moses, R., 2005, Spectral analysis of signals: Upper Saddle River, New Jersey, Prentice Hall, 427 p.

Welch, P.D., 1967, The use of fast Fourier transform for the estimation of power spectra—A method based on time averaging over short, modified periodograms: Institute of Electrical and Electronics Engineers (IEEE) transactions on audio and electroacoustics, v. AU-15, p. 70–73.
Whittaker, A.S., Aho, J.L., Crouse, C.B., Frosch, R., Kelly, D.J., Lizundia, B., Lowes, L.N., Miranda, E., Nigbor, R.L., Sanders, D.H., and Stewart, J., 2005, Guideline for ANSS seismic monitoring of engineered civil systems, version 1.0: Open-File Report 2005–1039.